2-2020

# Electrical Characterization and Detection of Blood Cells and Stones in Urine

Nida Nasir

United Arab Emirates University

College of Engineering

ELECTRICAL CHARACTERIZATION AND DETECTION OF
BLOOD CELLS AND STONES IN URINE

Nida Nasir

This dissertation is submitted in partial fulfillment of the requirements for the degree
of Doctor of Philosophy

Under the Supervision of Dr. Mahmoud F. Al Ahmad

February 2020

# Declaration of Original Work

I, Nida Nasir, the undersigned, a graduate student at the United Arab Emirates University (UAEU), and the author of this dissertation entitled "*Electrical Characterization and Detection of Blood Cells and Stones in Urine*", hereby, solemnly declare that this dissertation is my own original research work that has been done and prepared by me under the supervision of Dr. Mahmoud F. Al Ahmad, in the College of Engineering at UAEU. This work has not previously been presented or published or formed the basis for the award of any academic degree, diploma or a similar title at this or any other university. Any materials borrowed from other sources (whether published or unpublished) and relied upon or included in my dissertation have been properly cited and acknowledged in accordance with appropriate academic conventions. I further declare that there is no potential conflict of interest with respect to the research, data collection, authorship, presentation and/or publication of this dissertation.

Student's Signature: _____     Date: _____

## Advisory Committee

1) Advisor: Mahmoud F. Al Ahmad

Title: Associate Professor

Department of Electrical Engineering

College of Engineering

2) Member: Tahir A. Rizvi

Title: Professor

Department of Microbiology

College of Medicine and Health Sciences

3) Member: Ali Hilal Al-Naqbi

Title: Associate Professor

Department of Mechanical Engineering

College of Engineering

4) Member: Farah Mustafa

Title: Associate Professor

Department of Biochemistry

College of Medicine and Health Sciences

# Approval of the Doctorate Dissertation

This Doctorate Dissertation is approved by the following Examining Committee Members:

1) Advisor: **Dr. Mahmoud F. Al Ahmad**

Title: Associate Professor

Department of Electrical Engineering
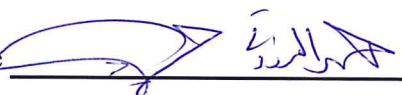
College of Engineering, UAEU, Al Ain, UAE

Signature _____ Date _20/2/20_

2) Member: **Dr. Ahmed H. Al-Marzouqi**

Title: Associate Professor

Department of Biochemistry

College of Medicine and Health Sciences, UAEU, Al Ain, UAE

Signature _____ Date _20/2/2020_

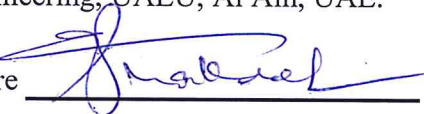3) Member: **Dr. Mohammad Shakeel Laghari**

Title: Associate Professor

Department of Electrical Engineering

College of Engineering, UAEU, Al Ain, UAE.
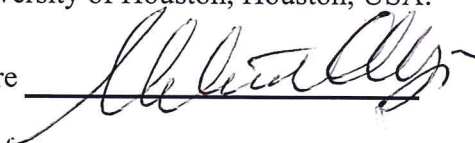
Signature _____ Date _20 – 02 – 2020_

4) Member (External Examiner): **Dr. Metin Akay**

Title: John S Dunn Endowed Chair Professor

Department of Biomedical Engineering

Institution: University of Houston, Houston, USA.

Signature _____ Date _20/2/2020_

This Doctorate Dissertation is accepted by:

Dean of the College of Engineering: Professor Sabah Alkass

Signature _____ Date 19/6/2020

Dean of the College of Graduate Studies: Professor Ali Al-Marzouqi

Signature _____ Date 19/6/2020

Copy ____ of ____

# Abstract

Urine contains an immense amount of information related to its physical, chemical, and biological components; hence, it is a promising tool in detecting various diseases. Available methods for detecting hematuria (blood in the urine) are not accurate. Results are influenced by many factors, such as, health and vitals of the patients, settings of the equipment and laboratories, which leads to the false positive or false negative outputs. This necessitates the development of new, accurate and easy-access methods that save time and effort. This study demonstrates a label-free and accurate method for detecting the presence of red and white blood cells (RBCs and WBCs) in urine by measuring the changes in the dielectric properties of urine upon increasing concentrations of both cell types. The current method could detect changes in the electrical properties of fresh urine over a short time interval, making this method suitable for detecting changes that cannot be recognized by conventional methods. Correcting these changes enabled the detection of a minimum cell concentration of $10^2$ RBCs per ml which is not possible by conventional methods used in the labs except for the semi-quantitative method that can detect 50 RBCs per ml, but it is a lengthy and involved procedure, not suitable for high volume labs. This ability to detect a very small amount of both types of cells makes the proposed technique an attractive tool for detecting hematuria, the presence of which is indicative of problems in the excretory system.

Furthermore, urolithiasis is also a very common problem worldwide, affecting adults, kids, and even animals. Calcium oxalate is the major constituent of the urinary tract stones in individuals, primarily due to the consumption of high-oxalate foods. The occurrence of urinary oxalate occurs by endogenous synthesis, especially in the upper urinary tract. In a normal, healthy individual, the excretion of oxalate ranges from 10 to 45 mg/day, depending on the age and gender, but the risk of stone formation starts at 25 mg/day depending on the health history of the individual. This study also addresses the detection of the presence of calcium oxalate in urine following same label free approach. This can be done by measuring the changes in the dielectric properties of urine with increasing concentrations of calcium oxalate hydrate ($CaC_2O_4.H_2O$). The current method could detect dynamic changes in the electrical

properties of urine over a time interval in samples containing calcium oxalate hydrate even at a concentration as low as 10 μg/mL of urine, making this method suitable for detecting changes that cannot be recognized by conventional methods. The ability to detect very small amount of stones makes it an attractive tool for detecting and quantifying stones in kidney.

Using a non-invasive method which also works as a precautionary measure for early detection of some severe ailments, hold a good scope. It forms the basis of the cytological examinations and molecular assays for the diagnosis of several diseases. This method can be considered a point-of-care test because the results can be instantaneously shared with the members of the medical team. Based on these results, it is anticipated that present approach to be a starting point towards establishing the foundation for label-free electrical-based identification and quantification of an unlimited number of nano-sized particles.

**Keywords**: Biological analysis, blood cells, calcium oxalate, capacitance–voltage method, detection, dielectric constant, label free, urine.

**Title and Abstract (in Arabic)**

# الخصائص الكهربائية للكشف عن خلايا الدم و الحصى في البول

*الملخص*

يحتوي البول على كمية هائلة من المعلومات المتعلقة بمكوناته الفيزيائية والكيميائية والبيولوجية؛ مما يجعله أداة واعدة في الكشف عن الكثير من الأمراض المختلفة. الطرق المتاحة للكشف عن البيلة الدموية (الدم في البول) ليست دقيقة. كما تتأثر النتائج بالعديد من العوامل من المرضى وإعدادات المختبر، مما يؤدي إلى نتائج سلبية أو إيجابية كاذبة. وهذا يستلزم تطوير أساليب جديدة ودقيقة وسهلة الوصول توفر الوقت والجهد. توضح هذه الدراسة طريقة خالية من الملصقات ودقيقة للكشف عن وجود خلايا الدم الحمراء والبيضاء (كرات الدم الحمراء و كرات الدم البيضاء) في البول عن طريق قياس التغيرات في خصائص العزل الكهربائي للبول عند زيادة تركيز كلا النوعين من الخلايا. يمكن للطريقة الحالية اكتشاف التغيرات في الخواص الكهربائية للبول الطازج خلال فترة زمنية قصيرة، مما يجعل هذه الطريقة مناسبة لاكتشاف التغيرات التي لا يمكن التعرف عليها بالطرق التقليدية. أتاح تصحيح هذه التغيرات اكتشاف الحد الأدنى لتركيز الخلية من $10^2$ كرات دم حمراء لكل مل، وهو أمر غير ممكن من خلال الطرق التقليدية المستخدمة في المختبرات باستثناء الطريقة شبه الكمية التي يمكن الكشف عن 50 كرة دم حمراء لكل مل، لكنها طويلة ومعقدة، وغير مناسبة للمختبرات ذات الإنتاج الكبير. هذه القدرة على اكتشاف كمية صغيرة جدًا من كلا النوعين من الخلايا تجعل التقنية المقترحة أداة جذابة للكشف عن بيلة دموية، التي تدل على وجود مشاكل في جهاز الإخراج.

علاوة على ذلك، تعتبر الحصى البولية أيضًا مشكلة شائعة في جميع أنحاء العالم، حيث تصيب البالغين والأطفال وحتى الحيوانات. أكسالات الكالسيوم هي المكون الرئيسي لحصى المسالك البولية في الأفراد، ويرجع ذلك أساسا إلى استهلاك الأطعمة عالية الأكسالات. يحدث تكون أكسالات البول عن طريق التخليق الداخلي، وخاصة في الجهاز البولي العلوي. في الفرد الطبيعي والصحي، يتراوح إفراز الأكسالات بين 10 و 45 ملغ/يوم، حسب العمر والجنس، لكن خطر تكوين الحجر يبدأ من 25 ملغ/يوم حسب التاريخ الصحي للفرد. تتناول هذه الدراسة أيضًا اكتشاف وجود أكسالات الكالسيوم في البول باتباع نفس الطريقة الخالية من الملصقات. يمكن القيام بذلك عن طريق قياس التغيرات في الخواص العازلة للبول مع زيادة تركيز هيدرات أكسالات الكالسيوم

(CaC$_2$O$_4$.H$_2$O). يمكن للطريقة الحالية اكتشاف التغيرات الديناميكية في الخواص الكهربائية للبول على مدى فترة زمنية في العينات التي تحتوي على هيدرات أكسالات الكالسيوم حتى بتركيز منخفض يصل إلى 10 ميكروغرام/مل من البول، مما يجعل هذه الطريقة مناسبة للكشف عن التغييرات التي لا يمكن التعرف عليها بواسطة الأساليب التقليدية. القدرة على اكتشاف كمية صغيرة جدًا من الحصى يجعلها أداة جذابة لاكتشاف وقياس الحصى في الكلى.

استخدام طريقة غير جراحية تعمل كتدبير وقائي للكشف المبكر عن بعض الأمراض الشديدة يعد نطاق جيد. هذا الأسلوب يشكل أساس الفحوصات الخلوية والمقايسات الجزيئية لتشخيص العديد من الأمراض. يمكن اعتبار هذه الطريقة بمثابة اختبار عند نقطة الرعاية لأنه يمكن مشاركة النتائج على الفور مع أعضاء الفريق الطبي. استنادًا إلى هذه النتائج، نتوقع أن يكون نهجنا الحالي بمثابة نقطة انطلاق نحو بناء الأساس لتحديد الهوية الكهربائية بدون ملصقات وتقدير عدد غير محدود من الجزيئات النانوية.

**مفاهيم البحث الرئيسية:** تحليل حيوي، خلايا الدم، أكسالات الكالسيوم، قياس، البول، ثابت العزل الكهربائي.

# Acknowledgments

I am especially grateful to Dr. Mahmoud F. Al Ahmad, who introduced me to the exciting field of biomedical engineering. His endless ideas and encouragement helped me in shaping my future.

I would like to thank my committee for their guidance, support, and assistance throughout my preparation of this dissertation. My thanks goes to the Department of Electrical Engineering at the United Arab Emirates University for assisting me in all parts of my studies and research.

Special thanks go to my Mom and Dad, along with my siblings Mudassar, Hiba and Meran, who encouraged me along the way. Moreover, I am sincerely grateful to my grandparents and my uncles and aunts, who have unwavering faith in me. In addition, special thanks are extended to my friends Amir, Anusha, Areen, Asma, Aysha, Hussam, Indu, Neeraj, Nisreen, Rehman, Saif, Shama, Shahnawaz and Sonu for their love and support.

# Dedication

*To my beloved parents and family*

# Table of Contents

# List of Tables

# List of Figures

# List of Abbreviations

| | |
|---|---|
| AFM | Atomic Force Microscopy |
| B | Boron |
| BioMEMS | Biomedical (or Biological) Micro-Electro-Mechanical Systems |
| BMI | Body Mass Index |
| CAP | Cell Attached Patch |
| Ca | Calcium |
| CaP | Calcium Phosphate |
| CaOx | Calcium Oxalate |
| $CaOx.xH_2O$ | Calcium Oxalate Hydrate |
| Cd | Cadmium |
| CF | Capacitance-Frequency |
| CKD | Chronic Kidney Disease |
| CM | Capacitance-Mass |
| CMOS | Complementary Metal Oxide Semiconductor |
| CNP | Carbon Nanoparticle |
| COD | Calcium Oxalate Dihydrate (weddellite) |
| COM | Calcium Oxalate Monohydrate (whewellite) |
| CPA | Constant Phase Angle |
| CT | Computed Tomography |
| CV | Capacitance-Voltage |
| DEPIM | Dielectrophoretic Impedance Measurements |
| dMRI | Diffusion Magnetic Resonance Imaging |
| DMEM | Dulbecco's Modified Eagles Medium |

| | |
|---|---|
| DNA | Deoxyribonucleic Acid |
| EBIS | Electrical Bioimpedance Spectroscopy |
| EDX | Energy Dispersion X-ray |
| EDTA | Ethylenediaminetetraacetic Acid |
| EFM | Electrostatic Force Microscopy |
| eGFR | Estimated Glomerular Filtration Rate |
| EMU | Early Morning Urine |
| ESEM | Environmental Scanning Electron Microscope |
| ESRD | End-Stage Renal Disease |
| FET | Field Effect Transistor |
| fMRI | Functional Magnetic Resonance Imaging |
| HPF | High-Power Field |
| IgA | Immunoglobulin A |
| IOP | Inside Out Patch |
| IR | Infrared Spectroscopy |
| LA-ICP-MS | Laser Ablation Inductively Couple Plasma Mass Spectroscopy |
| LIBS | Laser Induced Breakdown Spectroscopy |
| LoC | Lab on a Chip |
| LPF | Low-Power Field |
| MALDI–TOF/MS | Matrix-Assisted Laser Desorption/Ionization–Time of Flight Mass Spectrometry |
| MEMS | Microelectromechanical Systems |
| MRI | Magnetic Resonance Imaging |
| μEIS | Micro Electrical Impedance Spectroscopy |
| μTAS | Micro Total Analysis Systems |

| | |
|---|---|
| nDEP | Negative Dielectrophoresis |
| NIR | Near Infrared Region |
| OOP | Outside Out Patch |
| PET | Positron Emission Tomography |
| ppWC | Permeabilized Patch Whole Cell |
| RBC | Red Blood Cell |
| ROT | Electrorotation |
| SCA | Single Cell Analysis |
| SEM | Scanning Electron Microscopy |
| SNR | Signal to Noise Ratio |
| STM | Scanning Tunneling Microscopy |
| TG | Thermogravimetry |
| UFC | Urinary Flow Cytometer |
| UTI | Urinary Tract Infection |
| UV | Ultraviolet |
| UWB | Ultra-Wide Band |
| WBC | White Blood Cell |
| WC | Whole Cell |
| XAS | X-ray Absorption Spectroscopy |
| Zn | Zinc |

# Chapter 1: Introduction

Many diseases can be detected and identified by conventional urine tests together with the label-free techniques employing capacitance–voltage plots, to identify abnormalities in the urine. Enhanced methods are always needed to address the demands of biomedical engineering advancement. In the research for comprehensive knowledge of the human body, urine always plays a key role.

## 1.1 Motivation

Globally, the number of deaths per year caused by kidney disease is increasing at a very fast pace, with a rate even higher than that of breast cancer, heart failure, prostate cancer, diabetes, etc. [1]. Kidney diseases are silent in the initial stage and do not initially reveal prominent symptoms, thus resulting in delayed diagnosis. These diseases cannot be detected until they become severe, but basic tests of urine can help analyze symptoms of any form of kidney ailments.

Urine, which contains an immense amount of information related to its physical, chemical, and biological components, is secreted by the kidneys and excreted through the urethra [2]. Urine is widely used as a biomarker for the early recognition of liver and kidney malfunction. The typical chemical composition of urine contains approximately 95% water and 5% nitrogenous molecules, such as urea, chloride, sodium, potassium, creatinine, and other dissolved ions. Moreover, organic and inorganic compounds such as proteins, hormones, and metabolites, in addition to other metabolic waste components, are also includes in urine composition [3].

Available laboratory analysis techniques for renal problems are depicted in Figure 1.1. However, no solitary procedure can provide thorough information about the

composition of renal calculi, implying that a combination of aforementioned methods is required for analysis [4, 5]. There are several conditions that can cause atypical components to be excreted in urine, such as proteinuria (a high protein content due to abnormal glomeruli), oliguria (a much lower amount of urine excretion, generally caused by kidney damage), polyuria (a very large amount of urine excretion, usually caused by diabetes), dysuria (regular painful urination due to urinary tract infections, UTIs), hematuria (red blood cells, RBCs, present in urine, often due to infection or injury), and glycosuria (excess plasma glucose because of diabetes) [3]. Thus, urinalysis provides crucial data for monitoring individual health and disease states. This field mainly focuses on disease detection at the initial stage [2].
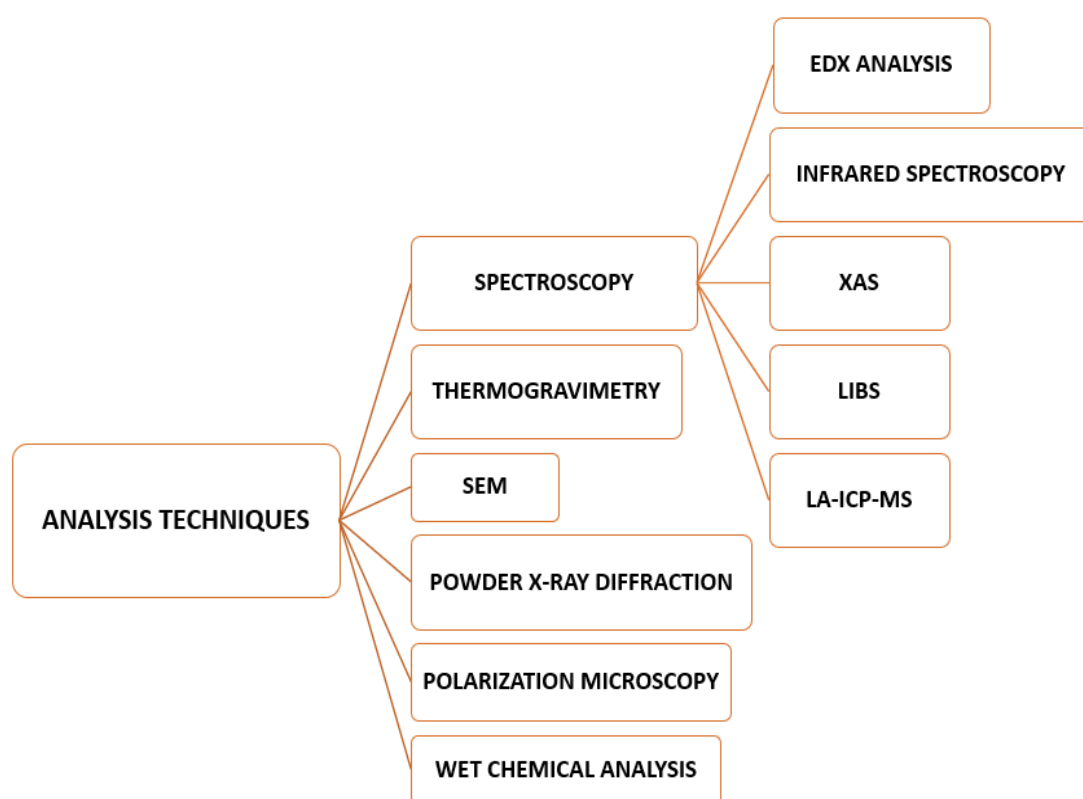


Figure 1.1: A schematic depiction of available laboratory analysis techniques for renal problems.

**1.2 Research Significance and Objectives**

The evolution of kidney diseases can be slowed by early detection and treatment, which is the focus of the study. Hence, the early diagnosis of diseases requires subsequent steps of disease treatment, prevention, and management that might even involve curing the disease. This study is intended to help improve healthcare techniques so that individuals can monitor their health by using their urine samples while engaging in normal activities.

The primary research objectives of this study are to introduce label-free, noninvasive, fast and reliable techniques for aberrations in the urine and to develop a simple clinical tool to predict the likelihood of developing kidney disorder in conjunction with characterizing biotic materials' peculiarities in this context. These goals can be achieved by detection, identification, and quantification of various types of abnormalities in urine using electrical and validation using the same, as mentioned in Figure 1.2.
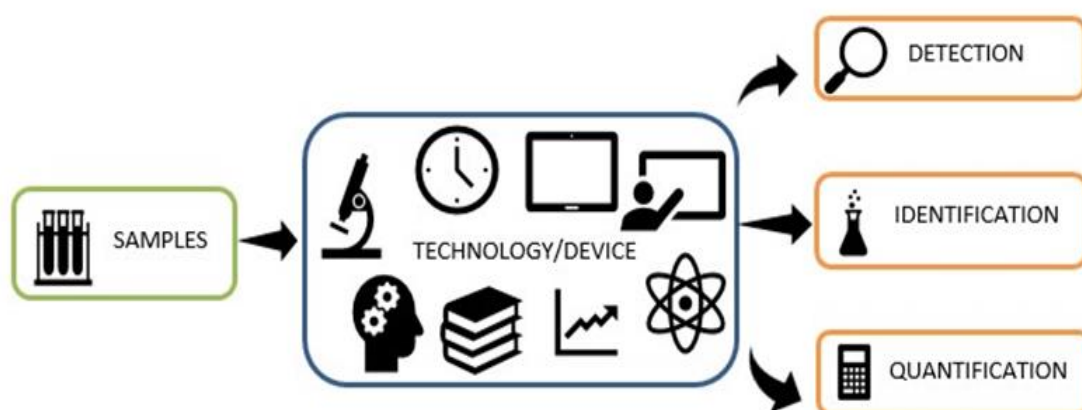


Figure 1.2: A schematic depiction of employing engineering techniques to analyse biomedical samples.

**1.3 Rationale**

The electrical attributes of urine can provide enhanced comprehension regarding various clinical aspects. Numerous studies have been conducted to determine the disparities of normal urine. For instance, variations in the dielectric properties of urine samples can be used to determine different stages of breast cancer [4, 5]. Using the electrical impedance, a significant difference was observed between the mean impedance of normal urine and urine containing higher numbers of RBCs and white blood cells (WBCs) or other constituents [6, 7].

Moreover, the electrical conductivity and total dissolved solids are correlated; any change in the concentration of cells and other components in urine can easily cause a change in electrical conductivity [8, 9]. Various capacitive sensors are available to detect UTIs [10, 11]. Furthermore, urine components such as protein and glucose can be detected through microfluidic technology [12–14]. Kidney stones can be detected using the electrical conductivity and dielectric properties [15, 16].

**1.3.1 Kidney Stones in Urine**

The presence of renal stones is a typical disorder, with a predictable recurrence rate of five years in 50% of the cases. Kidney calculi have no specific origin but numerous factors that sharply increase the risk. Lithiasis occurs when the urine becomes concentrated and contains an excess of crystal-forming elements, such as uric acid calcium, oxalate, etc. Concurrently, urine can be deficient in substances that prevent crystals from aggregating. The identification of kidney stones can also be performed based on their various properties. Knowing the type helps in determining the source and enables precautions to be taken.

Due to the continuous change in dietary proclivity and lifestyle, there has been a steady growth in the susceptibility to calculi over the past decades, as shown in Figure 1.3. Most kidney stones are of calcium type, typically in the form of calcium oxalate, which is highly prevalent. Oxalate is a naturally existing substance that is found in various food items and produced by the liver on a daily basis. Calcium oxalate is a calcium salt of dicarboxylic acid and oxalic acid that occurs as a dihydrate or monohydrate, i.e., calcium whewellite and weddellite, respectively. Certain types of chocolate, nuts, vegetables, and fruits have high oxalate quantities. Dietary proclivity and lifestyle along with heavy doses of vitamin D, certain surgeries and several metabolic disorders can enhance the concentration of calcium oxalate in urine.



Struvite Stone          Cystine Stone

Calcium Stone          Uric Acid Stone

Figure 1.3: Common types of kidney stones.

Calcium phosphate is an additional type of calcium calculus found in metabolic problems such as renal tubular acidosis. Moreover, these problems are usually correlated with migraine headaches and seizure medications. Struvite stones form in reaction to an infection, for instance, a UTI. These stones can grow quickly, without any visible symptoms. Uric acid stones form from a lack of fluid intake in the diet or in cases where a person loses too much fluid. Certain genetic factors (cystinuria), a high protein intake or even gout can increase the risk of uric acid stones.

Many factors increase the risk of developing kidney stones, such as hereditary aspects in people who have a genetic proclivity to developing stones, not drinking enough water daily, living in warm climates, which leads to heavy sweating, and having a diet that is high in protein, salt, and sugar. A high salt intake increases the amount of calcium that the kidneys must filter and significantly increases the risk. Additionally, a high body mass index (BMI), intestinal surgery, inflammatory bowel disease and diarrhea affect the digestive process and disturb the absorption of calcium and water, enhancing the concentrations of stone-forming elements in urine.

**1.3.2 Blood in Urine**

Hematuria is a condition in which blood cells to leak into the urine from the kidneys or any other parts of the urinary tract. Many reasons are there for this leakage, such as UTIs, stones, enlarged prostate glands, and glomerulonephritis. A quantity of three or more RBCs per high-power field (HPF) is considered an abnormal finding. Hematuria can be of two types: gross and microscopic, as mentioned in Figure 1.4. The type is considered gross when the color of blood is visible in the urine sample and microscopic when the RBCs are few, which is detectable by urine dipsticks or microscopic urinalysis.

In gross hematuria, depending on the source of the blood, the urine color can range from light pink to dark brown. A light-colored shade usually arises because of a lower urinary tract problem, while dark-colored shades are due to a glomerular origin. Gross hematuria is caused by UTIs, ureteral irritations, congenital abnormalities, coagulopathy tumors, acute nephritis, etc. Microscopic hematuria occurs due to disorders such as hereditary hematuria, sickle cell trait or anemia, alport syndrome, and IgA vasculitis. The various types of hematuria have different etiologies, but in some cases, they share common causes.
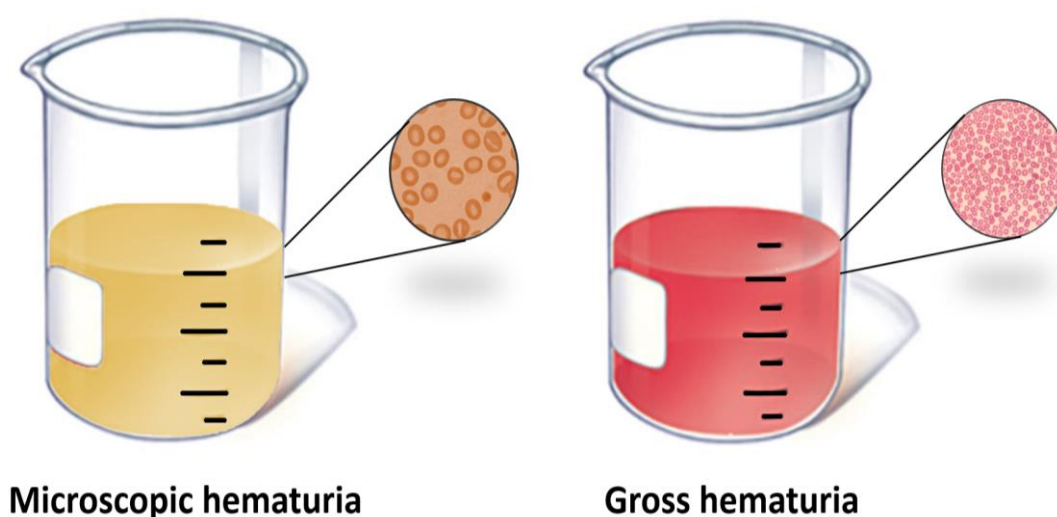


Figure 1.4: Types of hematuria: a) microscopic hematuria and b) gross hematuria.

Blood in the urine can be due to many factors. UTIs happen when microorganisms enter the body via the urethra and grow inside the bladder. Sometimes the only sign of sickness is a microscopic presence of blood cells in the urine sample. Kidney infections happen when microorganisms reach kidneys either from the bloodstream or the ureter. Stone formation occurs when crystal-forming minerals are present in concentrated form within the urine, leading to bladder or kidney stones that cause both types of

hematuria. Prostate gland enlargement often occurs in men approaching middle age. The effects include squeezing of the urethra, somewhat blocking the urine flow. Glomerulonephritis, an infection in the kidney filtering system, either occur by itself or can be the part of a systemic disease such as diabetes. It is caused by viral infections, vasculitis, IgA nephropathy, etc.

Advanced renal, prostate or bladder cancer may lead to visible bleeding in urine, which is mostly detectable at later stages, when these cancers are less curable. Alport syndrome also disturbs the filtering membranes in the kidney glomeruli. Congenital disorders such as sickle cell anemia, a hemoglobin defect in the RBCs, causes both gross and microscopic hematuria. Kidney injury due to accident can cause evident blood in the urine. Furthermore, medications like cyclophosphamide and penicillin, along with anticoagulants such as aspirin and the blood thinner heparin, can cause the bladder to bleed.

Hematuria may be a sign of kidney damage or may lead to kidney damage, such as hemoglobinuria-induced tubular injury. The presence of metabolites released by RBCs in the lumen of nephron tubules can initiate a cascade of intracellular reactions, leading to the generation of reactive oxygen species and consequently lipid peroxidation caspase activation and eventually programmed cell death (apoptosis). Thus, hematuria can act as a diagnostic factor for the presence of kidney disease and as a prognostic marker for chronic kidney disease (CKD). Gross hematuria is more frequent at the early stages of the disease, while micro-hematuria is associated with worse renal outcomes and a higher incidence of patients with end-stage renal disease (ESRD). All of these results suggests that detecting microscopic haematuria is critical to predicting and recognizing patients at high risk of developing CKD, which enables healthcare

professionals to take proactive measures to stop initial stages of CKD from progressing to ESRD.

### 1.3.3 Cells in Urine

Cells are counted as the number observed per low power field (LPF) or per high power field (HPF) or as few, moderate, or many. A disadvantage of this method is that the examination of the urinary sediments should be done by nephrologist to provide more comprehensive information. Urinalysis mostly consists of analysis by dipsticks, in certain cases, it is followed by microscopy of urine sediments. Urinary flow-cytometers (UFC) are used for better count and accuracy, but the absence of a reference measurement is shortcoming for this method.

Cystoscopy examination is a standard procedure in the evaluation of lower urinary tract diseases but is invasive in nature. Several molecular techniques like immunocyte use the immunocyte fluorescence technique (using a fluorochrome to indicate an antigen-antibody reaction), which employs three antibodies to detect cellular markers of bladder cancer using exfoliated cells from urine. However, these techniques are costly and lengthy and are not appropriate for routine identification. Diseases such as UTI that are caused by bacteria are confirmed by culture methods and WBC counts.

A combination of various methods can result in higher diagnostic efficiency and improved precision. A microscopic examination (which was introduced into clinical practice in the 1900s) is part of the routine urinalysis conducted when findings in the physical or chemical examination are not normal. This lengthy process is generally performed on urine sediments obtained by centrifuging urine.

**1.4 Scope**

The aim of the study is to provide a precautionary measure for kidney ailments, especially for patients who cannot avail themselves of expensive healthcare technology. The study emphasizes improving the current situation of lacking a single, fast, non-invasive and comprehensive method. All other techniques require preprocessing steps, while the proposed technique can be directly used. The idea behind the research is to develop electrical models of urine, treating urine as a medium with a variety of abnormal particles in it, to detect these abnormalities, as depicted in Figure 1.5. The abnormal particles can be renal cells, blood cells, kidney stones, etc.
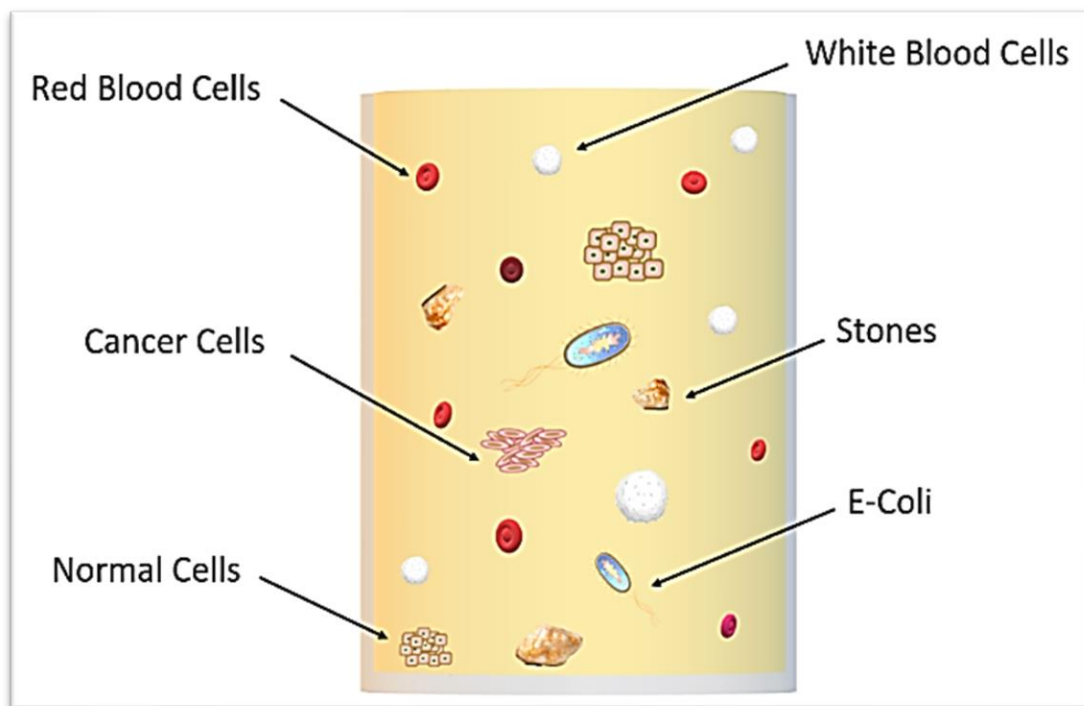


Figure 1.5: A schematic depiction of a urine sample with various uncommon particles.

**1.5 Dissertation Organization**

This dissertation is organized as follows:

Chapter 1 (Introduction): This chapter introduces the main objective of the thesis along with the scope, significance, and motivation. Furthermore, it briefly explains the rationale behind this topic.

Chapter 2 (Electrical Characterization Techniques): This chapter summarizes the relevant studies that have been conducted in this field on various biotic materials such as DNA, viruses, cells. Highlights of urinalysis along with comparison of various available electrical characterization techniques has been done in this section.

Chapter 3 (Fundamentals of Electrical Properties of cells): This chapter summarizes the fundamental theory of electrical characterization of biological cells and discusses the various electrical properties related to it. Moreover, modelling of dielectric properties of cells and mixture theory has been explained.

Chapter 4 (Electrical Detection of Blood Cells in Urine): This chapter discusses the results of the proposed approach along with the methodology, related with Hematuria.

Chapter 5 (Electrical Characterization of Calcium Oxalate in Urine): This chapter reports the results obtained from performing the experiments on calcium oxalate in urine, along with the processing and discussion of the results.

Chapter 6 (Conclusions and Future Work): This chapter summarizes the research findings and relates them to the objectives presented in the first chapter, in addition to future work that could be performed to enhance and elaborate the present work.

# Chapter 2: Electrical Characterization Techniques

Electrical characterization is a technique used to apply an electrical framework to various materials. The electrical properties of a material are built on the basic elements that are atoms. For illustration, the number of electrons in a material, their arrangement, their movements, and whether they become ionized when exposed to external factors such as photons, temperature, and an electric field are all related to the electrical properties of the material. Hence, every living and nonliving material exhibits electrical properties such as resistivity, electrical conductivity, and permittivity. These electrical properties of dielectric materials are obtained to enable their electrical characterization.

## 2.1 Why to use Electrical Characterization?

The electrical characterization of biological materials has been gaining popularity for several decades. The world is approaching the microelectronic and nanoelectronics era. With the progression of CMOS, MEMS, BioMEMS and other technologies, the popularity of this field has surged. The miniaturization of large and heavy devices is made possible through developments in the field of electronics. For building smaller electronic devices and gadgets, electrical characterization of materials plays a pivotal role. Thus, this tool has become a crucial technique in numerous fields, such as medical, science and engineering. Apart from the miniaturization aspects, the analysis of electrical equivalent circuits can be carried out in both the domains of time and frequency by making use of various tools, such as the Fourier transform, Z-transform, and Laplace transform, to provide insight into the analysis process.

## 2.2 Electrical Characterization of Biotic Materials

The new advances in the biomedical and health field are developing in great leaps. In this section, a generalized description of the famous trends in the biomedical field is presented. The review includes the electrical detection and identification of undesirable or pathological biotic materials.

### 2.2.1 Electrical Characterization of DNA

DNA is the source of the traits of all living creatures and is required to balance the homeostasis of life [17]. An extensive variety of biotic process research requires an understanding of the basic electrical properties of DNA, such as restoring impaired cell bonds, identifying genetic alterations, and characterizing the links between proteins and DNA [18]. Various electrical-based DNA characterization techniques have been studied, such as the use of carbon nanoparticles (CNPs) [19–21], field effect transistors (FET) [22, 23], cyclic voltammetry [24, 25], molecular wires [26, 27], graphene quantum dots [28, 29], and dielectrophoresis [30, 31].

### 2.2.2 Electrical Characterization of Viruses

Viruses are microscopic creatures that may induce mild to severe ailments in humans, animals, and plants [32]. These diseases may range from the common flu or cold to fatal diseases. The virus element attacks the cells and controls their mechanism for its own survival and to proliferate and spread. Thus, the contaminated cell generates viral products instead of its usual ones [33]. There are many fatal viruses, such as HIV, dengue, enterovirus, norovirus, and many more. Several techniques are available to detect and identify these viruses, such as scanning tunneling microscopy (STM) [34],

nanotechnology [35], carbon nanotube networks [36, 37], microstrip cavity resonant measurement [38], and dielectrophoretic impedance measurement (DEPIM) [39, 40].

### 2.2.3 Electrical Characterization of Cells

The study of various kinds of cells has developed as a diverse new domain and is recognized as one of the fundamentals in the medical field. Cells have distinctive physical and chemical properties to sustain them within their environment to complete their explicit functions [41]. Moreover, the biophysical properties of cells provide critical information, especially the characterization of cells based on their electrical, mechanical, optical and thermal properties [42]. These properties give early indications of sickness or an atypical state of the body, offering promising markers for detecting various cancers [43–47], bacteria [11, 48–51], toxins [52, 53] and tissue status [54–56]. Fast-emerging technologies have been developed and advanced by scientists in the past few decades to study the biophysical traits of cells, applying extensive influences to biology and the clinical research field, especially in the area of microfluidics [45, 57, 58].

### 2.2.3.1 Single-cell Analysis

Single-cell analysis (SCA) is a significant subject to engineers and scientists in the area of biomedical engineering to develop the available experimental tools and technologies for single-cell characterization [59, 60]. For example, complex analysis and detailed investigation of the differentiation between normal and cancerous cells can be achieved only with the help of SCA [61]. In conventional approaches, population-based procedures have been used, such as cell growth, proliferation, metabolism and motility. These procedures use average values of the cell traits to calculate and forecast the cells' physical and chemical constraints [62]. Although this

technique can present erroneous results and usually omits crucial data due to mixture of various cells [63]. Hence, single-cell researches offers to explore the molecular structure of distinct cells. SCA is important in determining treatment plans for cancer patients [64].

Electrical traits of cells offer rigorous data about complicated physiological states. Cells which undergo aberrations or have been contaminated by microorganisms, exhibits altered ion channel movement [65], cytoplasm conductivity and resistance [66–69] and deformability [70]. Such as, RBCs tainted by Plasmodium falciparum, exhibit reduced deformability [46, 71, 72]. The disease-altered RBCs undergo a change in resistivity, moreover, the normal RBCs and rigidified RBCs have 14.2 and 19.6 $\Omega$ of average resistance, respectively [71]. The electrical traits of cells are beneficial in counting, separating, trapping and characterizing a single cell.

a) Conventional Techniques

The conventional technique to analyze cell electrical properties was initiated in 1791 by measuring the electrical activity in animals by electrical stimulation with metal wires [73]. Over the years, the tools for electrical characterization have been improved. The classical techniques, such as patch clamps and probing, are quite promising for electrical property characterization of a single cell.

i)   Patch Clamp

This technique supports the high-resolution of the ionic currents in the cell membrane. Neher and Sakmann in 1976 introduced the patch-clamp technique; since then, the patch clamp has been used by scientists for crucial data regarding the electrical traits of biological cells [74–76]. A micropipette is used to draw out the cell membrane and

to create a high electrical resistance between 10 and 100 GΩ, known as giga-seals [77].

Then, the ion current which flows through the electrode of the pipette, is measured via

an amplifier.
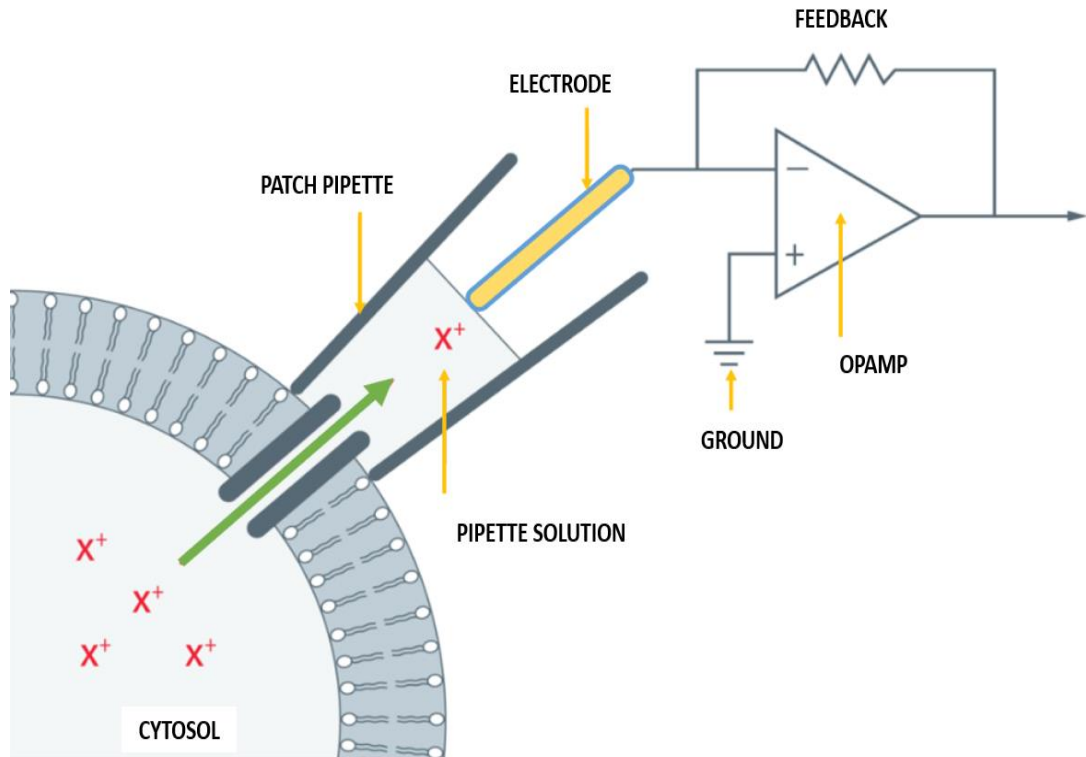


Figure 2.1: The principle of patch-clamp measurements [78].

In Figure 2.1, a pipette comprising an electrolytic mixer is firmly inserted into the

membrane, electrically isolating the membrane patch. A current ($X^+$) flows via the

passage in the patch, which helps in measuring the flow into the pipette using an

electrode. The electrode is linked to a differential amplifier. The overall configuration

of the voltage clamp includes a current which is applied inside the cell through

negative feedback (using a resistor) to compensate for variations in the voltage of the

membrane. The current measurements are used to calculate the membrane

conductance.

This method has following drawbacks:

- It is time consuming [79–84]. The complete cell population has to be changed after the extra-cellular fluid has been used.

- The quality and condition of the cells along with their suspension should retain certain properties for homogenous channel measurements [62].

- Experienced researcher is essential to move the glass pipette without harming the cell.

Further concerns are the recording quality and heat control. However, the patch-clamp gives high sensitivity and low-noise measurement of the currents [73-85].

ii)    Nanoprobes
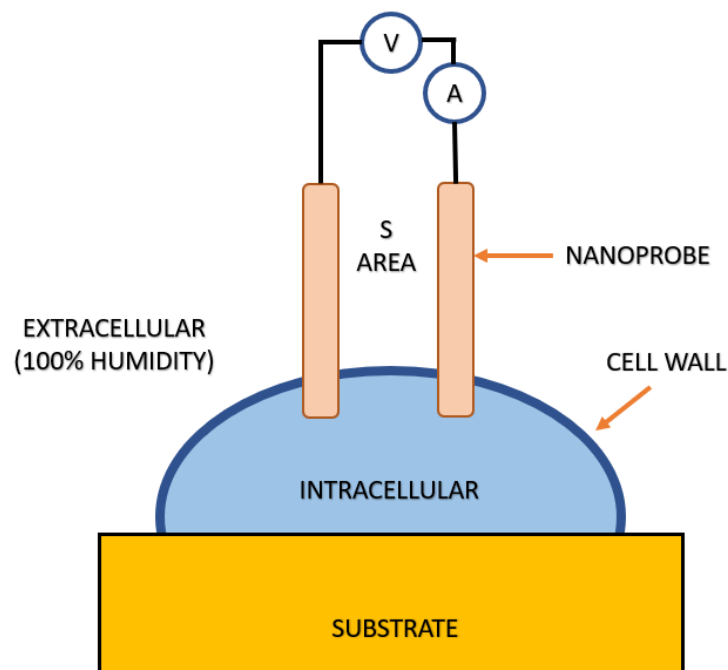


Figure 2.2: Single-cell analysis (SCA) using a dual nanoprobe within an ESEM [62].

Nanoprobes can be used for single-cell electrical characterization. Nanoprobes are well suited for measuring the electrical features of cells and statistically determining their capabilities, as shown in Figure 2.2. Some studies have established dual nanoprobes combined with nanomanipulators within an environmental scanning electron microscope (ESEM) to achieve electrical penetration of single cells [86].

ESEMs can be utilized for high-resolution while maintaining the cell's natural state [87]. This method has been used to effectively differentiate live and dead yeast cells based on their electrical properties [86]. Recently, for high precision and reproducibility, electrostatic force microscopy (EFM) has been used to calculate the electric polarization of single bacterial cells [88].

Generated topographic images helps in acquiring the geometry and finite-element numerical models of bacteria to calculate the dielectric constants of the cell [88]. The complete method requires a large apparatus that can be implemented only in an environmentally controlled area, for instance, a clean room [89].

b) Advanced Techniques

The development of microfabrication procedures, such as soft lithography, opens new prospects for economical and rapid manufacturing of micrometer-size structures [90].

i)   Microfluidic Systems

Rapid advancements in microfluidic systems have been observed, both for biology and medical investigations [91]. Microfluidic structures are used to study materials at the millimeter scale in microscale fluidic passages. Microfluidic structures known as micro total analysis systems (µTASs) [92] or lab on a chip (LoC) devices offer the potential to advance diagnostics and medical studies.

Microfluidic systems are broadly implemented in modern clinical studies. For instance, DNA [93] and cellular analysis [94] is reproducible, requires little power usage and reagent consumption, is cost effective and open to modifications and can be combined with the other technologies [95, 96]. The capability of microfluidic methods to detect initial stage cancer and handle complications in its review which allows it to switch conventional methods in electrical SCA.

Various microfluidic methods have been established for studying the electrical constraints of the cell, such as Micro-electrical impedance spectroscopy (µEIS), electrorotation (ROT), and impedance flow cytometry. Some of these techniques are shown in Figure 2.3.

ii) Electrorotation

A cell rotates when placed in a revolving electric field ($\vec{E}$) in a medium that itself has a nonuniform $\vec{E}$ field. This ROT generally helps in determining the dielectric constraints of cells. The ROT concept is centered on the revolution speed of cells per unit particle by considering the frequency of a rotational field $\vec{E}$. The $\vec{E}$ is produced through four electrodes which are linked to ac signal with a ninety degree out of phase with respect to each other [97].
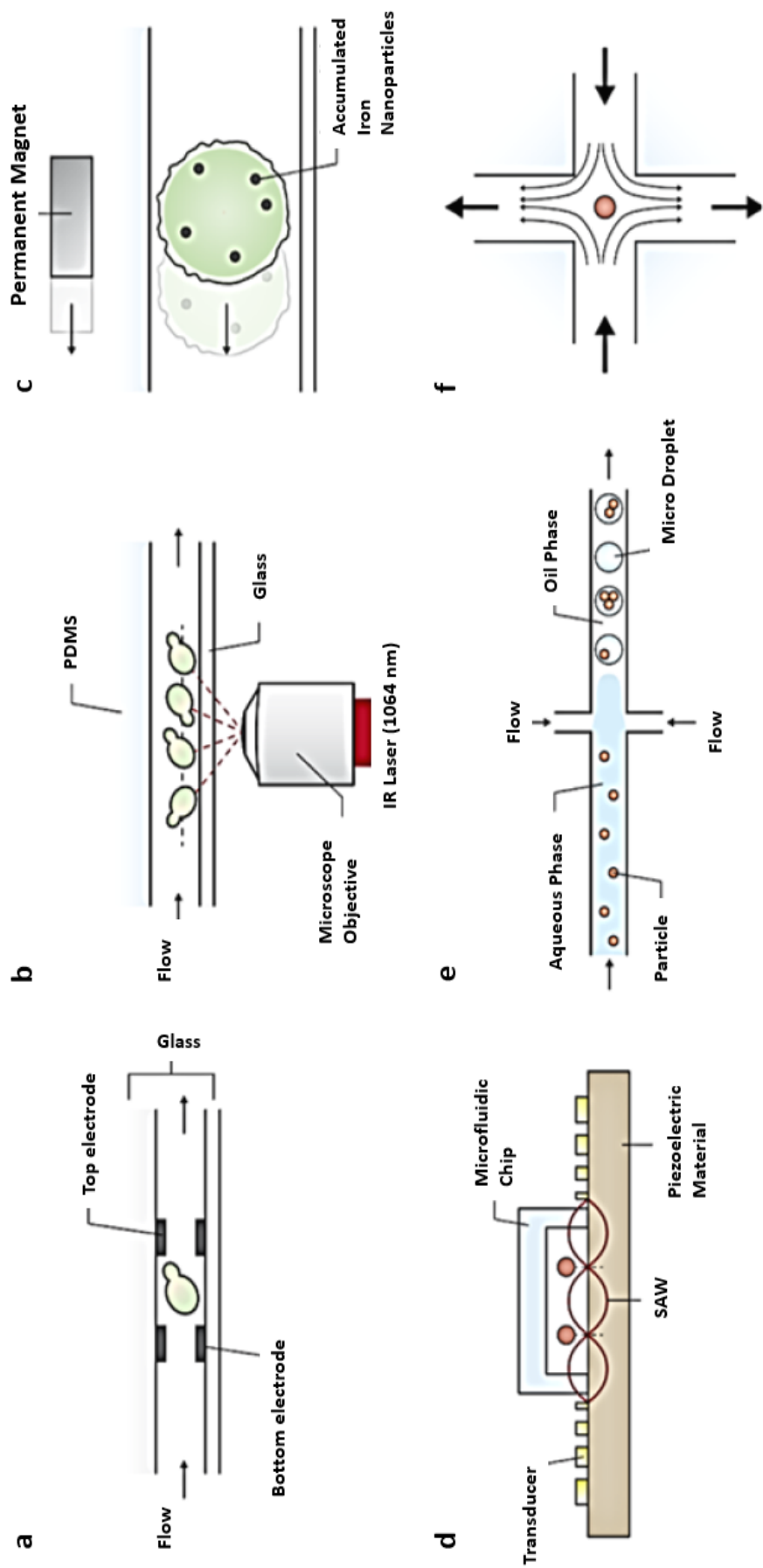
Figure 2.3: Overview of non-surface-contact-based microfluidic methods:: (a) negative dielectrophoresis (nDEP) [78], (b) optical tweezers [79], (c) magnetic tweezers, adapted from [80]; (d) standing acoustic waves (acoustic tweezers), adapted from [81], (e) droplet
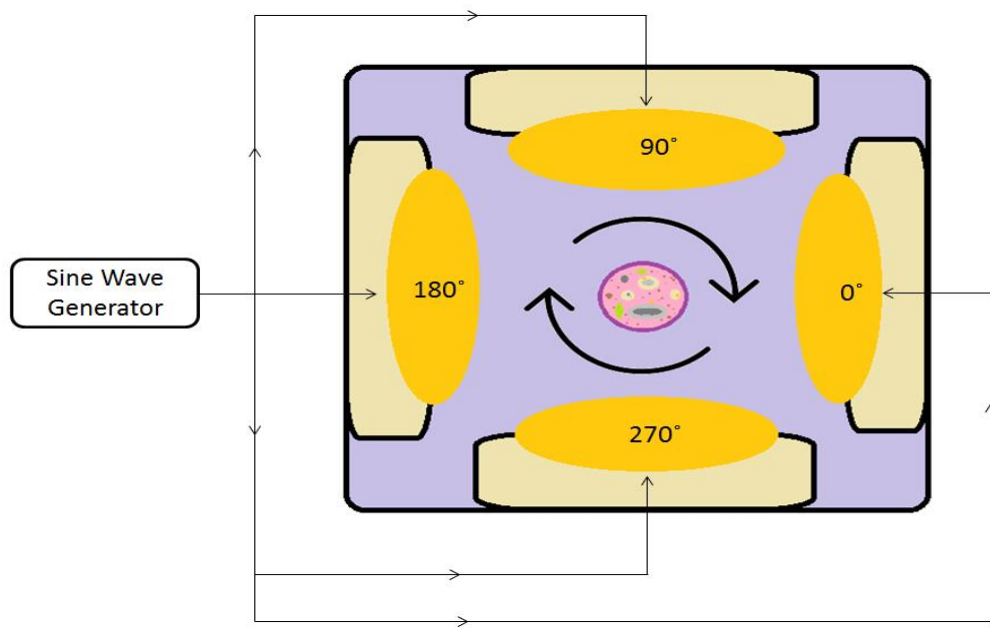
Figure 2.4: Illustration of the working principle of ROT.

The cross-connection of quad-electrodes is set to get sine wave 90° apart, which is chief in ROT technique [98–100]. Figure 2.4 depicts the working principle of ROT where probes fed by an ac signal generator creating a revolving $\vec{E}$. The $\vec{E}$ pulls the cell into the middle of the setup and then rotates it in a direction either similar to or opposite that of the rotating field [101]. The dielectric properties of the cell can be deduced using Maxwell's theory which correlates cell's complex permittivity with its suspension [81]. The theory description and ROT working principle can be found in numerous articles [102–104] and books [105].

In this setup, the electric field magnitude is not affected by the cells, as they are rotating only at a certain site within the electric field [54, 106]. Therefore, a suitable frequency is within the range of 1 kHz up to 200 MHz to identify characteristics such as the cytoplasm conductivity and permittivity along with the membrane capacitance [107, 108]. Wang et al. [98] applied frequencies from 1 to $1.2 \times 10^5$ KHz to extract the

dielectric properties of leukocytes in cell combinations. Moreover, ROT was applied to obtain practical cell information in real-time calculations [109, 110]. Dalton proved that ROT resolved the viability of intestinal parasites [111].

### 2.2.3.2 Electrical Detection of Cancer Cells

There are numerous types of cells that can be detected electrically. The main idea behind this method is to detect abnormalities inside the human body. The atypical presence of cells in body fluids can be used to indicate any of several diseases. The cells might be normal, cancerous or tumorous, depending upon the stage of the disease. The most crucial cells to detect are cancer cells. The following sections describe several techniques used to detect cancer.

 a) X-ray Mammography

It employs electromagnetic radiation to detect early stage cancer in a controlled manner (else it can exaggerate cancer due to the ionizing nature at high frequencies). The total dose for a screening mammogram for both breasts is approximately 0.4 mSv [112, 113].

An X-ray Imaging setup has been shown in Figure 2.5. The proportionality of X-ray transmission energy is inversely with wavelength and directly with transmission frequency. Therefore, high-frequency X-rays cause photons of higher energy and generate better mammography results. However, the higher the penetrating power, the more the ionizing effect of the X-rays is.

Conventional X-ray mammography cannot maintain a balance between higher penetrations or less ionization of low-frequency X-rays while simultaneously maintaining high-energy X-rays. As mentioned by Abbosh and Zhao [115, 116], the

error rate of X-ray mammography in detecting tumors is quite significant, which includes false-positive and false-negative prospects.
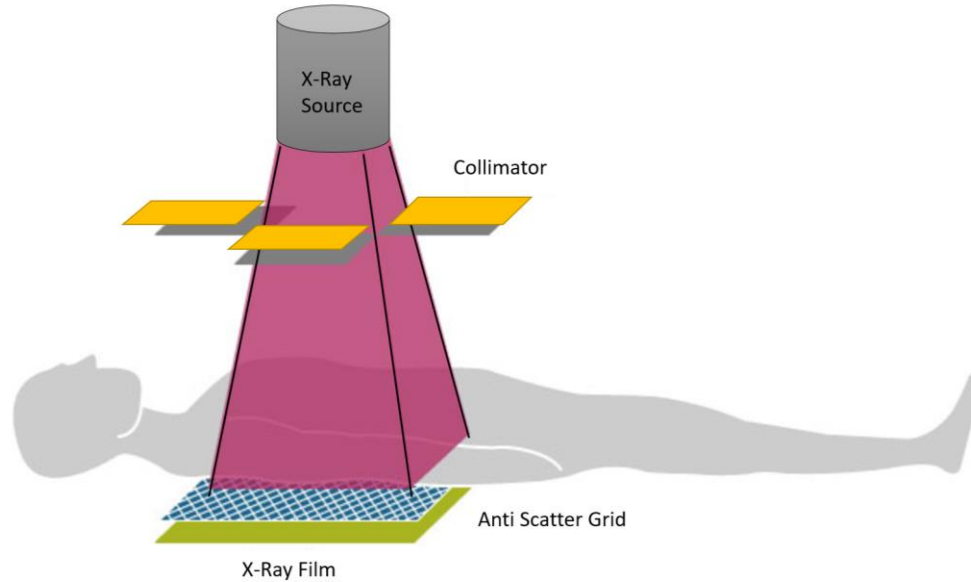


Figure 2.5: X-ray imaging setup [114].

b) Magnetic Resonance Imaging

There is a substitute for X-rays, i.e., magnetic resonance imaging (MRI), for detecting cancer tumors. MRI offers better sensitivity, but the specificity is quite low and sometimes give false-positive results [117], however its frequency range is about 60 MHz [117]. It generates a powerful magnetic field (from 0.2–3 T), which line up the protons of water molecules present inside human body. The protons absorb the energy from field and reverse their spins. Protons in different body tissues return to their normal spins at diverse rates, so the scanner can differentiate among various types of tissues. The basic MRI setup has been shown in Figure 2.6.
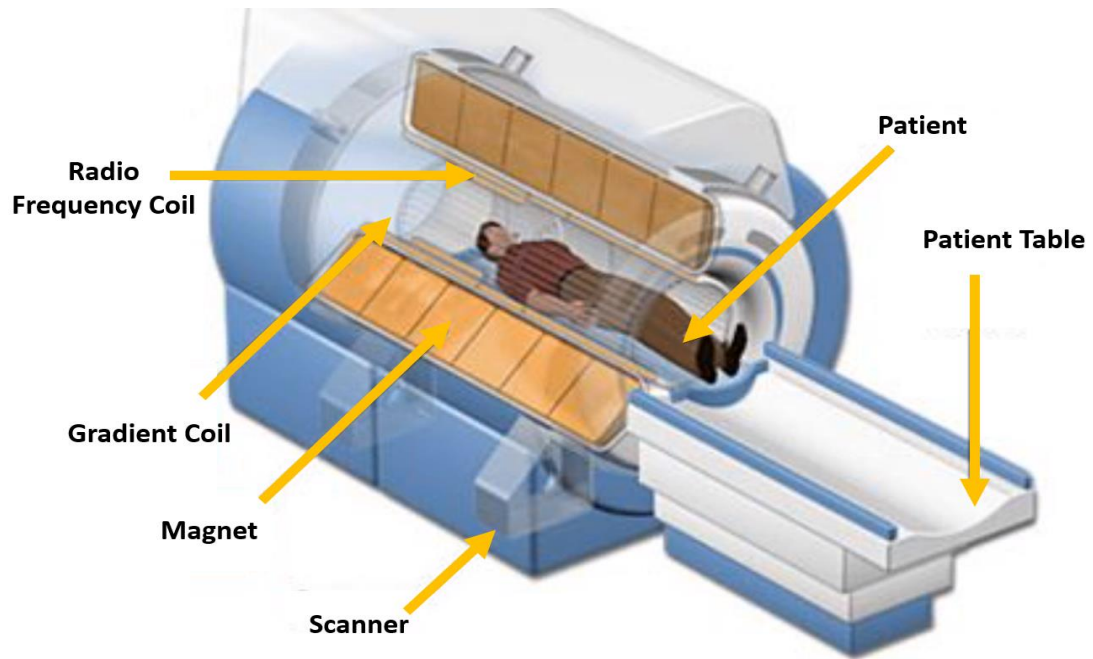
Figure 2.6: The basic setup for MRI [118].

The MRI techniques include two types normally used in biomedical imaging: diffusion MRI and functional MRI (fMRI). Diffusion MRI focuses on how water molecules diffuse in body cells and tissues. This method can easily detect tumors, as tumors are relatively impermeable to water molecules. However, fMRI provides images of structural and functional activities. In addition, fMRI helps in detecting variations in blood flow to various tissues and organs.

 c)  Ultrasound Waves

It is an alternative for sensing and examining the occurrence of tumors. Sound waves at high frequency are applied on affected area and the receiver transforms signals into images, as shown in Figure 2.7. It is not as effective as mammography or MRI but it helps in checking the condition of cancerous lumps.
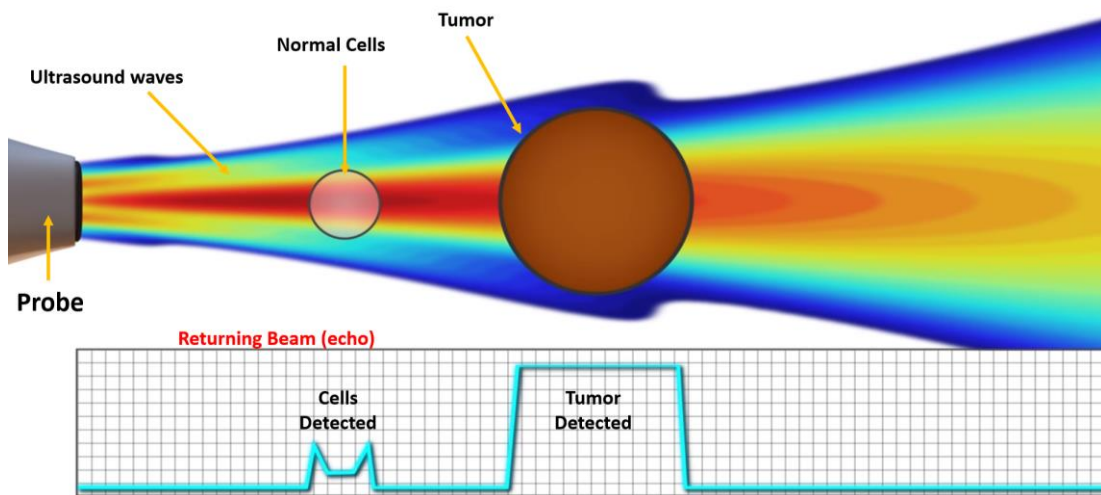
Figure 2.7: Tumor detection using ultrasound.

Ultrasound can help characterize the tumor category and is considered a valuable extension of manual palpitations to detect the presence of any tumors. Although ultrasound waves have frequencies above approximately 20 kHz, they exhibit inadequate penetration because their frequency is still lower than that of the MRI and X-ray methods [119, 120].

 d) Positron Emission Tomography (PET)

It is an imaging technique which classifies malignancy by injecting mixture of radioactive materials with sugar, followed by observation of how cells react. Detection using PET has been depicted in Figure 2.8. Cancer cells multiplies at quicker rate and absorbs more nutrients of the injected mixture. During this process, positrons are released, allowing the generation of an image. PET can find initial stage cancer; however, it is limited by less resolution. PET can be joined with other procedures, like CT scan, for further estimation.
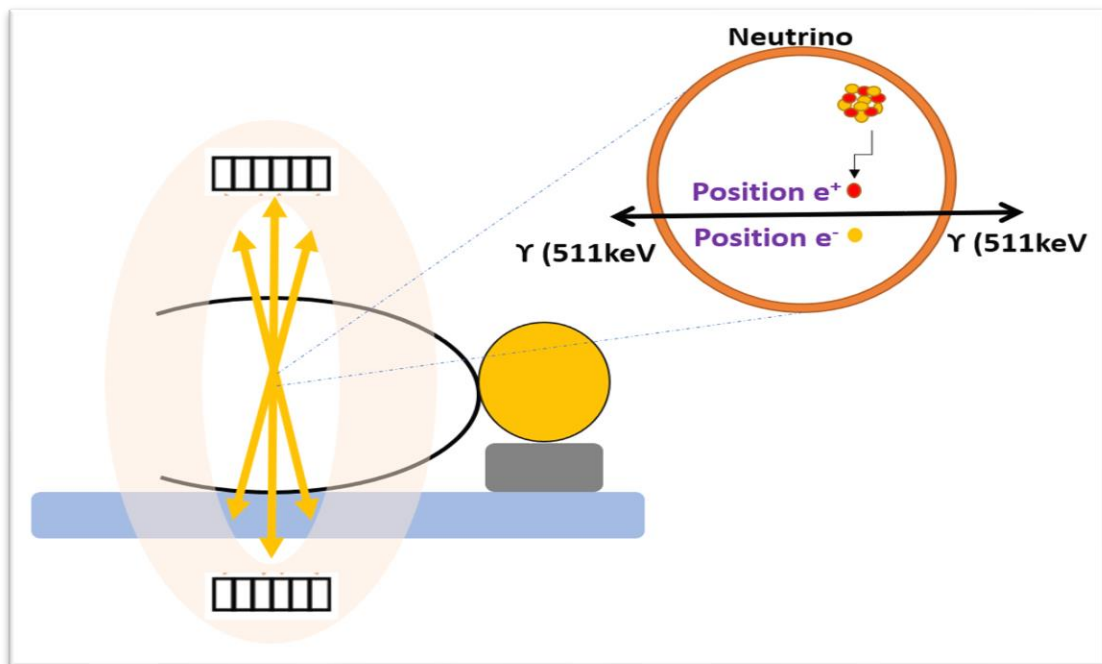
Figure 2.8: Detecting cancer using PET [121].

e) Ultra-wideband Techniques

Microwaves offer improved tumor detection without the danger of ionization effects on cells and tissues. Its radar imaging characterizes the power of waves to differentiate between normal and abnormal tissues as shown in Figure 2.9. Its pros are power efficiency and noise cancellation. As a result, this method is economical for real-time body imaging. The main features of UWB are as follows:

- High penetration
- High precision
- Less electromagnetic radiation
- Less processing energy consumed
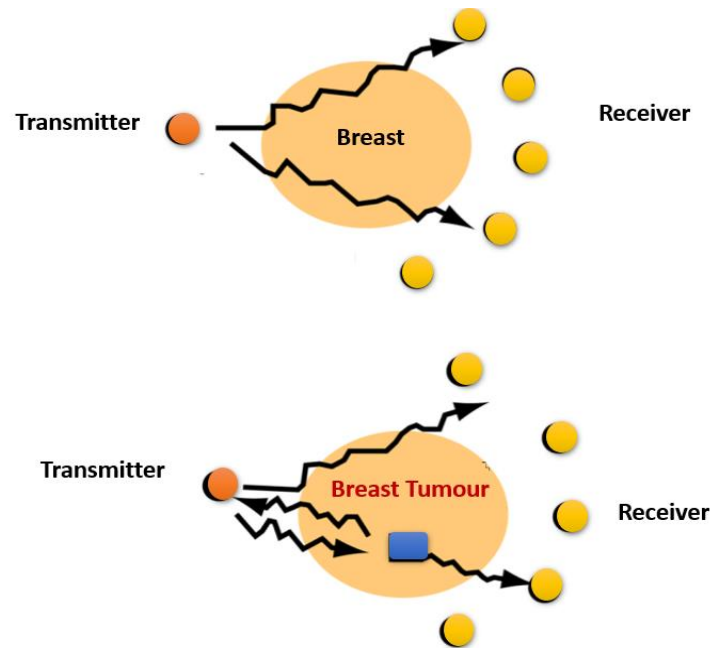
Figure 2.9: Detecting breast tumors using microwaves [122].

## 2.3 Urinalysis

### 2.3.1 Dipstick Test

This is the most basic method of the urinalysis which still has been used.



Figure 2.10: Dipstick analysis using testing sticks and comparison with standard markings.

The dipstick is a plastic stick with strips of various chemicals placed on it, which are used to detect abnormalities within a urine sample. The chemical pads vary in color to indicate the presence of substances such as blood, bilirubin, urobilinogen, ketone, protein, nitrite, glucose, leukocytes, pH level and specific gravity. Figure 2.10 shows dipstick analysis and comparisons with standard marking.

### 2.3.2 Matrix-assisted Laser Desorption Ionization–Time of Flight Mass Spectrometry (MALDI–TOF/MS)

It is an ionization process in which a matrix (saturated organic solution) is added to the sample (a microbial colony or blood, urine, cerebrospinal fluid, or protein extracts), after which the concoction is kept on a metallic plate. The matrix helps in ionization by providing protons to the sample. The sample and matrix crystallize on the metal plate and are targeted by the beam of a UV laser. The irradiation is brief to avoid variations in the sample caused by overheating. The contact between the photons of the laser and targeted molecules causes the matrix to change into gaseous form, followed by sample ionization. A schematic depiction of MALDI–TOF/MS analysis techniques for protein has been depicted in Figure 2.11 while for multiple samples in Figure 2.12.

In the case of the urine analysis for UTIs, before using MALDI–TOF/MS, the occurrence of bacteria or blood inside the urine sample has to be known, which can limit the usefulness of the urinary proteomic analysis [123]. A high bacterial concentration in the urine samples improves the likelihood of bacterial detection at the expense of not detecting the remaining proteome profile.

Various studies have shown that it is a good option for the direct recognition of any bacteria in urine samples. The reliability is suitable for specimens with bacterial

densities up to $10^3$ CFU/mL [124]. Studies have been performed to enhance the performance of the methodology and to eliminate leukocytes, proteins and many other components for the identification of urinary pathogens [125, 126]. This method avoids the requirement of urine culture in complex cases.

However, MALDI–TOF/MS cannot accurately classify assorted bacteria existing in urine samples [125, 127]. Moreover, no consistent procedure currently exists regarding the preprocessing of specimens.
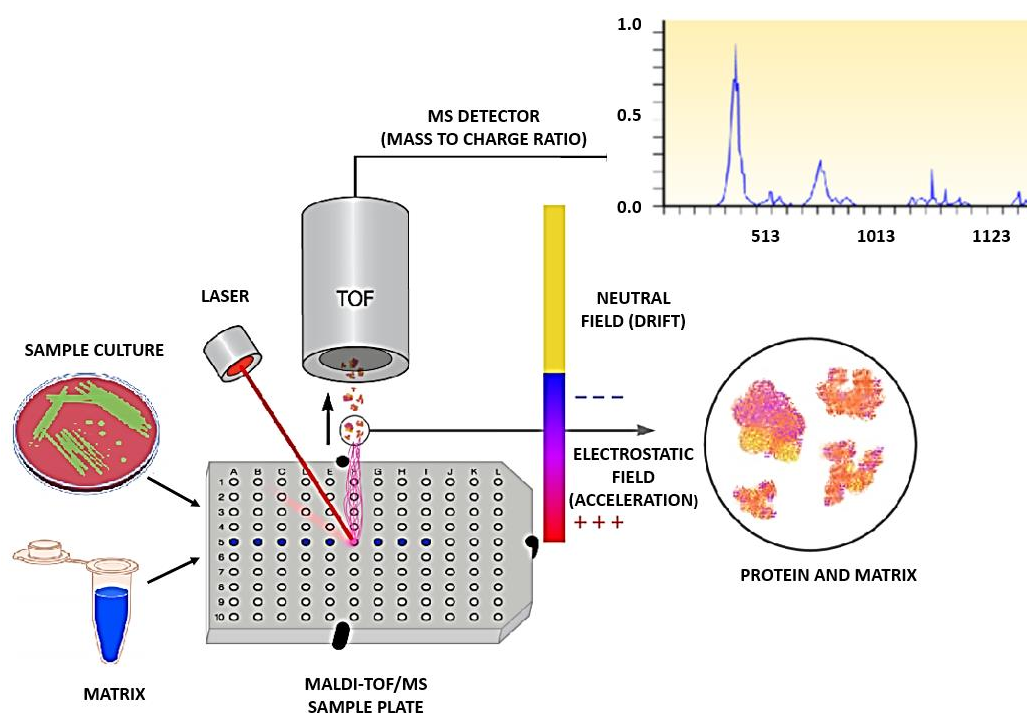


Figure 2.11: A schematic depiction of MALDI–TOF/MS analysis techniques for protein. Reprinted with permission from the American Society for Microbiology.
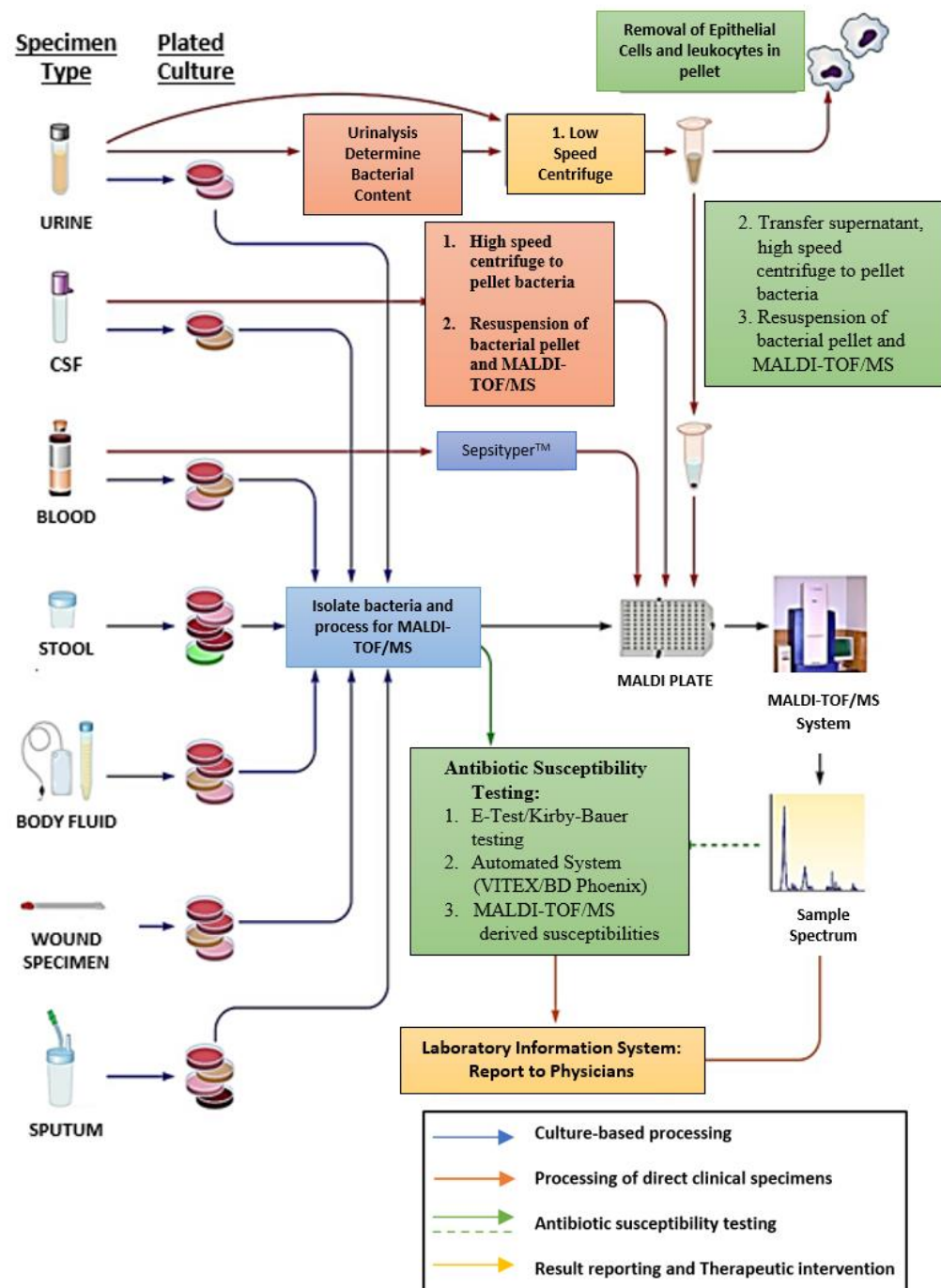
Figure 2.12: A schematic depiction of MALDI–TOF/MS analysis techniques with multiple sample types. Reprinted with permission from the American Society for Microbiology.

**2.4 Comparison of the Various Techniques**

In this section, comparisons of various available techniques for cell detection and their identification, has been discussed.

**2.4.1 Electric Field-based Techniques for Cell Manipulation**

For tissue engineering, various types of electric fields are used for cell manipulation, such as electrical, optical [128–131], ultrasound [132, 133] and magnetic [134, 135], which are undergoing advancements. The main methods are compared in Table A.1 [136] (mentioned in Appendix). Physical force field-based methods rely on low-conductivity buffers to be fully operative, as opposed to other methods that work directly in the growth medium. Methods based on an electric field lack spatial resolution, but only the electrode array size limits the number of cells that can be manipulated.

In contrast, the laser tweezer methods are fundamentally limited by their spatial resolution, and the number of manipulated cells is also very limited. Ultrasound-based methods are also subject to significant spatial resolution limitations. One of the main disadvantages of magnetic methods is that cells are not usually magnetizable. Hence, the cells are forced to take up paramagnetic materials. This alteration is not required by the other approaches.

**2.4.2 Characterization of Nanomaterials**

The preparation of nanomaterials requires approaches for their crystal structure, shape and size, chemical alignment, energy levels and dynamics of chemical and physical processes. Diverse methods for the study of these materials have been

discussed to evaluate their shortcomings at the nano-level, as shown in Table A.2-A.5 [137], mentioned in Appendix.

### 2.4.3 Cancer-detecting Methods and their Modalities

Cancer-detecting methods and their modalities are compared in Table A.6 (mentioned in Appendix), which indicates that despite their capability to find tumors, these methods still lack various capabilities. The erroneous result rates are quite significant. False-positive results lead to several unnecessary additional tests, while false-negative results miss tumors at the initial stage that could lead to cancer growing and spreading throughout the body. Sometimes the difference in the parameter of interest between the tumor and the adjacent tissue is very low, thereby leading to errors.

# Chapter 3: Fundamentals of the Electrical Properties of Cells

## 3.1 History

The electrical-based passive properties of cells were first scientifically investigated in the 1770s by Henry [138], who found that the current was directly proportional to the voltage and that salt mixtures showed greater conductivity than normal water. The famous relationship connecting the voltage, current, and resistance was given by Georg Ohm, who formulated the well-known Ohm's law [139]. In 1902, Bernstein [140] combined all of the relevant information about the cell membrane and articulated certain features. First, cells have an electrolyte enclosed by an impermeable membrane that allows the flow of ions. Second, a steady-state potential difference exists across the membrane. Third, the membrane allows potassium ion flow over a certain range of currents and voltages, known as the Nernst diffusion potential. Fourth, living tissue exhibits a relatively high dc resistivity.

Höber [141, 142] deduced that at different frequencies, the current path changes; he focused mainly on the current penetration into the conductive part of the cell at higher frequencies. He also developed the concept of $\beta$-dispersion, which describes the phenomenon that the outer membrane of the cell has a high resistivity for dc and (low-frequency) ac currents and has a very high capacity for collecting ions at its surface, which is known as Maxwell–Wagner interfacial polarization.

Various equivalent circuits have been proposed by many scientists. Figure 3.1(a) shows the equivalent circuit of RBCs developed by Philippson [143], where R and r are the resistances of the cytoplasm and membrane, respectively, while C is the capacitance of the membrane. As shown in Figure 3.1(b), Fricke and Morse proposed an equivalent

circuit of RBC suspensions, where $R_0$ is the resistance around the cell and $R_i$ is the resistance of the cytoplasm [144]. Cole and Baker discovered an inductive reactance within the membrane structure [145] and developed the equivalent circuit depicted in Figure 3.1(c). The resistance and capacitance of the cell can be measured by a parameter ($\phi$) that signifies the ratio of the actual area of the cell membrane to the area of the membrane ($4\pi r^2$) formed by smooth and spherical layers of the cytoplasm or nucleoplasm [146]. The calculated membrane capacitance ($C_m$) and membrane resistance ($R_m$) are:

$$C_m = \phi C_0 \tag{3.1}$$

$$R_m = \frac{1}{\phi} R_0 \tag{3.2}$$

where $C_o$ and $R_o$ are the values associated to $\phi=1$.



| (a) | (b) | (c) |
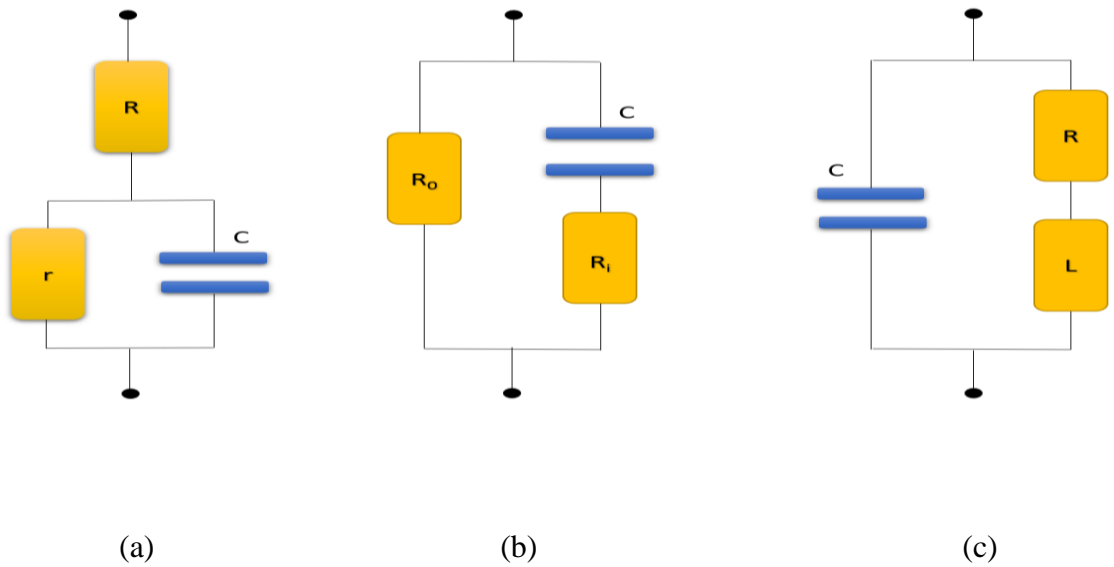
Figure 3.1: Equivalent circuits proposed by (a) Philippson, (b) Fricke and Morse, and (c) Cole and Baker.

**3.2 Electrical Properties of Cells**

There are various electrical properties related to biological cells that not only help in better understanding the characteristics of cells but also help acquire indications about the abnormalities within them. Some of the electrical properties are the dielectric dispersions (α, β, γ, and δ dispersions), polarization (electronic, atomic and orientation polarization), and relaxation (static and dynamic permittivity). These aspects are explained as follows:

**3.2.1 Dielectric Dispersions**

The dielectric properties of the cells at the cellular and molecular levels can be determined by the interaction of EM radiation. The relative permittivity ($\varepsilon_r$) can reach up to $10^6$ to $10^7$ below 100 Hz. The permittivity variation at high frequencies can be described via the so-called α, β, γ, and δ dispersions [147]. The dispersions indicate the dielectric relaxations that arise from the polarization mechanisms that occur in complex biological environments.
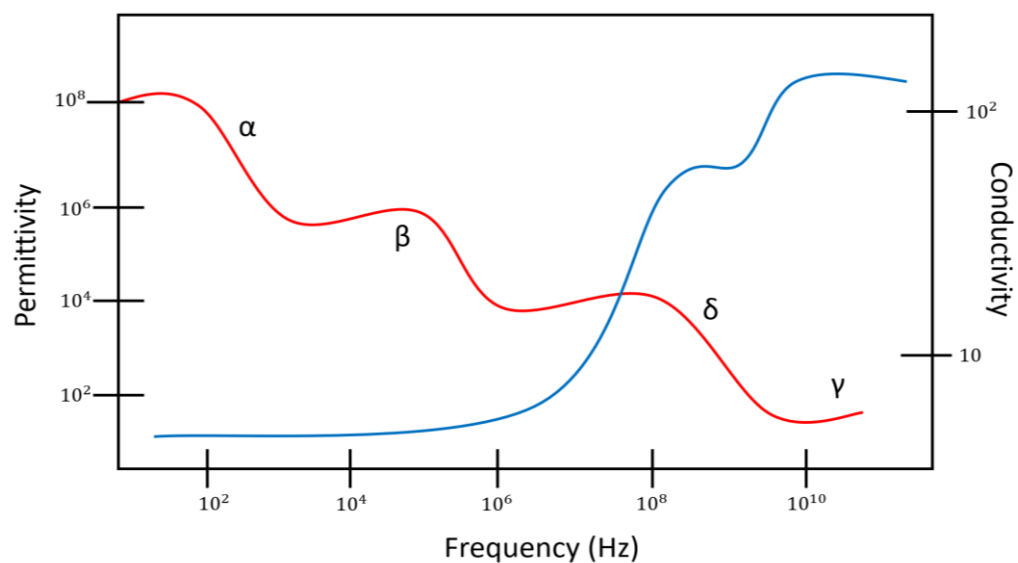


Figure 3.2: Permittivity and conductivity over the frequency spectrum.

The step changes in relative permittivity ($\varepsilon_r$) over the frequency spectrum are called dispersions and are often occurs because of the loss of certain type of polarization modes, as depicted in Figure 3.2. The α, β, γ, and δ dispersions consequently are described by the dielectric relaxation and frequency range and mainly by the total dielectric decrements, i.e., $\Delta\varepsilon_\alpha$, $\Delta\varepsilon_\beta$, $\Delta\varepsilon_\gamma$ and $\Delta\varepsilon_\delta$, respectively.

a) α-dispersion

α dispersion occurs in a low-frequency range, i.e., 10 Hz–10 kHz, while the relaxation time (τ) is 6 ms. This mode is categorized by a very high permittivity increment and very high dielectric decrement values ($\Delta\varepsilon_\alpha \approx 10^6$). This dispersion occurs near the cell membrane where the movements of charged particles are limited. The cell membrane is a complex structure consisting of phospholipids, cholesterol, proteins, and carbohydrates. There is a potential difference (approximately 60–70 mV) between the intracellular and extracellular media due to the ions which is distributed around the membrane (about 10 kV/mm). The phospholipids and cholesterol maintain the fluidity of the cell membrane whole proteins help in ion and signal transport. Penetration into the membrane is possible from the ion channels and membrane-spanning protein. However, the change in conductivity is about 5 mS/m for a $10^6$-permittivity increment, with a relaxation frequency of 100 Hz [148-150]. This shows that with a large permittivity increment, there is very small corresponding conductivity decrement.

b) β-dispersion

It arises within the frequency range of 10 kHz–10 MHz with a relaxation time of about approximately 300 ns. The cellular membranes and other intracellular bodies become charged (capacitive), leading to this dispersion type. The cell membranes are

electrically shorted, while the current can penetrate through the cytoplasm. This penetration decreases the impedance and leads to the β-dispersion or interfacial polarization or the Maxwell–Wagner relation. This effect occurs at the interface of membrane-electrolyte structures, which have two different dielectrics, leading to the formation of charges.

The polarization magnitude depends on the conductivity, permittivity, and structure of the distinct intracellular components. With increasing frequency, the number of resistive elements is nullified by their related parallel capacitances, making the intracellular structures more electrically similar. Usually, blood shows interfacial polarization at the 3 MHz frequency with a 50 ns relaxation time and $\Delta\varepsilon_\alpha \approx 2000$. This arises due to charging cell membranes through the electrically conductive cytoplasm cell. The effect is an extension of β-dispersion and hence is called β$_1$-dispersion [151]. Certain tissues have larger cell sizes and hence exhibit larger permittivity values than those of blood.

c) δ-dispersion

Some protein solutions exhibit δ-dispersion, which lies between the β and γ dispersions. If present, the effect falls in the range of 0.1 to 5 GHz, and comparatively, its magnitude is small. δ-dispersion was first categorized in a study by Pethig [152] and was credited to the dipolar moments of proteins and other large molecules such as biopolymers, cellular organelles [153] and protein-bound water [154]. The total water content of tissue consists of free water and the bound water. The bound water is rotationally hindered and has a relaxation frequency lower than that of the free water (approximately 50–150 times lower).

d) γ-dispersion

In 1989, Foster and Schwan discovered γ-dispersion [155], which occurs due to the presence of water content in the cells and tissues. The dielectric properties of cells and tissues at frequencies above 0.1 GHz depend on the intracellular electrolytes and water (dipole polarization). At frequencies above a few hundred megahertz, the complex permittivity can be decoupled into a Cole-Cole term and a conductivity term, corresponding to the dipolar dispersion of water and the electrolytic behavior, respectively, written as:

$$\varepsilon^{*}(\omega) = \varepsilon_{\infty} + \frac{(\varepsilon_{S} - \varepsilon_{\infty})}{1 + (j\omega\tau)^{(1-\alpha)}} + \frac{\sigma}{j\omega\varepsilon_{0}} \tag{3.3}$$

where σ is the conductivity from ionic currents and low-frequency polarization and α is the distribution parameter. γ-dispersion arises at microwave frequencies of approximately 25 GHz with a relaxation-time of approximately 6 ps and dielectric decrement of $\Delta\varepsilon_{\gamma} \approx 50$.

### 3.2.2 Polarization

Polarization is a process that occurs when a field E is employed on a dielectric material and the charges start moving within the structure. The amount of charge passing through a unit area within the dielectric, perpendicular to the direction of the applied field E, is called the polarization. The three types of polarization [156] are as follows:

a) Electronic Polarization ($P_e$): As the name suggests, electronic polarization occurs due to the displacement of electrons with respect to the atomic nucleons and occurs in

atoms in the dielectric material. The duration of the phenomenon is very small ($\sim 10^{-15}$ s), which corresponds to the period of ultraviolet light.

b) Atomic Polarization ($P_a$): Atomic polarization occurs due to the shifting of atoms or groups of atoms within the structure. The duration of the phenomenon corresponds to the period of infrared light.

c) Orientation Polarization ($P_o$): Orientation polarization arises from polar molecules. It occurs in dielectric materials because of the rotation of permanent dipoles. The orientation of molecular dipoles occurs in the path of the applied field and depends on the molecule size, viscosity, temperature, and applied field frequency. The duration of the phenomenon corresponds to the period of the microwave frequency region. Thus, the overall polarization ($P_t$) is:

$$P_t = P_e + P_a + P_o \tag{3.4}$$

Therefore, polar materials have a higher dielectric permittivity than nonpolar materials because of the presence of additional polarization due to orientation.

**3.2.3 Dielectric Relaxation**

The theories of dielectric relaxation are based on static permittivity and dynamic permittivity:

a) Static Permittivity: When a dielectric material has a constant dipole, the moment is placed in a steady electric field so that all types of polarization can maintain equilibrium. The permittivity under this condition is known as the static permittivity [157].

b) Dynamic Permittivity: With the change in the frequency of the applied field, the frequency-dependent permittivity of the dielectric material is called the dynamic permittivity [158].

### 3.2.3.1 Static Permittivity and Its Models

Different models are used to describe the static permittivity, some of which are described below:

a) Clausius–Mossotti Relation

The Clausius–Mossotti relation expresses the permittivity in terms of the atomic polarizability [159]. Under the influence of an electric field (F) acting on a molecule, the molecules possess an electric moment (m):

$$m = \alpha_0 F \tag{3.5}$$

where $\alpha_o$ is the polarizability of each molecule. The dipole moment may be permanent or induced. The average moment ($\bar{M}$) in the path of the field is the average dipole moment and the displacement of elastically bound charges [160]:

$$\bar{M} = \frac{\mu^2 \cos^2 \theta}{KT} F + e.r \tag{3.6}$$

The force F applies a unit positive charge bounded by a small sphere [161]. This force consists of three components: one related to the surface charge density ($\delta$) of the plates ($F_1$), one related to external surface polarization ($F_2$) and one related to molecules inside the small sphere ($F_3$).

$$F = F_1 + F_2 + F_3 \tag{3.7}$$

$$F_1 = 4\pi\delta \tag{3.8}$$

$F_2$ has been divided two parts, the first due to conducting plates and the second due to small spherical cavity.

$$F_2 = 4\pi P + \left(\frac{4\pi P}{3}\right) \tag{3.9}$$

where P is the polarization of the medium. A general expression for $F_3$ is used in special cases; in a cubic crystal, however, $F_3=0$. The total force F is:

$$F = 4\pi\delta - 4\pi P + \left(4\pi P / 3\right) \tag{3.10}$$

However, the dielectric displacement is $D = E + 4\pi P = 4\pi\delta$ :

$$F = E + 4\pi P - 4\pi P + \left(4\pi P / 3\right) \tag{3.11}$$

$$F = E + \left(4\pi P / 3\right) \tag{3.12}$$

Moreover, the dielectric displacement can be represented as:

$$D = \varepsilon E = E + \left(4\pi P\right) \tag{3.13}$$

$$E\left(1 - \varepsilon\right) = \left(4\pi P / 3\right) \tag{3.14}$$

$$\therefore F = E + E(1 - \varepsilon)/3 \tag{3.15}$$

$$F = E\frac{(\varepsilon + 2)}{3} \tag{3.16}$$

This relation expresses the coupling between the actual force and electric field from the electrostatic calculations [162]. Let $N_1$ is the number of molecules/cubic centimeter; then polarization is:

$$P = N_1 m = N_1 \alpha_0 F \tag{3.17}$$

$$P = N_1 \alpha_0 \left( \frac{\varepsilon + 2}{3} \right) \tag{3.18}$$

By using Equations (3.14) and (3.18), the link between the dielectric constant and molecular polarizability ($\alpha_o$) is obtained:

$$\frac{(\varepsilon - 1)}{(\varepsilon + 2)} = \frac{4\pi}{3} N_1 \alpha_0 \tag{3.19}$$

In pure substances, $N_1 = N_d / M$, where M is the molecular weight, d is the density and N is the number of molecules per mole.

$$\frac{(\varepsilon - 1)}{(\varepsilon + 2)} \frac{M}{d} = \frac{4\pi}{3} N \alpha_0 \tag{3.20}$$

This relation is known as the Clausius–Mossotti equation [159, 160]. The RHS of Equation (3.20) shows the molar polarization (p), which describes the electric properties of the molecule as follows:

$$p = \frac{4\pi}{3} N \alpha_0 \tag{3.21}$$

Using Equations (3.20) and (3.21),

$$p = \frac{(\varepsilon - 1)}{(\varepsilon + 2)} \frac{M}{d} \tag{3.22}$$

The permittivity depends on the amount of polarization, which is a function of the frequency of the applied field. At increasingly elevated frequencies, there is less polarization, and therefore, the permittivity value decreases with increasing frequency.

b) Debye Theory of Static Permittivity

To derive the relation for static permittivity, the field at a single molecule is considered by imagining a spherical surface of molecular dimension in the dielectric medium. Assume that the medium inside the sphere is composed of individual molecules and that outside the sphere lies a medium of homogeneous permittivity. The field at the center of the sphere can be divided into three parts: first, the external charges and applied field; second, the surface polarization charges; and third, the field due to the sphere material.

Debye's theory depends on the suppositions that no neighboring forces act on the dipoles and that the field component due to molecules inside the spherical region is zero. With these assumptions, the equation given by Debye is:

$$\frac{\varepsilon_0 - 1}{\varepsilon_0 + 2} = \frac{4\pi N_1 \left( \alpha + \frac{\mu^2}{3KT} \right)}{3\varepsilon} \tag{3.23}$$

where $N_1$ is the number of molecules per unit volume, $\alpha$ is the polarizability ($\alpha = \alpha_{electronic} + \alpha_{atomic}$), $\mu$ is the dipole moment, $K$ is the Boltzmann constant, $\varepsilon_0$ is the static permittivity, and $\varepsilon$ is the permittivity of free space. If the material has molecular weight

M and density p, then $N_1 = N_P / M$, where N is Avogadro's number. Therefore, Equation (3.23) can be written as

$$\frac{\varepsilon_0 - 1}{\varepsilon_0 + 2} \times \frac{M}{p} = \frac{4\pi N\left(\alpha + \dfrac{\mu^2}{3KT}\right)}{3\varepsilon} \tag{3.24}$$

In this expression, $\dfrac{\varepsilon_0 - 1}{\varepsilon_0 + 2} \times \dfrac{M}{p}$ is called the molar polarization.

The following inferences have been obtained from Debye's theory [163]. First, for non-polar substances, the polarizability must be constant and unaffected by the temperature and pressure. The density is directly proportional to the permittivity. Second, in the case of polar materials, the dipolar polarization decreases due to thermal agitation. Third, below a certain temperature (T), the polarization becomes quite large, which makes the molecules align themselves even without the field.

$$T = \frac{4\pi N\rho\mu}{9MK\varepsilon} \tag{3.25}$$

Some limitations in Equation (3.23) arise because of assumptions made to derive the Debye relation. As the validity of the equation is restricted to fluids due to first assumptions, it is not applicable to crystal materials. According to the Debye relation and Equation (3.25), liquids act as ferroelectric materials at T < T$_c$ (where the molar polarizability tends to $M / p$ at $\varepsilon_0 \to \infty$), but ferroelectricity is quite uncommon. This failure of the Debye equation is due to the statement that the medium force inside the sphere is zero which is invalid.

c) Kirkwood Theory

Kirkwood considered a material specimen with N dipoles, each having moment $\mu$, within a sphere of volume V inside a uniform external field. Using this assumption, Kirkwood developed an equation for non-polarizable dipoles:

$$\frac{(\varepsilon-1)(2\varepsilon+1)}{3\varepsilon}\frac{M}{d} = 4\pi N_A \frac{g\mu^2}{3KT} \tag{3.26}$$

where g is a correlation parameter. Further, Kirkwood incorporated distortion polarization by attaching the polarizability ($\alpha$) of each dipole. Thus, Kirkwood's equation is written as:

$$\frac{(\varepsilon-1)(2\varepsilon+1)}{3\varepsilon}\frac{M}{d} = 4\pi N_A \left[\alpha + \frac{g\mu^2}{3KT}\right] \tag{3.27}$$

d) Cole Theory

Cole [162] proposed a theory similar to Kirkwood's for the static permittivity which differs in the behavior of the direction of polarization. He obtained the expression for static permittivity as follows:

$$\frac{(\varepsilon_0-1)}{(\varepsilon_0+2)} = \frac{(n^2-1)}{(n^2+2)} + \frac{4\pi N}{3v\varepsilon} \times \frac{3\varepsilon_0(n^2+2)}{(\varepsilon_0+2)(2\varepsilon_0+n^2)} \times \frac{g\mu^2}{3KT} \tag{3.28}$$

which reduces to:

$$\frac{\varepsilon_0 - n^2(2\varepsilon_0+n^2)}{\varepsilon_0(n^2+2^2)} = \frac{4\pi N}{3v\varepsilon} \times \frac{g\mu^2}{3KT} \tag{3.29}$$

### 3.2.3.2 Dynamic Permittivity and its Models

Various models are used to describe the permittivity in terms of frequency. Some of the most widely used models are described below.

a) The Debye Model

Debye [163] gave a model for complex permittivity and dielectric loss by the equation:

$$\varepsilon^* = \varepsilon_\infty + \frac{\varepsilon_0 - \varepsilon_\infty}{1 + j\omega\tau} \qquad (3.30)$$

where $\varepsilon^* = \varepsilon' - j\varepsilon''$ is the complex permittivity, $\varepsilon'$ is known as the dielectric dispersion, $\varepsilon''$ is known as the dielectric loss, $\varepsilon_0$ is the static permittivity and $\varepsilon_\infty$ is the permittivity at infinite frequency. $\omega$ is the angular frequency and $\tau$ is the relaxation time. The physical significance of these equations is that at the frequency for which $\omega\tau \ll 1$, i.e., below the absorption curve, equilibrium occurs in a short time compared with that for which the field points in one direction. In this case, the maximum value of permittivity is obtained, and little energy is absorbed. When the frequency approaches that for which $\omega\tau = 1$, the field reverses over a time which makes the polarization to reach its maximum value. Thus, the energy absorbed per cycle is maximized. At frequencies for which $\omega\tau \gg 1$, there is no significant orientation of dipoles in each cycle, and the measured $\omega\tau \gg 1$ permittivity does not contain a contribution from this polarization. The dielectric loss approaches zero for small and large values of frequencies, while it is maximum for $\omega\tau = 1$, i.e., $\varepsilon''_{max} = \left( \left( \varepsilon_0 - n^2 \right) / 2 \right)$ at a frequency $\omega = 1/\tau$, and this parameter falls to half its maximum when $\omega\tau = \left( \left( 1 + \omega^2\tau^2 \right) / 4 \right)$. Another way to represent the experimental result is to construct a diagram by plotting $\varepsilon''$ against $\varepsilon'$ at the same frequency. The above equations for $\varepsilon'$ and $\varepsilon''$ are parametric equations of a circle. Upon reducing and reordering, below result has been obtained:

$$\left(\varepsilon^{'}-\frac{\varepsilon_0+\varepsilon_\infty}{2}\right)^2+\varepsilon^{''}=\left(\frac{\varepsilon_0-\varepsilon_\infty}{2}\right)^2 \tag{3.31}$$

which is the equation of a circle with center $\left[\dfrac{\varepsilon_0+\varepsilon_\infty}{2},0\right]$ and radius $\dfrac{\varepsilon_0-\varepsilon_\infty}{2}$. Thus,

by plotting ε" against ε', a semicircle is obtained, as shown in Figure 3.3(a), called the

Debye semicircle.
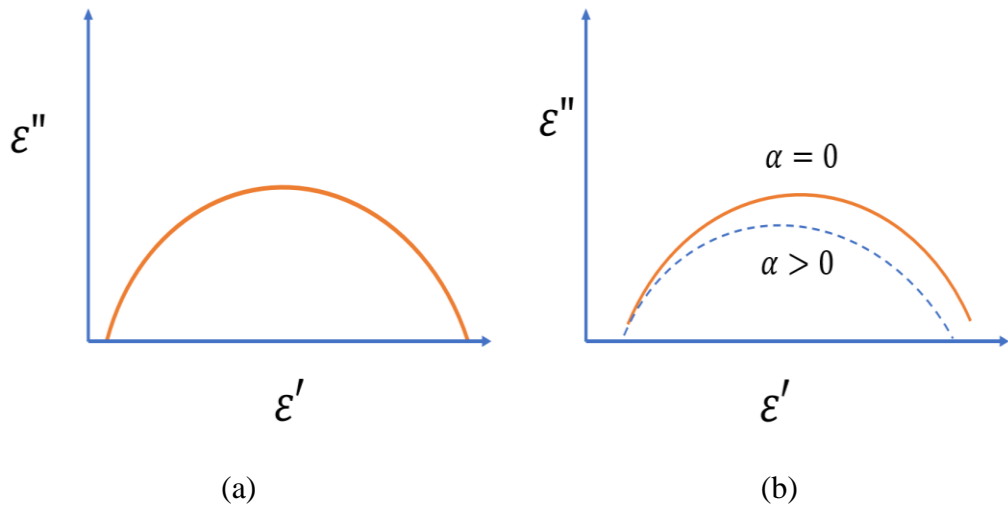


Figure 3.3: Illustration of (a) the Debye semicircle and (b) a Cole-Cole plot.

b) The Cole-Cole Model

It describes the experimental observations of many materials with particularly long-chain molecules and polymers, which show a broader dispersion curve and the maximum loss at lower frequency than would be expected from the Debye relationship. According to Cole and Cole [162], in such cases, the permittivity might follow the empirical equation:

$$\varepsilon^{*}=\varepsilon_\infty+\frac{\varepsilon_0-\varepsilon_\infty}{1+j\omega\tau^{1-\alpha}} \tag{3.32}$$

where $0 \leq \alpha < 1$. When α = 0, the above equation reduces to the Debye equation, as shown in Figure 3.3(b). The plotted curve of ε" vs ε' obeys the following equation of a circle:

$$\left[\frac{1}{2}\varepsilon_0 + n^2 - \varepsilon'\right]^2 + \left[\varepsilon'' + \frac{1}{2}\varepsilon_0 - n^2 \tan\left(\frac{\pi\alpha}{2}\right)\right]^2 \tag{3.33}$$

$$\frac{1}{4}\left(\varepsilon_0 - n^2\right)\sec^2\left(\frac{\pi\alpha}{2}\right) \tag{3.34}$$

with its center at:

$$\left\{\frac{1}{2}\varepsilon_0 + n^2, -\frac{1}{2}\varepsilon_0 - n^2 \tan\left(\frac{n\alpha}{2}\right)\right\} \tag{3.35}$$

The radius is:

$$\frac{1}{2}\left(\varepsilon_0 - n^2\right)\sec\left(\frac{n\alpha}{2}\right) \tag{3.36}$$

## 3.3 Theoretical Modeling: Maxwell's Mixture Theory

The dielectric properties of biological cells that are suspended in media are usually defined by Maxwell's mixture theory [164]. In the frequency domain, this theory gives an equivalent complex dielectric permittivity of the cells ($\tilde{\varepsilon}_{cell}$) at a low volume fraction:

$$\tilde{\varepsilon}_{mix} = \tilde{\varepsilon}_m \frac{1 + 2\varphi\tilde{f}_{cm}}{1 - \varphi\tilde{f}_{cm}} \tag{3.37}$$

where $\tilde{f}_{cm} = \dfrac{\tilde{\varepsilon}_p - \tilde{\varepsilon}_m}{\tilde{\varepsilon}_p + 2\tilde{\varepsilon}_m}$ (the Clausius–Mossotti factor)

where mix represents the mixture, p represents the particle, m represents the membrane, $\tilde{\varepsilon}$ is the complex permittivity, $\varepsilon$ is the permittivity, $\sigma$ is the conductivity, $\omega$ is the angular frequency, $\varphi$ is the volume fraction of the cells in the suspension, and complex permittivity can be represented as:

$$\tilde{\varepsilon} = \varepsilon - j\frac{\sigma}{\omega} \tag{3.38}$$

However, Maxwell's mixture theory is effective only for low volume fractions, such as φ < 10%. Later, Hanai and Koizumi [165, 166] extended the theory for all volume fractions, depicted below:

$$1 - \varphi = \left(\frac{\tilde{\varepsilon}_{mix} - \tilde{\varepsilon}_p}{\tilde{\varepsilon}_m - \tilde{\varepsilon}_p}\right)\left(\frac{\tilde{\varepsilon}_m}{\tilde{\varepsilon}_{mix}}\right)^{1/3} \tag{3.39}$$

For the one-shelled model, as depicted in Figure 3.4(a), the complex permittivity of the biological cell is given by [164]:

$$\tilde{\varepsilon}_p = \tilde{\varepsilon}_{mem} \frac{\gamma^3 + 2\left(\dfrac{\tilde{\varepsilon}_i - \tilde{\varepsilon}_{mem}}{\tilde{\varepsilon}_i + 2\tilde{\varepsilon}_{mem}}\right)}{\gamma^3 - \left(\dfrac{\tilde{\varepsilon}_i - \tilde{\varepsilon}_{mem}}{\tilde{\varepsilon}_i + 2\tilde{\varepsilon}_{mem}}\right)} \tag{3.40}$$

where $\gamma = \dfrac{R+d}{R}$, $\tilde{\varepsilon}_{mem}$ is the complex permittivity, $\tilde{\varepsilon}_i$ is cytoplasm permittivity, R is cell radius and d is the membrane width. Thus, $\tilde{\varepsilon}_{cell}$ depends on the cell size, membrane dielectric properties, and internal properties, which are related predominantly to the cytoplasm. The complex bio-impedance ($\tilde{Z}_{mix}$) of cells in suspension is given by [164]:

$$\tilde{Z}_{mix} = \frac{1}{j\omega\tilde{\varepsilon}_{mix}G} \tag{3.41}$$

where G is a geometric constant ($G = A/g$), A = electrode area and g = gap between

the electrodes.



(a)                                                (b)
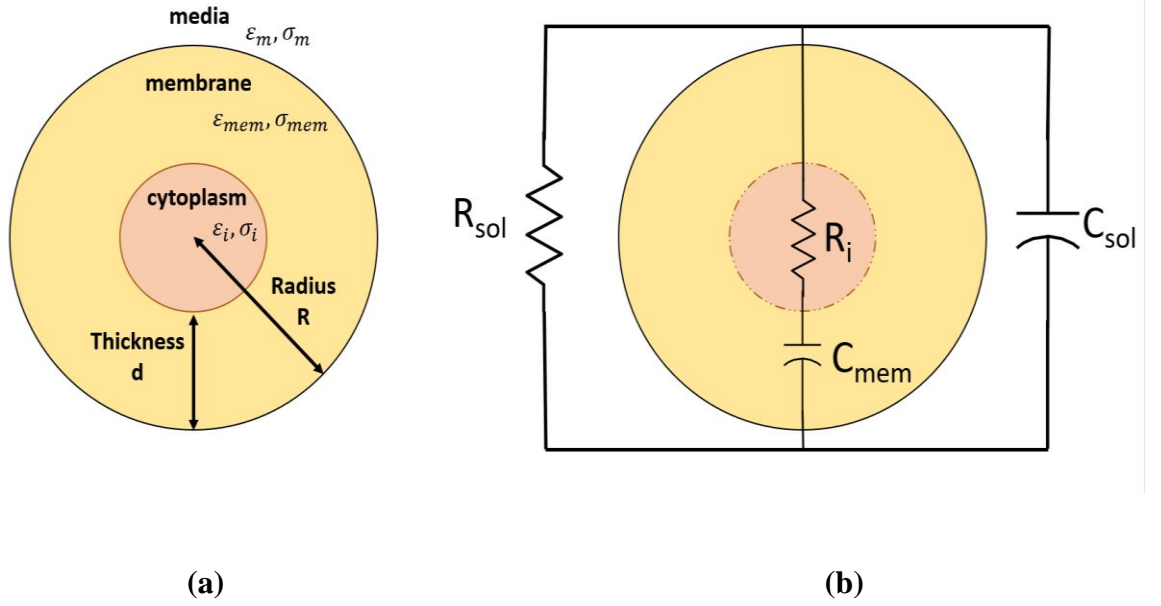
Figure 3.4: Schematic of the (a) one-shell model of a cell; (b) equivalent circuit model of a cell in suspension by Foster and Schwan [155].

### 3.3.1 The Equivalent Electrical Model of a Single Cell

Although analysis of the equivalent circuit model is generally quite intricate, the membrane conductivity and the cytoplasm permittivity are usually low [166-167]. Simplified expressions are as follows:

$$\tilde{\varepsilon}_i = -j\sigma_i / \omega \tag{3.42}$$

$$\tilde{\varepsilon}_{mem} = \varepsilon \tag{3.43}$$

where $\sigma_i$ is the cytoplasm conductivity and $\varepsilon_{mem}$ is the membrane permittivity.

Inserting the above expressions into Equation (3.40) and simplifying,

$$\tilde{\varepsilon}_p = \varepsilon \frac{\gamma^3 + 2\left(\dfrac{-j\sigma_i/\omega - \varepsilon}{2\varepsilon - j\sigma_i/\omega}\right)}{\gamma^3 - \left(\dfrac{-j\sigma_i/\omega - \varepsilon}{2\varepsilon - j\sigma_i/\omega}\right)} \tag{3.44}$$

$$\frac{\mathrm{Re}\left[\tilde{\varepsilon}_p\right] + j\,\mathrm{Im}\left[\tilde{\varepsilon}_p\right]}{\varepsilon} = \left(\frac{2b\varepsilon^2 + a(\sigma_i/\omega)^2}{b^2\varepsilon^2 + (\sigma_i/\omega)^2}\right) + j\left(\frac{\varepsilon\sigma_i/\omega(2-ab)}{b^2\varepsilon^2 + (\sigma_i/\omega)^2}\right) \tag{3.45}$$

$$\text{where } a = \left(\frac{\gamma^3 + 2}{\gamma^3 - 1}\right) \quad b = \left(\frac{2\gamma^3 + 1}{\gamma^3 - 1}\right) \tag{3.46}$$

By dividing the real and imaginary parts of $\tilde{\varepsilon}_p$ in Equation (3.45):

$$\frac{a}{\omega}\left(\frac{\sigma_i}{\varepsilon}\right)^2 - K(2-ab)\left(\frac{\sigma_i}{\varepsilon}\right) + 2b\omega = 0 \tag{3.47}$$

$$\text{where } K = \left(\frac{\mathrm{Re}\left[\tilde{\varepsilon}_p\right]}{\mathrm{Im}\left[\tilde{\varepsilon}_p\right]}\right) \tag{3.48}$$

Assuming $\dfrac{\sigma_i}{\varepsilon} = 1$ and calculating the imaginary part of Equation (3.45), $\varepsilon_{cell}$ is:

$$\varepsilon = \left(\frac{b^2 + \left(1/\omega^2\right)}{(1/\omega)(2-ab)}\right)\mathrm{Im}\left[\tilde{\varepsilon}_p\right] \tag{3.49}$$

The total impedance of suspension comprises the impedance of medium and its cells. As described in [155], one cell is equivalent to a cytoplasmic resistance ($R_i$) in series with a membrane capacitance ($C_{mem}$), as manifested in Figure 3.4(b).

$$C_{mem}(\omega) = \frac{9\varphi \, \mathrm{R} \, \varepsilon}{4d} G \qquad (3.50)$$

$$R_i(\omega) = \frac{4\left(\dfrac{1}{2\sigma_m} + \dfrac{1}{\sigma_i}\right)}{9\varphi G} \qquad (3.51)$$

## 3.4 Modeling of Dielectric Properties of Cells

Maxwell noted that to calculate the resistivity of composite matter, the resistivities of all particles of the medium should be counted together [168-169]. Later, this model was extended by Wagner [171], who demarcated the elements of such materials in terms of the complex conductivities. Some of them are mentioned below.

## 3.4.1 Permittivity of Cells in Dilute Suspensions

Consider a field E employed on a fluidic medium (with permittivity $\varepsilon_m$) comprising suspension of cells, each cell with radius $R_c$ and permittivity $\varepsilon_c$. Inside a sphere of mixture with radius $R_m$ that comprises n number of cells, then the potential at a distance r from the center of the spherical region is [170]:

$$\phi_1 = \left(\frac{nA}{r^2} - Br\right) E \cos\theta \qquad (3.52)$$

$$\text{where} \quad A = \left(\frac{\varepsilon_c - \varepsilon_m}{\varepsilon_c + 2\varepsilon_m}\right) R_c^3 \qquad (3.53)$$

The volume ($v_c$) fraction of suspended cells is:

$$v_c = \frac{nR_c^3}{R_m^3} \qquad (3.54)$$

Inserting Equations (3.53) and (3.54) into (3.52) yields:

$$\phi_1 = \left( v_c R_m^2 \frac{\varepsilon_c - \varepsilon_m}{\varepsilon_c + 2\varepsilon_m} \frac{1}{r^2} - Br \right) E \cos\theta \tag{3.55}$$

Now consider another similar sphere where the permittivity of the cells enclosed inside is homogeneous, with effective permittivity ($\varepsilon_{eff}$). Thus, the new potential is as follows:

$$\phi_2 = \left( R_m^3 \frac{\varepsilon_{eff} - \varepsilon_m}{\varepsilon_{eff} + 2\varepsilon_m} \frac{1}{r^2} - Br \right) E \cos\theta \tag{3.56}$$

If both spheres have the same dielectric properties, then:

$$\left( \frac{\varepsilon_{eff} - \varepsilon_m}{\varepsilon_{eff} + 2\varepsilon_m} \right) = v_c \left( \frac{\varepsilon_c - \varepsilon_m}{\varepsilon_c + 2\varepsilon_m} \right) \tag{3.57}$$

### 3.4.2 Effective Medium Theory

### 3.4.2.1 Mixture Equations by the Maxwell–Wagner Relation

Equations describing the permittivity and conductivity of cells in a mixture are called mixture equations. The measured permittivity value in a dielectric measurement of a cell mixture is $\varepsilon_{eff}$. To study the conduction effects in terms of the complex permittivity, in Equation (3.57), replace $\varepsilon_{eff}$ and $\varepsilon_m$ by $\varepsilon_{eff}^*$ and $\varepsilon_m^*$, respectively.

$$\left( \frac{\varepsilon_{eff}^* - \varepsilon_m^*}{\varepsilon_{eff}^* + 2\varepsilon_m^*} \right) = v_c \left( \frac{\varepsilon_c^* - \varepsilon_m^*}{\varepsilon_c^* + 2\varepsilon_m^*} \right) \tag{3.58}$$

Upon rearranging Equation (3.58), the effective complex permittivity of the fluid medium $\varepsilon_m^*$ in the spherical volume is given in terms of the complex permittivity of the suspended cells $\varepsilon_c^*$:

$$\varepsilon_{eff}^{*} = \frac{2\varepsilon_{m}^{*} + \varepsilon_{c}^{*} + 2v_{c}(\varepsilon_{c}^{*} - \varepsilon_{m}^{*})}{2\varepsilon_{m}^{*} + \varepsilon_{c}^{*} - v_{c}(\varepsilon_{c}^{*} - \varepsilon_{m}^{*})}\varepsilon_{m}^{*} \qquad (3.59)$$

The expression of complex permittivity and conductivity is as follows [170]:

$$\sigma^{*} = i\omega\varepsilon_{0}\varepsilon^{*} \qquad (3.60)$$

The above expression Equation (3.60) leads to the same relation $\varepsilon_{eff}^{*}$ as that defined by Wagner [171]. Equation (3.59) describes the average permittivity of the cells in the suspension. Assume that $\varepsilon_{eff}^{*}$ and $\varepsilon_{m}^{*}$ are approximately equal, then a heterogeneous mixture behaves as a homogeneous one. Using this fact, in Equation (3.61):

$$\varepsilon_{eff}^{*} = \varepsilon_{m}^{*}\left(1 + 3v_{c}\frac{\varepsilon_{c}^{*} - \varepsilon_{m}^{*}}{\varepsilon_{c}^{*} + 2\varepsilon_{m}^{*}}\right) \qquad (3.61)$$

This equation is called the Maxwell–Wagner equation, which states that if $v_{c}$ increases from zero, then the suspension permittivity rises linearly with the rise in cell concentration. To obtain the effective mixture equations, segregate the real and imaginary terms of Equation (3.61). The relationships of $\varepsilon_{eff}'$ and $\sigma_{eff}'$ appear as follows:

$$\varepsilon_{eff}' = \varepsilon_{\infty}' + \frac{\varepsilon_{s}' - \varepsilon_{\infty}'}{1 + i\omega\tau} \qquad (3.62)$$

$$\sigma_{eff}' = \sigma_{\infty}' + \frac{\sigma_{s}' - \sigma_{\infty}'}{1 + i\omega\tau} \qquad (3.63)$$

$$\text{with } \tau = \varepsilon_{0}\frac{\varepsilon_{c}' + 2\varepsilon_{m}'}{\sigma_{c}' + 2\sigma_{m}'} \qquad (3.64)$$

$$\left(\varepsilon_s^{'}-\varepsilon_\infty^{'}\right)=\Delta\varepsilon_{eff}^{'}=9v_c\frac{\left(\varepsilon_c^{'}\sigma_m^{'}-\varepsilon_m^{'}\sigma_m^{'}\right)^2}{\left(\varepsilon_c^{'}+2\varepsilon_m^{'}\right)\left(\sigma_c^{'}+2\sigma_m^{'}\right)^2} \quad (3.65)$$

$$\left(\sigma_\infty^{'}-\sigma_s^{'}\right)=\Delta\sigma_{eff}^{'}=\frac{1}{\tau}\Delta\varepsilon_{eff}^{'} \quad (3.66)$$

The foundation of effective medium theory is the approximation that states that heterogeneous and homogeneous materials are considered equal for a large observation scale.

### 3.4.2.2 Mixture Equations by Hanai

Hanai [172] extended the Maxwell–Wagner equation for highly concentrated suspensions, which involves gradually increasing the volume fraction $v_c$ in increments $\Delta v_c$, which increases the mixture permittivity from $\varepsilon_{mix}^{*}\rightarrow\varepsilon_{mix}^{*}+\Delta\varepsilon_{mix}^{*}$. The new volume fraction is $\frac{\Delta\widehat{v}_c}{1-\widehat{v}_c}$, while $\varepsilon_m^{*}$ changes to $\varepsilon_{mix}^{*}$. Insert these substitutions into the Maxwell–Wagner Equation (3.59):

$$\Delta\varepsilon_{mix}^{*}\simeq\frac{3\varepsilon_{mix}^{*}\Delta\widehat{v}_c(\varepsilon_c^{*}-\varepsilon_{mix}^{*})}{(1-\widehat{v}_c)(\varepsilon_c^{*}+2\varepsilon_{mix}^{*})} \quad (3.67)$$

Integrate the above equation with limits from 0 to $v_c$ and $\varepsilon_m^{*}$ to $\varepsilon_{mix}^{*}$. The following relationship arises:

$$(1-\widehat{v}_c)=\frac{(\varepsilon_{mix}^{*}-\varepsilon_c^{*})}{(\varepsilon_m^{*}-\varepsilon_c^{*})}\left(\frac{\varepsilon_m^{*}}{\varepsilon_{mix}^{*}}\right)^{1/3} \quad (3.68)$$

This is called the Hanai mixture equation, and this relationship is typically used to analyze dielectric measurements performed with cell suspensions.

### 3.4.3 Modeling of a Cell

Cell modeling can be performed on two bases: the single-shell model of the cell and the two-shell model of the cell which denotes by the number of membranes. Figure 3.5 shows both types of cell structure modeling. The basic model of the spherical cell does not contain a nucleus or internal organelles. The volume fraction is given by $v_c = (R_1/R_2)^3$ and the following relationship is derived:

$$\varepsilon_{cell}^* = \frac{\left(2\varepsilon_{mem}^* + \varepsilon_{cyt}^*\right)R_2^3 + 2\left(\varepsilon_{cyt}^* - \varepsilon_{mem}^*\right)R_1^3}{\left(2\varepsilon_{mem}^* + \varepsilon_{cyt}^*\right)R_2^3 - \left(\varepsilon_{cyt}^* - \varepsilon_{mem}^*\right)R_1^3}\varepsilon_{mem}^* \tag{3.69}$$

where the cell radius is $R_2$ and the membrane width d is given by $d = R_2 - R_1$.
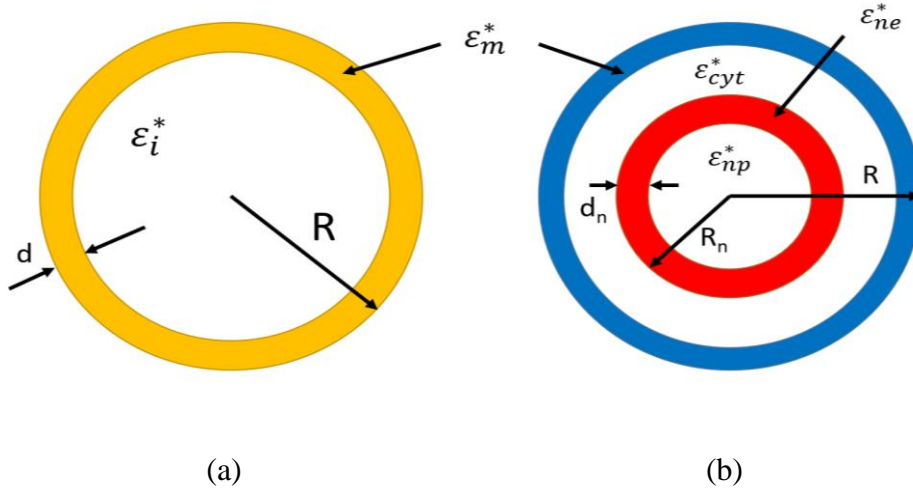


Figure 3.5: Illustration of (a) the one-shell model of a shell. (b) two-shell model. The subscripts for the complex permittivity designate the plasma membrane (m), inner phase of the cell (i), cytoplasm (cyt), nuclear envelope (ne), and nucleoplasm (np).
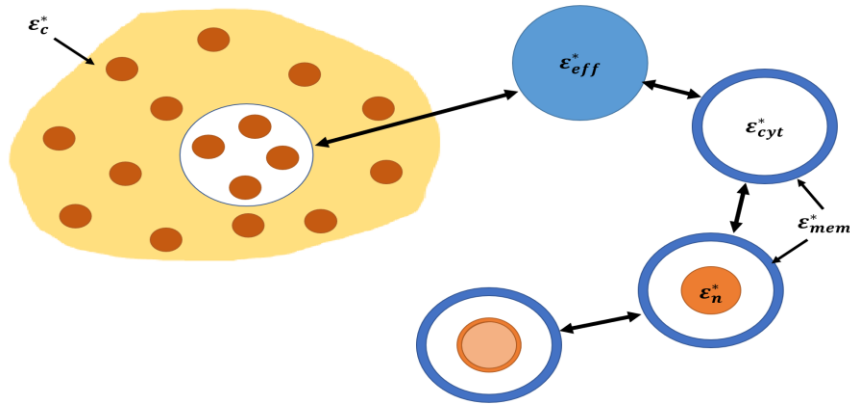
Figure 3.6: A schematic depicting how to derive the effective complex permittivity of a cell in suspension.

It is inferred that the single-shell model has limitations in describing the dielectric properties of the cells completely, as cells contain many organelles itself have membranes [173]. The single-shell model considers only the plasma membrane for a cell without including the nucleus, whereas the double-layer model includes the nuclear envelope of homogeneous membrane [173, 174]. Figure 3.6 schematizes the extraction of the effective complex permittivity via Equations (3.59) and (3.69).

**3.5 Chapter Summary**

This chapter deals with the various electrical properties related to biological cells. Some of the electrical properties have been discussed, such as the dielectric dispersions, which include the α, β, γ, and δ dispersions; polarization and its types, such as electronic, atomic and orientation polarization; relaxation with related theories and modeling of the static and dynamic permittivity. Maxwell's mixture theory has been explained along with the modeling of the dielectric properties of cells. The modeling of cells includes the permittivity of dilute suspensions of cells and the effective medium theory of Maxwell and Hanai.

## Chapter 4: Electrical Detection of Blood Cells in Urine

Available methods for detecting blood in urine (hematuria) can be problematic since the results can be influenced by many factors of patients and in the lab setting, resulting in false positive or false negative results. This issue necessitates the development of new, accurate and easy-access methods that save time and effort. This study demonstrates a label-free and accurate method for detecting the presence of red and white blood cells (RBCs and WBCs) in urine by measuring the changes in the dielectric properties of urine with increasing concentration of both cell types.

The current method can detect changes in the electrical properties of fresh urine over a short time interval, making this method suitable for detecting changes that cannot be recognized by conventional methods. Correcting for these changes enables the detection of a minimum cell concentration of $10^2$ RBCs per ml, which is not possible with the conventional methods used in the lab except for the semi-quantitative method that can detect 50 RBCs per ml; however, this method involves a lengthy and complicated procedure that is not suitable for high-volume labs. The ability to detect a very small number of both types of cells makes the proposed technique an attractive tool for detecting hematuria, the presence of which is indicative of problems in the excretory system.

### 4.1 Hematuria

The kidney is a vital organ in the human body with excretory, endocrine and metabolic functions [175]. Any abnormalities in or damage to the kidneys can lead to serious complications and can be lethal [176]. Chronic kidney disease (CKD) is a term used to describe kidney damage characterized by abnormal and increased levels of albumin

secretion in urine (albuminuria) or decreased kidney function that lasts for more than three months [177]. Renal functions are evaluated by estimated glomerular filtration rate (eGFR), which is compared to a standardized criterion that aids in determining the severity of CKD and thus in stratifying patients. This determination allows for better medical interventions and treatments associated with complications, avoiding possible progression to end-stage disease.

The urine of a healthy individual should be clear, with no or very few cells [178]. Observation of an increased number of cells in urine can be indicative of a serious problem that requires intervention. Hematuria or the existence of RBCs in urine is an abnormal condition that might indicate serious kidney problems or can be a sign of progression to CKD, if not managed. Thus, accurate detection of hematuria can be of high prognostic value, in addition to being important for diagnosis.

A patient is considered to have hematuria if the number of RBCs is more than five per high-powered field (HPF) in microscopy [179]. Under other criteria, even three or more cells per HPF are considered an abnormal finding, and this finding should be observed in at least two of the sediments of three collected urine samples [180]. Hematuria is described as gross/macroscopic when the color of blood is visible to the naked eye or as microscopic when the RBCs are few. Microscopic hematuria is only detectable by dipsticks or microscopic urinalysis. The two types of hematuria have different etiologies, but in some cases, they share common causes. In gross hematuria, the urine color can range from pink to red to brown depending on the source of the blood. Light colored blood usually comes from the lower urinary tract (non-glomerular), while dark colored blood is of glomerular origin.

The two types of hematuria can be caused by various conditions, such as trauma, nephrolithiasis, post infectious glomerulonephritis, and immunoglobulin A (IgA) nephropathy. Gross hematuria is also caused by urinary tract infections, perineal and ureteral irritations, congenital anomalies, anatomic abnormalities (e.g., tumor), acute nephritis, and coagulopathy. Microscopic hematuria, in contrast, can occur in some diseases, such as familial hematuria, sickle cell anemia, alport syndrome nephritis and henoch-schönlein purpura [181]. Glomerular hematuria is more critical since it implies damage to the nephrons that filter the blood that passes through them. The leakage of RBCs into the urinary space during glomerular hematuria indicates defects in the glomerular basement membrane. These defects can result from abnormalities in the structure or composition of the basement membrane in some diseases, leading to notches and membrane rupture [182]. Similarly, inflammation or glomerulonephritis can also lead to glomerular membrane weakening and leakage as a result of leukocyte infiltration into the basement membrane, in addition to the production of reactive oxygen species such as $H_2O_2$ [179, 183] and proteinases, which damage and degrade the components of the membrane, respectively [184].

Interestingly, hematuria not only is a sign of kidney damage but also can itself lead to kidney damage, such as hemoglobinuria-induced tubular injury [185]. The presence of metabolites released by RBCs in the lumen of nephron tubules can initiate a cascade of intracellular reactions, leading to the generation of reactive oxygen species [186] and consequently lipid peroxidation [187], caspase activation, and eventually programmed cell death (apoptosis) [188]. Taken together, these results indicate that hematuria can act as a diagnostic factor for the presence of renal ailments and can, at the same time, act as a prognostic marker for CKD. Notably, gross hematuria is more

frequent at the early stages of the disease, while microhematuria is associated with worse renal outcomes and a higher incidence of patients with end-stage renal disease (ESRD).

All of these results suggest that detecting microscopic hematuria is critical to predicting and recognizing patients at high risk of developing CKD, which enables healthcare professionals to take proactive measures to stop the initial stages of CKD from progressing to ESRD [189, 190]. In the following section, the discussion of different methods to assess hematuria has been done. This discussion will be followed by the presentation of a new approach for investigating the dielectric properties of urine samples with blood cells as a new, real-time, noninvasive method that can be of great use in the clinical setting.

### 4.1.1 Methods Used for Testing Hematuria

Dipstick urinalysis is an old standard for testing the presence of blood cells. A blood sample with hematuria generates a greenish-blue color, which results from the oxidation of a chromogenic substrate, tetramethylbenzidine, by the peroxidase activity of hemoglobin [187]. Different companies use different chromogenic substrates for this purpose. A dipstick is believed to detect as low as 2-5 RBCs/HPF, which is equivalent to 10 RBCs per µl. However, this method has some pitfalls, such as false positive results in certain cases like hemoglobinuria and myoglobinuria, which have different etiologies from hematuria, in which the urine does not contain any blood cells [191, 192]. The positive results in these conditions do not result from the presence of RBCs but rather from the pigments released from lysed blood cells or from muscle damage, respectively. Dipsticks can also give false positive results when bacterial peroxidases are released into urine because of infection or because of contamination

of urine with oxidizing agents used in cleaning solutions or with menstrual blood in women. Additionally, the urine of patients taking vitamin C supplements might generate false negative results [192]. The presence of RBCs in urine can also be confirmed by a microscopic examination of the sediment of spun urine under an HPF, what is known as microscopic urinalysis and the count is usually described as RBCs/HPF [192]. This approach is the conventional method but concerns regarding RBC loss as a result of cells sticking to the walls of the tube during centrifugation or during decanting of the supernatant remain. To avoid these artifacts, some researchers favor counting the cells in uncentrifuged urine using a Coulter counter [193]. A cytological semiquantitative method was shown to be more accurate than both the conventional and dipstick methods.

In this method, the sediment of urine is spread over many slides, fixed and stained, and then, cells are counted under a microscope. This method was able to detect blood cells at concentrations of less than 50 RBCs per ml, while the minimum concentration detected by the conventional method was 500 RBCs per ml. Surprisingly, dipsticks from different companies could detect minimum concentrations ranging from $2\times10^4$ to $1\times10^6$ RBCs per ml, which is much larger than the number claimed by companies [194]. Dipsticks are attractive for the initial screening of urine samples since they can detect several abnormalities in urine, in addition to being inexpensive, fast and easy to use. One study showed that the use of a dipstick is very reliable since further microscopic analysis of the same tested samples did not change the treatment decisions that were based on the dipstick results [195]. Regarding the detection of hematuria, dipsticks were found to be more accurate and consistent compared to flow cytometry

and microscopic analysis when used under unstandardized conditions (hyperhydration) [196].

Usually, a positive result for a dipstick is followed by a microscopic examination to confirm hematuria, which consumes a considerable amount of time. A false negative result is even worse and can result in misdiagnosis, which can be dangerous to patient health. More developed and sophisticated methods for urine analysis involve the use of automated analyzers. Different analyzers can have different analytical principles and might require different sample preparations. Some of these analyzers are based on flow cytometry, where fresh urine samples are used to determine the particle size and complexity by light scattering and additional sample staining can give more information about DNA [197]. Other analyzers are based on image analysis in which urine sediment is analyzed by obtaining particle images using integrated cameras, which are analyzed using predefined libraries [198, 199].

Although these automated methods can save time in high-volume labs, they still require the presence of well-trained professional technicians who need to accept or reject the results or reclassify them, especially for image-based methods. Moreover, one cannot ignore the costly charges of instrument maintenance [199], which has always been a motivation factor in finding newer, less expensive methods that allow accurate and instant results, thus saving time in addition to minimizing maintenance charges. This study investigates the use of the electrical properties of urine to detect both RBCs and white blood cells (WBCs) in urine, which can be cost effective and save time compared to previous methods.

## 4.2 The Current Approach
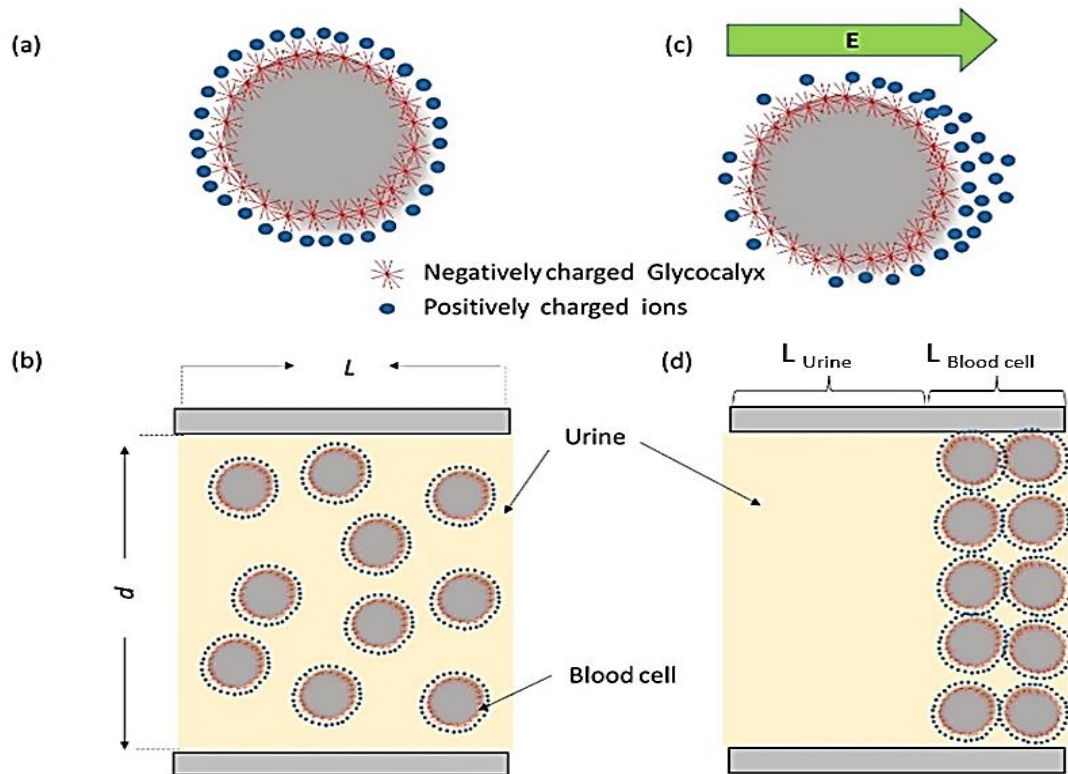


Figure 4.1: Illustration of cell with a negatively charged glycocalyx (a) blood cell with a negatively charged glycocalyx coated by positively charged ions in urine. (b) the random distribution of blood cells in a suspending medium (urine). L is the length of the total capacitor; d is the distance between the two electrodes of the capacitor. (c) Diagram showing how the surface-bound charged ions diffuse under the effect of an applied electric field, leading to cell polarization. (d) An alternative two-zone parallel capacitance model of the cell distribution inside a capacitive structure. $L_{Urine}$ and $L_{Blood}$ cell are the lengths of the capacitor zones occupied by the medium (urine) and blood cells, respectively.

Suspensions of biological cells are known to interact with an applied electric field by experiencing different levels of polarization; therefore, such suspensions can be treated as a dielectric material that affects the capacitance, which can be measured by a capacitor. The nonhomogeneous nature of cells arises from their complex composition; cells comprise proteins, carbohydrates, nucleic acids and lipids in addition to other minor constituents such as ions and vitamins. Cells tend to become

polarized when subjected to an electric field. The strength of the polarization depends on the composition and how cells interact with the suspending medium [200]. A cell suspension exhibits a unique response to an electric field since its response is frequency dependent with at least three incremental losses or dispersions, known as α, β and γ dispersions [201].

Figure 4.1(b) illustrates how cells suspended in urine are randomly distributed inside a capacitor. When a cell is placed under the effect of an applied electric field, it becomes polarized, and one type of polarization results from the diffusion of the charged ions present at the cell surface, resulting in a large dipole (see Figure 4.1(c)). For simplicity and modeling, the cell distribution inside a capacitive structure is assumed to consist of two separate zones, and a parallel model is shown in Figure 4.1(d). The volumes of the cell and medium zones are the same as their respective actual volumes in the suspension in both the parallel and series representations.

## 4.3 Materials and Methods

### 4.3.1 Collection of Urine Samples

A fresh, early morning urine (EMU) sample (30-50 ml) was collected in a sterile urine container with no additional preservatives.

### 4.3.2 Separation of RBCs and WBCs

Whole blood (5-10 ml) collected in an EDTA vacutainer was centrifuged at 377xg for 10 minutes at 4°C. Blood separates into three components: plasma (top), buffy coat (middle) and RBCs (bottom). The top plasma layer was carefully removed and discarded without disturbing the buffy coat. The buffy coat containing the WBCs was carefully transferred to a fresh 50-ml falcon tube using a Pasteur pipette. To remove

the contaminating RBCs in the buffy coat fraction, 10 ml of RBC lysis buffer (2 mM Tris HCl, 5 mM $MgCl_2$, pH 7.5) was added to the buffy coat and mixed so that the RBCs were lysed while maintaining the WBCs intact. The WBCs were pelleted at 672xg for 20 minutes at 4°C. The RBC lysis step was carried out twice to completely remove the RBCs. The WBCs were then suspended in 10 ml of Dulbecco's Modified Eagles Medium (DMEM, HyClone) and counted using a hemocytometer to prepare the required dilutions. Meanwhile, the bottom RBC-containing layer was transferred to a fresh 50-ml falcon tube and washed twice with 5 ml of PBS, suspended in 10 ml of DMEM, and counted using a hemocytometer to prepare the required dilutions.

### 4.3.3 Preparation of Dilutions

The purified RBC and WBC suspensions were separately prepared using fresh urine. The dilutions initially prepared were $10^6$, $10^4$, $10^2$, and $10^1$ cells/ml in DMEM for RBCs and WBCs. Immediately before being loaded into the coaxial adaptor for electrical characterization, the cell suspension in DMEM was centrifuged at 1,050xg for one minute. The supernatant was carefully separated and resuspended in 1 ml of fresh urine. The sample was then used for electrical characterization. After electrical characterization, the same sample was collected in a micro centrifuge tube and centrifuged at 1,050xg for one minute. The supernatant was carefully separated and loaded into coaxial cable for electrical characterization.

### 4.3.4 Electrical Measurements

The electric measurements were conducted by loading 500 µl of each cell suspension in urine or urine alone into an open-ended coaxial cable connected to Gamry 3000 equipment (USA). The instrument can measure current from 3 amps to 300 picoamps

over a range of frequencies from 100 MHz to 100 kHz. The instrument can record

different types of electrical measurements, such as capacitance-voltage (CV) profiles.

Due to the frequency and current ranges used, the device can measure capacitance with

a high precision (up to zeptofarad). Figure 4.2 illustrates the experimental setup used

and the electrical modeling and electric circuit for blood cells in urine.
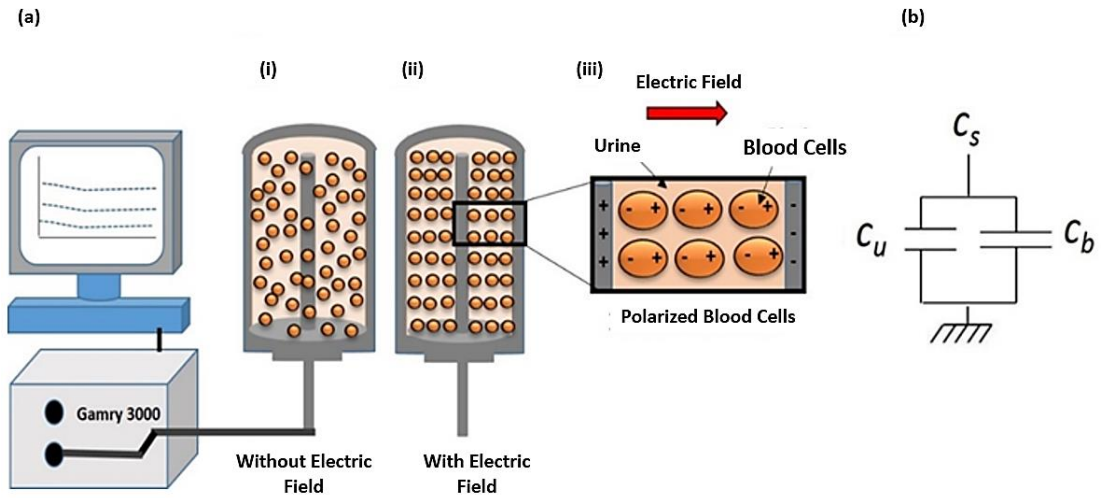


Figure 4.2: Illustration of the electrical modelling of blood cells suspended in urine. (a) Panel (i) demonstrates the random distribution of blood cells before the application of a DC bias, panel (ii) shows the distribution of blood cells after the application of a DC bias, and panel (iii) depicts how cells act as dipoles when exposed to an electrical field. (b) Depiction of the corresponding equivalent circuit model, where $C_S$ is the suspension (blood cells and urine) capacitance, $C_U$ is the urine capacitance, and $C_b$ is the capacitance of the blood cells.

## 4.4 Results

Figure 4.3 (a) displays capacitance curves measured over a range of frequencies (1-$10^5$ Hz) for urine samples spiked with increasing concentrations of RBCs ($10^2$ to $10^6$

cells/ml). The electrical measurements were made by loading the cell suspensions in

urine into the coaxial adaptor of the Gamry instrument, followed by recording their

electrical potential. In general, the capacitance curves displayed a smooth pattern, with the highest values occurring at low frequencies. A gradual decrease in capacitance occurred as the frequency applied to the capacitor increased.

The capacitance-frequency (CF) curve for urine alone (sample P0 in Figure 4.3 (a)), which acted as a control sample, was below the rest of the curves, indicating a low capacitance potential of urine. Unexpectedly, the capacitance values for urine/blood suspensions were inversely proportional to the RBC concentration; the sample with the highest number of cells ($10^6$) generated the lowest curve, while the curves shifted to higher values with decreasing concentration of blood cells (Figure 4.3 (a)). Figure 4.3 (b) displays curves of suspensions where the urine samples were spiked with increasing concentrations of WBCs. Similar to the pattern observed with RBCs, urine samples spiked with the highest concentrations of WBCs resulted in the lowest capacitance; thus, the capacitance was inversely proportional to the concentration of cells in urine.
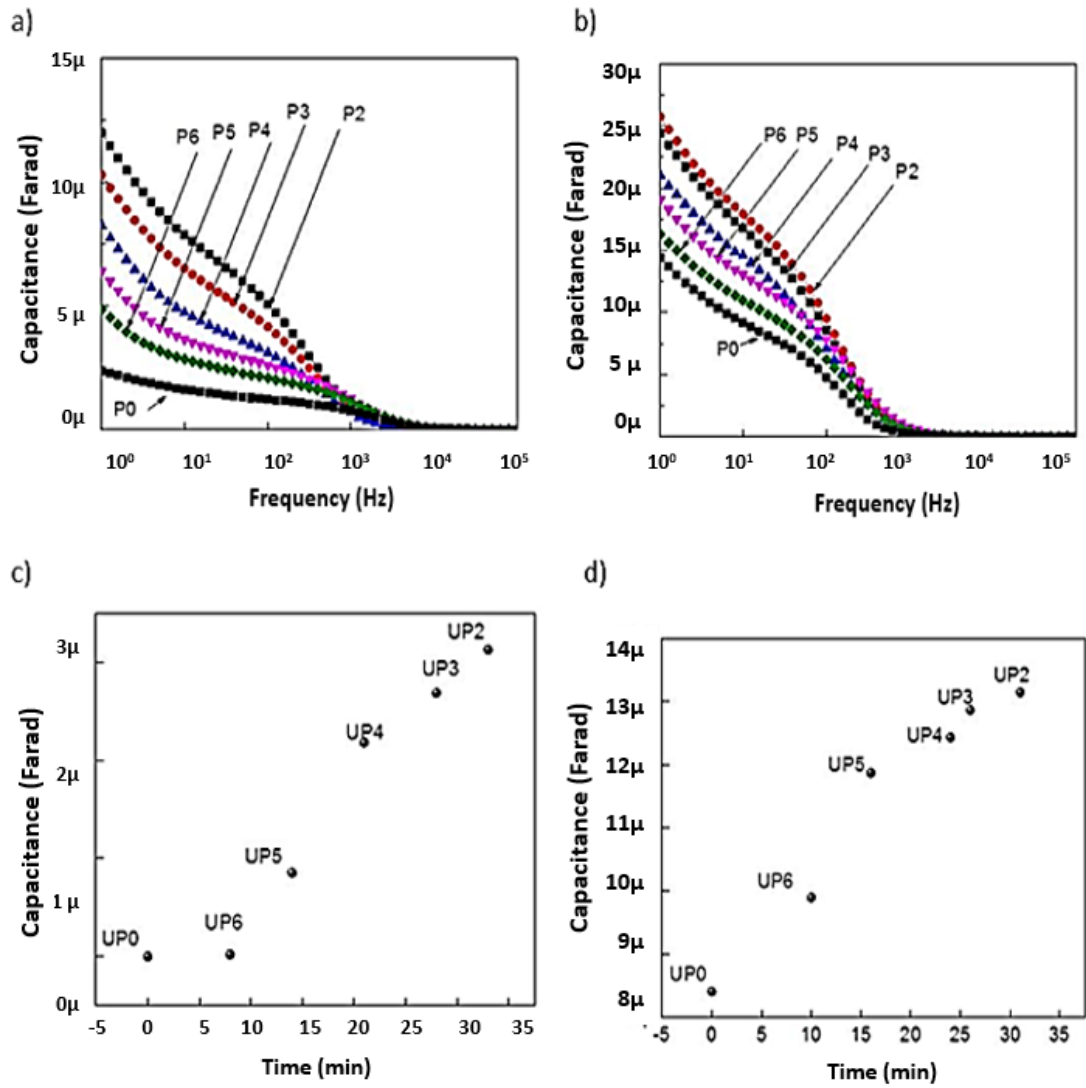
Figure 4.3: Dielectric properties of urine and cell suspensions measured over a range of frequencies. (a) Capacitance versus frequency profile for increasing concentrations of RBCs) and (b) WBCs in urine. The curves labeled P0, P2, P3, P4, P5, and P6 correspond to concentrations of 0, $10^2$, $10^3$, $10^4$, $10^5$ and $10^6$ cells/ml, respectively. (c) Time-dependent changes in the capacitance of the fresh urine sample devoid of cells used for RBC and (d) WBC suspensions. The changes in capacitance versus time were measured at 1 Hz. UP0, UP2, UP3, UP, UP5, and UP6 are urine samples measured electrically at the times shown in the figures, which were exactly the times at which different suspensions were freshly mixed and measured.
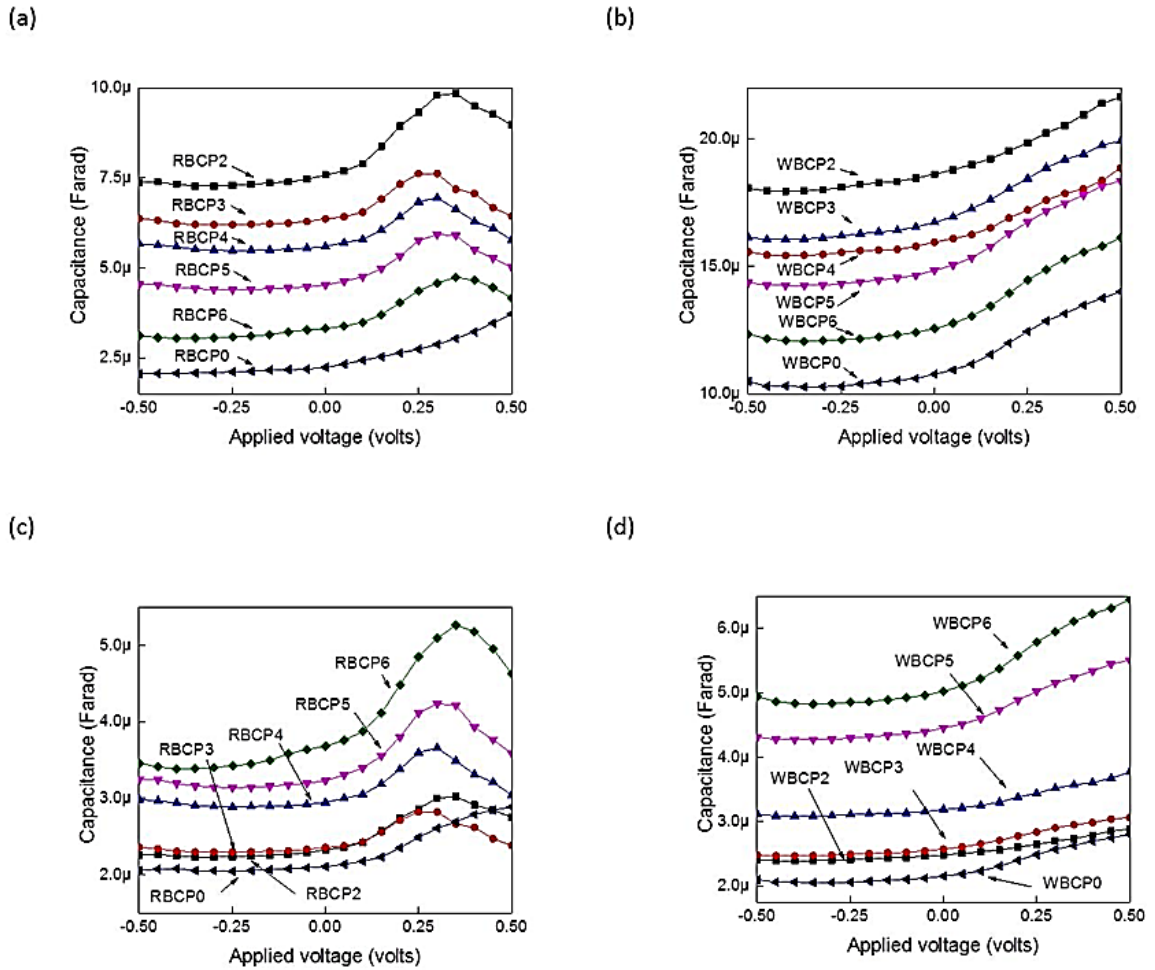
Figure 4.4: Capacitance-voltage (CV) profiles of urine samples containing increasing concentrations of RBCs and WBCs. (a) CV profile of the control urine sample and urine samples spiked with increasing concentrations of red blood cells (RBCs). Samples RBCP0, RBCP2, RBCP3, RBCP4, RBC5 and RBC6 had cell concentrations of 0, $10^2$, $10^3$, $10^4$, $10^5$ and $10^6$ cells/ml, respectively. (b) CV profile of urine only and urine samples with increasing concentrations of white blood cells (WBCs). Samples WBCP0, WBCP2, WBCP3, WBCP4, WBC5 and WBC6 had cell concentrations of 0, $10^2$, $10^3$, $10^4$, $10^5$ and $10^6$ cells/ml, respectively. (c) CV values of each suspension recalculated by de-embedding the capacitance of urine "alone" obtained by centrifuging the supernatant and measuring its capacitance after each suspension capacitance measurement from the capacitance of the RBC suspension. (d) Similarly, recalculated WBC suspension CV values as in (c) after de-embedding the values of urine alone.

Figures 4.3 (c) and (d) display the variations in the capacitance of the sample (fresh urine) used to make the cell suspensions over time. This figure was obtained by

repeatedly measuring the urine capacitance at the time points at which each suspension of RBCs or WBCs was made. In general, the capacitance for urine samples in both sets of experiments displayed a stable increase with time (measured over 35 minutes), as shown in Figures 4.3 (c) and (d), revealing that urine (the control sample) alone undergoes dynamic changes that can affect its electrical parameters, leading to a gradual increase in capacitance with time.

Figure 4.4 (a) displays capacitance curves measured over a range of voltages (-0.5 to +0.5 V) for urine samples containing increasing concentrations of RBCs. As with the CF profiles, the CV curve for the urine only sample (as a control) was below all the other curves, showing less capacitance potential for urine, while the capacitance values for the rest of the samples were inversely proportional to the concentration of cells in the samples.

A similar pattern was observed for urine samples containing increasing concentrations of WBCs (Figure 4.4 (b)), as shown in Figure 4.3 (b). To determine if the inverse relationship observed with increasing cell concentration was due to the instability observed with urine alone, the CV values observed for the cell suspensions were corrected for those of urine alone. Figures 4.4 (c) and (d) show corrected versions of the CV curves displayed in Figures 4.4 (a) and (b), respectively, after de-embedding the capacitance of the control urine sample from the suspension capacitance. Briefly, each cell suspension was reconstituted just before the measurement was performed. After the measurement, the sample was centrifuged, and the supernatant representing the fresh urine status at this time was subjected to electrical measurements.

The capacitance values of each supernatant urine sample were deducted from those of the corresponding cell suspension. By performing this step, the capacitance values

were corrected for any artifacts that might have arisen from any possible changes occurring in the urine over time. The curves plotted after the correction step revealed a more logical pattern, where spiking more cells into urine led to a stepwise increase in the capacitance potential of urine. These data also revealed that 100 cells/ml could easily be distinguished from urine alone for both cell types across most of the range of frequencies tested (Figures 4.4 (c) and (d)).
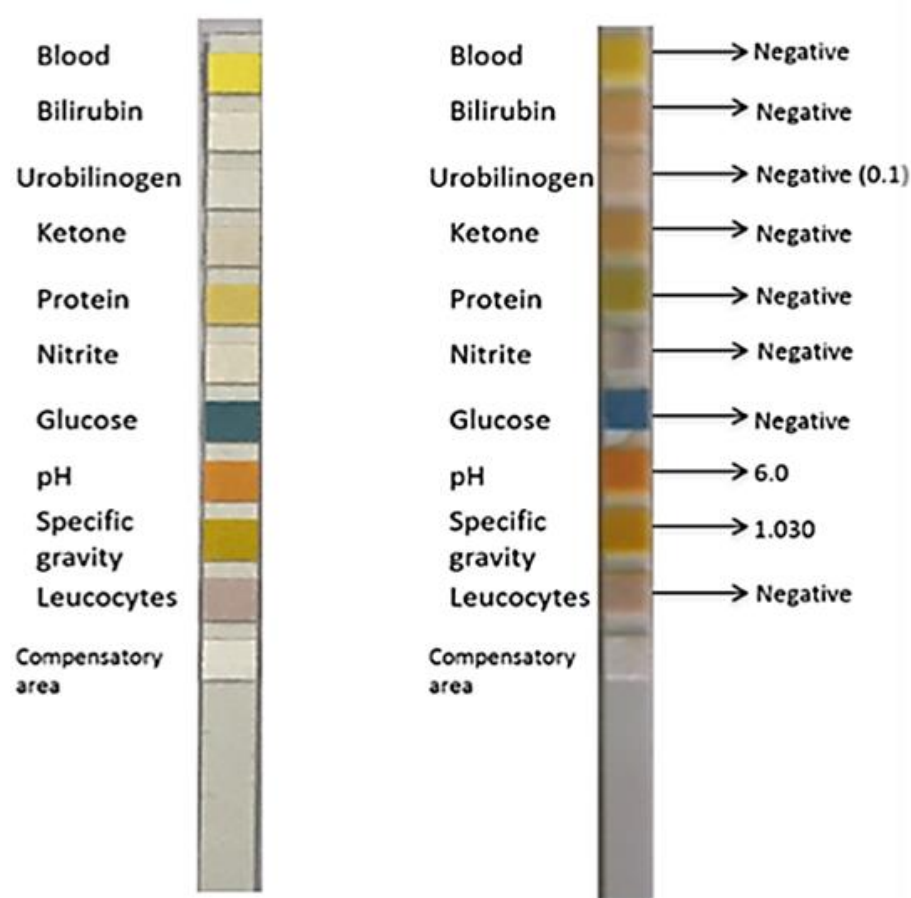


Figure 4.5: Dipstick analysis of fresh urine containing one million cells/ml. The image on the left shows the urine strip dipped in fresh urine without any cells, while the image on the right shows the strip dipped in urine with 106 cells/ml.

Next, the limit of detection of this electrical technique has been compared with that of the current method of choice for hematuria, the "urine dipstick" method. To this end, the red blood cell suspension in urine with the highest concentration of cells, $10^6$ RBCs/ml, was tested by a dipstick. Surprisingly, the dipstick revealed a normal urine status with no indication of the presence of RBCs, although dipsticks are claimed to be sensitive, with the ability to detect from $2\times10^4$ to $1\times10^6$ cells/ml, as shown in Figure 4.5. In contrast, proposed method could detect RBC concentrations with nearly 10,000-fold fewer cells/ml (as low as 100 cells/ml).

Next, the capacitance values in Figures 4.4 (c) and (d) were used to extract the dielectric constants for cell suspensions over a range of voltages, and these values were normalized by calculating the ratio between the dielectric constant of each suspension and the dielectric constant of the urine control sample measured at the very beginning of the measurement. The normalized values of the dielectric constants were plotted for both types of cell suspensions, as shown in Figures 4.6 (a) and (b). Calibration curves were generated by plotting the ratios calculated at -0.25 V (the middle of the negative voltage range) for each concentration of cells, as shown in Figure 4.6 (c). Figure 4.6(c) presents the change in the dielectric constant of the suspension versus the concentration of both cell types.

Figure 4.6 (d) was used to examine quantity of cells in urine by extracting the corresponding dielectric constant from the measured suspension capacitance. For a high cell concentration, Figure 4.6 (d) reveals the possibility of identifying the cell type if the value of the extracted normalized constant is greater than 1.75 (as indicated by the vertical line). For concentrations with less than 104 cells per ml, both RBCs and WBCs exhibited approximately the same trend, making the use of these calibration

curves for cell identification below this range difficult. Nevertheless, as can be concluded from the data displayed in Figures. 4.4 (c) and (d), the recorded capacitance values for the two types of cells at the same concentration were different. Hence, the capacitance per cell can be used to differentiate the cell types.
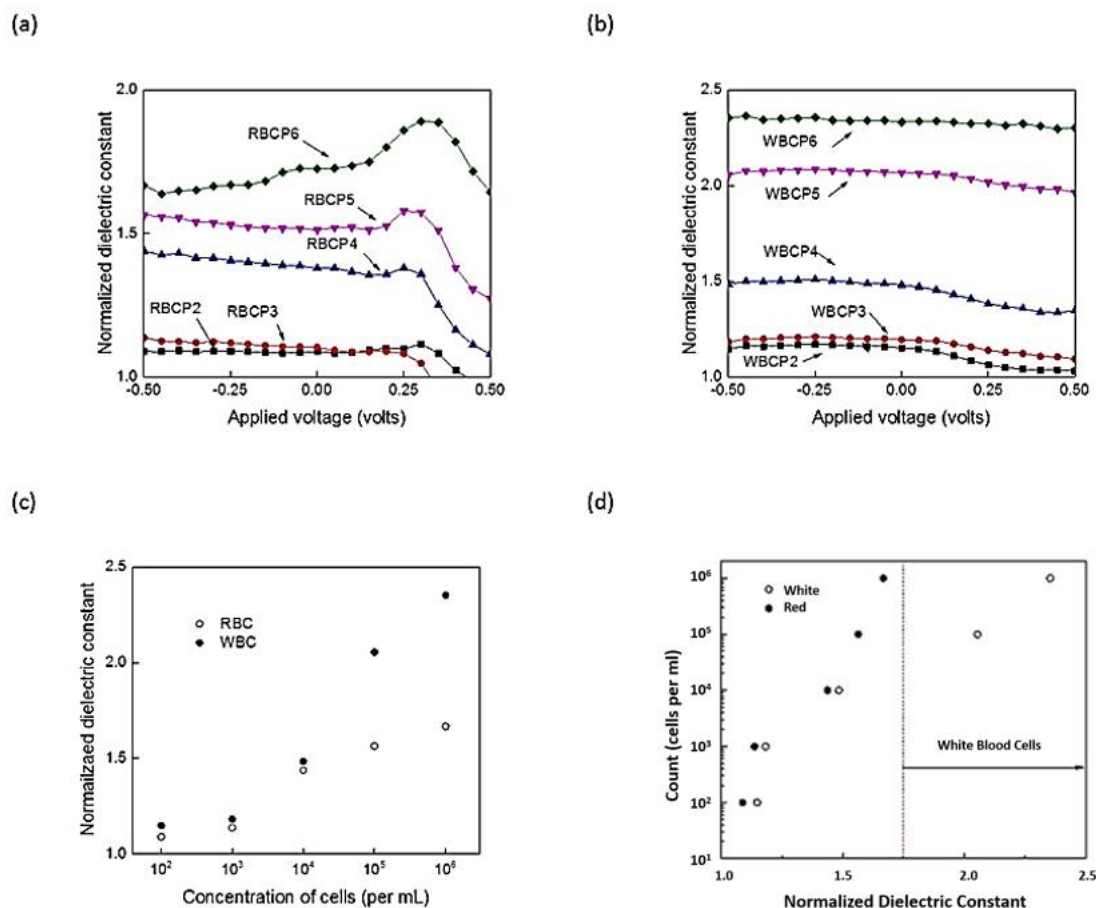


Figure 4.6: Extraction of the dielectric constants and cell counts from the electrical measurements.(a) Ratios of the dielectric constant of each cell suspension to the dielectric constant of the urine only sample plotted over a range of voltages (-0.5 to +0.5 V) for red blood cells (RBCs). Samples RBCP0, RBCP2, RBCP3, RBCP4, RPC5 and RPC6 had 0, $10^2$, $10^3$, $10^4$, $10^5$ and $10^6$ cells/ml, respectively. (b) Same calculations for the white blood cell (WBC) urine suspensions. Samples WBCP0, WBCP2, WBCP3, WBCP4, WBC5 and WBC6 contained 0, $10^2$, $10^3$, $10^4$, $10^5$ and 106 cells/ml, respectively. (c) Ratios calculated at a voltage of -0.25 V plotted against the cell concentration for RBCs and WBCs. (d) Replotting of figure (c) with reversed axes to calculate the cell count per ml based on electrical parameters.

**4.5 Discussion**

In this study, the dielectric properties of urine are characterized which presented the ability to detect, quantitate, and distinguish between two different types of blood cells present in urine based on their electrical parameters. The results show that using proposed approach, it can detect a minimum of $10^2$ blood cells/ml of urine. Study of the dielectric properties of urine has been gaining more interest in the last few years. Such studies can pave the way for fast and noninvasive methods that can be very practical for clinical utility. For example, in one study, electrical measurements were recorded for urine samples of normal patients and patients with CKD with proteinuria at frequencies from 0.2-50 GHz and at three different temperatures [202]. Below 7 GHz, the urine of patients with CKD had higher dielectric properties than that of normal subjects, with the differences becoming more significant at higher temperatures of 30°C and 37°C. This trend was reversed above 7 GHz. Similarly, a positive correlation between proteinuria level and dielectric properties was observed below 7 GHz, while a negative correlation was observed above this point. The lower relaxation frequency observed in samples with proteinuria was explained by a decrease in bulk water, leading to slower relaxation times [202]. Similar results were also shown when the urine of patients with diabetes and CKD was compared to that of normal subjects, but the differences were more significant between normal patients and patients with CKD [203]. Other studies have investigated the effect of glycosuria on the dielectric properties of urine and observed an increase in the dielectric constant with increasing glucose in urea [204–207]. All these studies demonstrate the biomaterial dependence of urine dielectric properties. Not much research has been done related to the dielectric properties of urea from patients exhibiting hematuria or on urine taken from patients with urinary tract infections have been conducted. As

discussed, the presence of RBCs is a very important prognostic factor for CKD, while WBCs can indicate the presence of infection.

In the present study, no real samples have been used from patients; rather, to establish the proof-of-principle, the effects of RBCs and WBCs on urine dielectric properties has been investigated. This investigation was achieved by spiking fresh urine with increasing concentrations of RBCs and WBCs. Surprisingly, the dielectric properties were not as expected because the urine CF curves, and the cell concentration exhibited an inverse correlation (Figures 4.3 (a) and (b)). This unexpected result raised the question of the stability of urine, which possibly affected its electrical properties, thus leading to this artifact. To test this possibility, the dielectric property of the fresh urine sample was measured after each suspension reading by spinning the suspension and removing the cells. Interestingly, it is observed a stepwise increase in the CF profile of urine alone with time (Figures 4.3(c) and (d)). This finding highlights the issue of urine stability over time. The observed dynamic changes in urine are possibly ascribed to some chemical reactions that can occur, altering the chemical composition of urine and consequently altering the intrinsic capacitance of urine over time. As a biological fluid, urine comprises of sodium chloride, phosphate, potassium, urea and trace levels of calcium, sulfate, and magnesium [208]. Fresh urine pH ranges from 5.6 to 6.8 [209]. Urea is one of the components degraded by the action of the urease enzyme found in some infectious microorganisms, breaking it into ammonia and carbon dioxide, thus raising the pH of urine to 9 [210]. One study showed that changes in the pH and ammonia concentration of fresh urine reach a steady state after 60 to 72 hours [207]. Moreover, this change is accelerated at higher temperatures (such as, 25°C and 30°C) [211]. In another study, no significant changes in urine sample parameters were

observed after one hour, but some parameters changed after a 24-hour period of refrigeration [212].

In this study, it has been showed that dynamic changes occur in urine in short periods of time (30 minutes) and that these changes can be electrically detected, but not by conventional methods. The electrode polarization (electric double layer) is augmented by the presence of free mobile ions in a suspension, and this phenomenon can lead to an increase in the capacitance of a suspension [213]. It has been suggested that the dynamic changes of urine with the generation of free ammonia ions and carbonate ions may lead to the increase in capacitance observed over time. Another explanation can be an increase in the density of dipoles as a result of dynamic chemical changes. In fact, this phenomenon was proposed to explain the high dielectric constant observed for the blood of people with diabetes [214]. Furthermore, the results revealed that the CV profiles of the cell suspensions in urine (Figures 4.4 (a) and (b)) had patterns similar to those observed in the CF profiles. The capacitance of cell suspensions using the following formula can be described as:

$$C_{Suspension} = C_{Urine} + C_{Cells\ (RBCs\ or\ WBCs)} \qquad (4.1)$$

This formula shows that de-embedding the CV values of each urine control sample from the CV values of the urine suspensions made at the corresponding times should yield the actual CV value of cells (Figures 4.4 (c) and (d)). As observed, after the de-embedding process, the CV curves became positively correlated with the cell concentrations in urine. The ratio of the dielectric constant of each cell concentration (RBCs/WBCs) to the dielectric constant of fresh urine was calculated for each value over the range of voltages, as shown in Figures 4.6 (a) and (b). The ratios calculated at -0.25 V were plotted against the cell concentration to obtain $\varepsilon_{RBC}/\varepsilon_{WBC}$ urine

concentration curves (Figure 4.6(c)). These curves were used to extract the concentration of cells in urine. This technique can detect cell numbers as low as 100 cells per ml, which is even more sensitive than any available urine dipstick test since these tests can detect a minimum of $2\times10^4$ to $1\times10^6$ RBCs per ml.

Similarly, WBCs could also be detected at low concentrations, 100 cells/ml. This study emphasizes on the ability to detect the dynamic changes in urine alone can also be important, especially if these changes result from bacterial activity that can result in even a higher rate of change in infected urine. This approach can be faster than conventional microbiological techniques that require lengthy microbial culture and proper interpretations. In proposed case, a high ratio of the rate of change of a suspect sample to the rate of a normal sample could act as an indication of infection since the urine sample was not handled in a sterile manner once it was used for the dilutions. Further investigation of this novel method and its validation can provide easier and more efficient modalities for urine examination, especially in high-volume labs where time is critical. The proposed method has been cross-checked using repeated electrical measurements against multiple cells stocks prepared at different times, i.e., all within the employed frequency range and over the same applied bias voltage. As detailed, the accuracy of these measurements using the outlined methodology is comparable with other conventional techniques such as dipstick.

# Chapter 5: Electrical Characterization of Calcium Oxalate in Urine

Urolithiasis is a very common problem worldwide, affecting adults, kids and even animals. Calcium oxalate is the major constituent of urinary tract stones in individuals, primarily due to the consumption of high oxalate foods. The occurrence of urinary oxalate arises due to endogenous synthesis, especially in the upper urinary tract. In a normal, healthy individual, the excretion of oxalate ranges from 10 to 45 mg/day, depending on the age and gender, but the risk of stone formation starts at 25 mg/day depending on the health history of the individual. This study demonstrates a label-free, accurate and sensitive method for detecting the presence of kidney stones in urine by measuring changes in the dielectric properties of urine with increasing concentration of calcium oxalate hydrate ($CaOx.H_2O$) powder. The current method can detect dynamic changes in the electrical properties of urine over time in samples containing $CaOx.H_2O$ at a concentration as low as $10\,\mu g/ml$ of urine, making this method suitable for detecting changes that cannot be recognized by conventional methods. The ability to detect very small amounts of stones makes this method an attractive tool for detecting and quantifying kidney stones.

## 5.1 Overview

Nephrolithiasis is a usual malady, with a predictable recurrence rate of five years in up to 50% of cases [215]. Due to the continuous change in dietary proclivity and lifestyle, the ubiquity of calculi has steadily grown over the past decades [216, 217]. The risk factors leading to urolithiasis are polydipsia [218–220], corpulence [221], hypertension [216, 220, 222] and insulin resistance syndrome [223], which may result in chronic kidney failure [216, 224–227]. Lithiasis occurs when urine becomes

concentrated with respect to certain minerals, resulting in crystallization in the kidneys; these crystals further grow and are retained within the kidneys ducts [228].

Many published reports have shown that all kinds of kidney calculi contain several trace elements, such as Ca, Mg, Mn, Cu, Fe, K, Zn, Cd, B, and Se [229–231]. However, calcium stones are the most prevalent, especially calcium oxide (CaOx) and calcium phosphate (CaP) crystals, which exist alone or as fusions. Hyperoxaluria is a metabolic disorder that might lead to end-stage renal failure and is defined as the excessive urinary excretion of oxalate anions [232]. CaOx is a calcium salt of dicarboxylic acid and oxalic acid that occurs as a dihydrate or monohydrate, i.e., whewellite (COM) and weddellite (COD). Among all calcium stones, COM stones are the most common ones that occur globally [233].

Precise analysis of renal calculi is a prerequisite for metaphylaxis. Currently, available analysis techniques include spectroscopy, thermogravimetry (TG), polarization microscopy, chemical analysis, scanning electron microscopy (SEM) and powder X-ray diffraction [234, 235]. Moreover, spectroscopy includes various effective analysis techniques, such as infrared spectroscopy (IR), energy dispersion X-ray analysis (EDX), laser-induced breakdown spectroscopy (LIBS), laser ablation-inductively coupled plasma-mass spectrometry (LA-ICP-MS) and X-ray absorption spectroscopy (XAS) [8, 236–239]. However, no solitary technique can provide comprehensive information on the chemical composition of kidney stones, indicating that combinations of these methods are needed for analysis [240].

Recently, various studies have been carried out on calculi behavior, detection, and quantification. The detection of kidney stones can be performed on the basis of physical, chemical and electrical properties, such as the electrical conductivity,

dielectric constant, polarization, and capacitance [15, 16]. Urinary pH affects the formation of stones; an alkaline pH supports the growth of Ca and P stones, whereas an acidic pH favors uric acid or cystine calculi [241].

In this proposed study, electrical characterization has been done along with urine strip analysis of urine samples with calcium oxalate hydrate powder (which is one of the main components of calcium oxalate kidney stones).

## 5.2 Results and Discussions

Calcium oxalate hydrate ($CaOx.H_2O$) (Sigma-Aldrich, United Kingdom) powder, which is a main component of kidney calculi, has been used for the experiments. A fresh urine sample was collected and centrifuged to prepare suspensions in urine. The same urine sample was used for both electrical characterization and urine strip analysis and was used as one of the reference samples for the study. The rest of the urine sample was centrifuged at $3x10^3$ rpm for five minutes and used as the diluent for suspending the $CaOx.H_2O$ powder. The quantity of $CaOx.H_2O$ powder varied from 10 mg to 1 mg, 100 µg and 10 µg per ml of urine sample. A fresh normal urine sample and pure oxalate powders were also used for the analysis.

### 5.2.1 Urinalysis

Urinalysis test strips (SD Uro-Color 10, Republic of Korea) has been used for the finding of key biomarkers (blood, bilirubin, urobilinogen, ketone, protein, nitrite, glucose, pH, specific gravity and leucocytes) in urine. The chemical pads react with urine and generates a color that could be analyzed by comparing to the color chart to determine the level of each parameter [241]. A complimentary area is also provided at the end of the urine strip.

The urine samples were collected, processed and stored in clean, dry containers. The tests were conducted one by one. A reagent strip was removed from the container and the cap was immediately replaced to minimize exposure of the remaining test strips to light and air. The chemical pads were completely immersed in the urine samples and instantly removed to prevent dissolution of the pads. The excess urine has been removed to prevent any cross-contamination of chemicals placed on adjacent reagent pads. The color change of pads has been compared to the corresponding color chart and the results were recorded for each panel.

Urinalysis was conducted by treating urine strips with urine samples. Figure 5.1 shows the urine strips treated with fresh urine and centrifuged urine containing different dilutions of $CaOx.H_2O$. Fresh and centrifuged urine were used as references. Comparison of the reference urine strips with those treated with urine containing different dilutions of $CaOx.H_2O$ showed a change in the pH value, which is a prominent parameter used for quick detection of pathological changes in urine [242].

The normal urine pH is approximately 6.0 but can range from 4.5 to 8.0 [243]. The reference samples exhibited a pH of 6.0. The $CaOx.H_2O$ urine suspensions at dilutions of 10 mg/ml and 1 mg/ml exhibited a pH of 6.0. The pH of urine with dilutions of 100 µg/ml and 10 µg/ml calcium oxalate decreased to 5.5.

The color pads on the reagent strips for the other parameters did not show considerable color changes compared to the reference sample strips. The other parameters used to indicate changes were as follows: glucose - 100, leukocytes – 75, bilirubin – 1.0 to 0.5, protein – 1 and specific gravity – 1.030. The urinalysis results are depicted in Table 5.1, which indicates that the pH and bilirubin have slight variations when the quantity of oxalate powder changes while the other properties remain constant.

83
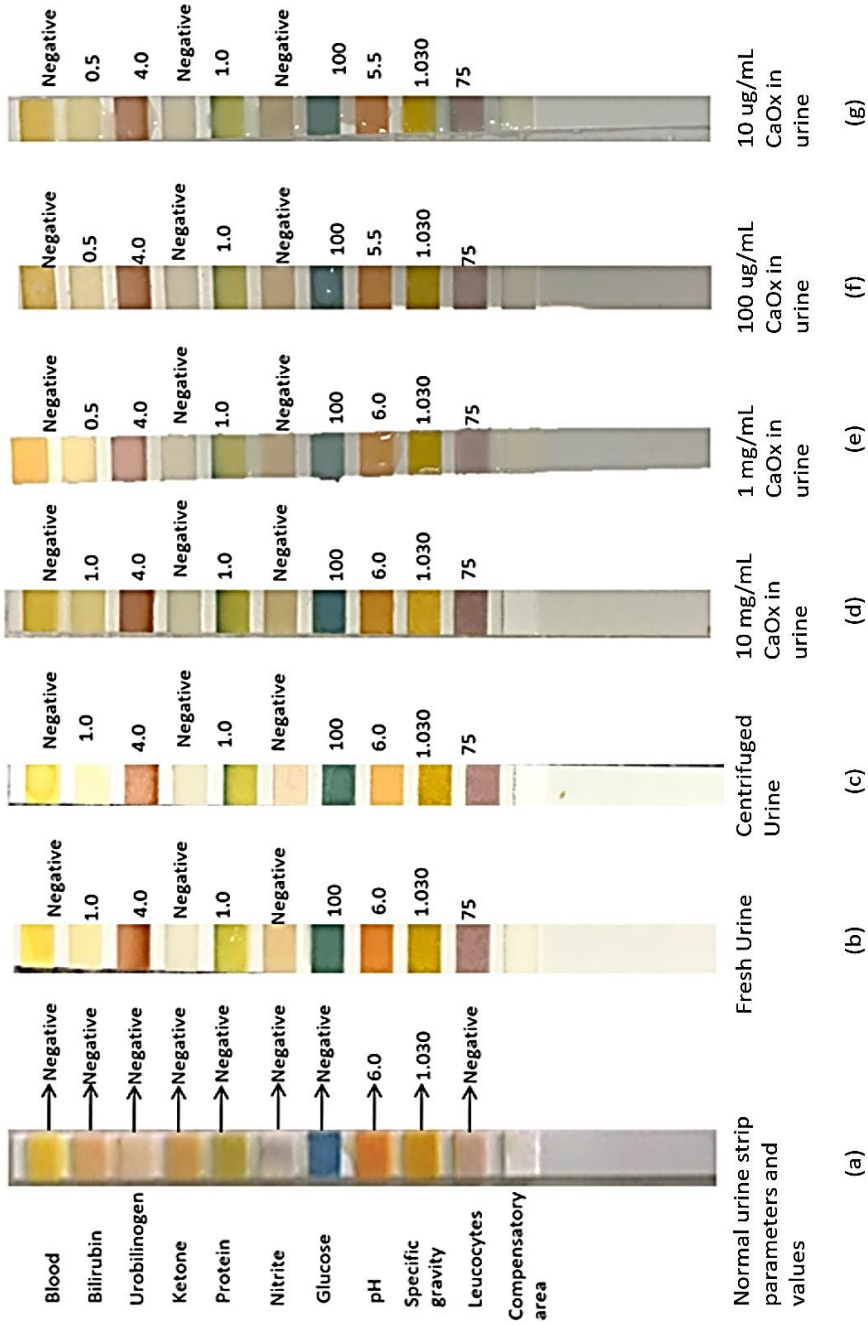


Figure 5.1:Urinalysis via test strips: a) without urine sample (normal values), b) fresh urine, c) centrifuged urine, d) 10 mg/ml CaOx.H2O in urine, e) 1 mg/ml CaOx.H2O in urine, f) 100 µg/ml CaOx.H2O in urine, and g) 10 µg/ml CaOx.H2O in urine.

Table 5.1: Urinalysis of Calcium Oxalate Hydrate Powder in Centrifuged Urine

| | Calcium oxalate hydrate powder (CaOx.$x$H$_2$O) in centrifuged urine | | | |
|---|---|---|---|---|
| | 10 mg/ml | 1 mg/ml | 100 µg/ml | 10 µg/ml |
| pH | 6.0 | 6.0 | 5.5 | 5.5 |
| Glucose | 100 | 100 | 100 | 100 |
| Blood | Neutral | Neutral | Neutral | Neutral |
| Bilirubin | 1 | 0.5 | 0.5 | 0.5 |
| Urobilinogen | 4 | 4 | 4 | 4 |
| Ketone | Neutral | Neutral | Neutral | Neutral |
| Protein | 1 | 1 | 1 | 1 |
| Nitrite | Neutral | Neutral | Neutral | Neutral |
| Specific Gravity | 1.030 | 1.030 | 1.030 | 1.030 |
| Leucocytes | 75 | 75 | 75 | 75 |

Calcium oxalate hydrate was artificially introduced into fresh, centrifuged urine samples at a range of dilutions based on mass, i.e., 10 mg/ml, 1 mg/ml, 100 µg/ml and 10 µg/ml of urine. A normal, healthy individual voids 1000-2000 ml of urine per day [242]. Normal levels of urine oxalate excretion are less than 45 mg/day (<0.50 mmol/day) [244]. Subjective to the age, gender, health history and numerous other parameters, the risk of calculi formation is higher even at small amount of 25 mg/day, which is considered to be a normal quantity [245]. Thus, 10 µg of CaOx.H$_2$O per ml of urine was selected as the lowest dilution for the test.

Urine strips are the preliminary and central diagnostic method for yielding quick and reliable information on pathological changes in urine [242]. This data shows that the presence of calcium oxalate crystals in urine results in a change in pH. The pH of the fresh, as well as centrifuged, urine samples remained at 6.0, which is the normal urine pH [243]. The color pads of the urine containing CaOx.H$_2$O dilutions showed slight changes in color. The pH remained at 6.0 for the 10 mg/ml and 1 mg/ml samples but was reduced to 5.5 for the 100 µg/ml and 10 µg/ml samples. The decrease in the urine

pH can be supported by the occurrence of calculi composed of calcium, oxalate, proteins, citrate and other macro-molecules; in proposed case, the decrease is due to the presence of oxalate powder [246]. The potential danger of calculi formation is associated with the formation of crystals present in urine. Studies have shown that COM crystal formation is associated with the occurrence of high amounts of oxalate [247]. Conte et al. showed that calcium oxalate hydrate present in the renal stones exhibits a relationship with the urinary parameters [248].

Other parameters that exhibit deviations from the normal values are glucose, leukocytes and bilirubin. The glucose component on the urine strip indicated a value of 100 due to the trace amounts of glucose normally excreted in urine [248]. The presence of leukocytes is indicated by the value of 75 in the test strip, which corresponds to a negligible amount and might not indicate an infection of the urinary tract [249]. Bilirubin conjugates with glucuronic or sulfuric acid and appears in urine. The presence of conjugated bilirubin in human urine (indicated by the values of 1.0 to 0.5 in the urine strip) is commonly associated with liver disorders such as hepatitis, cirrhosis, gallbladder disease and various hepatocellular cancers [250]. Urobilinogen is formed by bacterial action on conjugated bilirubin and its appearance in urine is caused mostly by hemolysis or hepatocellular dysfunction. The protein component in the test strip exhibits a color range corresponding to a value of 1 and protein enters urine due to either altered renal functions, such as permeability, or tubular damage [251]. Adults have a specific gravity of 1.005 to 1.030 [252].

### 5.2.2 Electrical Characterization

The sample dilutions prepared using the centrifuged urine were used for electrical characterization. The electrical characterization was performed by loading the

reference urine samples as well as the urine suspensions inside the coaxial cable of a Gamry Reference 3000 (Gamry/USA) instrument and measuring the electrical parameters of the samples. The GR-3000 is a high-performance, high-current, USB controlled potentiostat with various current ranges from 3 A to 300 pA and up to a 32 A compliance voltage. This instrument takes measurements over a frequency span from 10 μHz to 1 MHz. The capacitance values of the samples were measured over a voltage span from -0.4 V to 0.4 V at a frequency of 10 Hz, values suitable for polarizing the suspended particles without altering the traits of the components inside the sample. At this frequency, the SNR is improved, and the frequency impedance spectra exhibit constant phase angle (CPA) and amplitude. The experimental setup has been depicted in Figure 5.2.
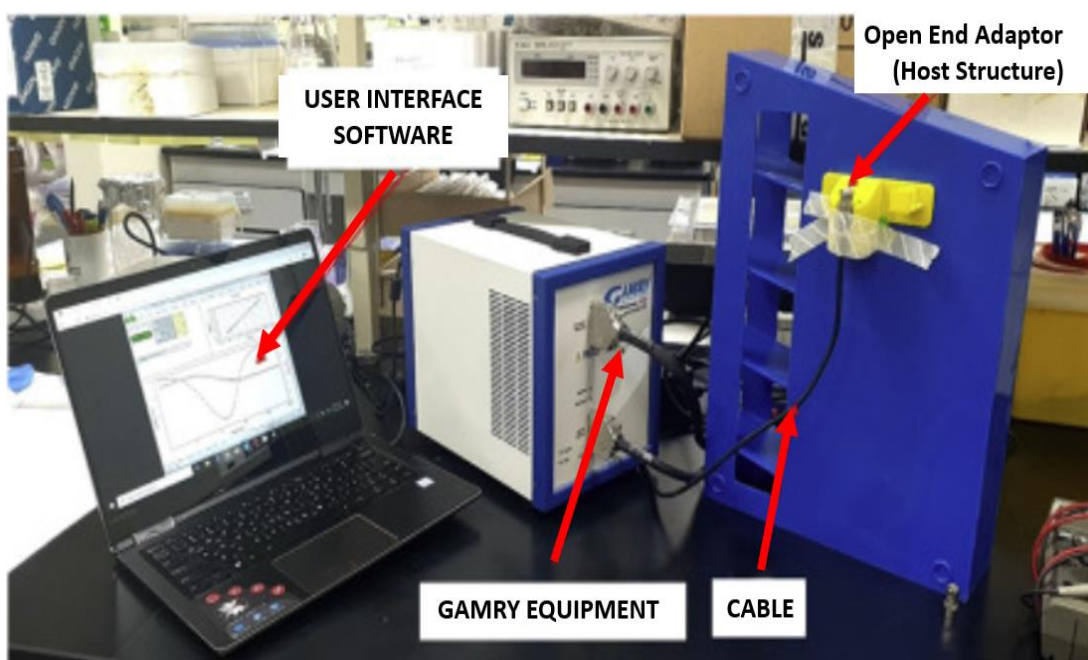


Figure 5.2: Experimental Setup.
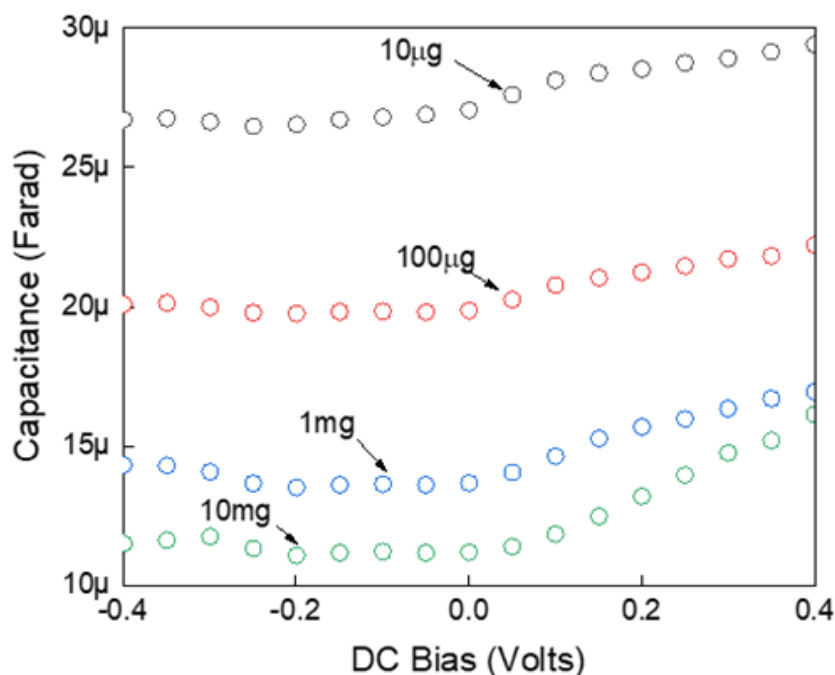
Figure 5.3:Capacitance-voltage (CV) measurements of calcium oxalate powder suspensions in urine.

The capacitance-voltage (CV) profiles for $CaOx.H_2O$ suspended in urine with increasing concentrations from 10μg/ml to 10mg/ml are depicted in Figure 5.3 (a). The capacitance of the samples was measured over a voltage span from -0.4V to 0.4V at a frequency of 10 Hz. The applied voltage range and frequency are suitable for polarizing the suspended particles; beyond this range, the traits of the components inside the sample may be altered [253]. Moreover, a low frequency of 10 Hz is desirable to improve the signal-to-noise ratio (SNR), and at this frequency, impedance spectra exhibit CPA and amplitude [254, 255]. As revealed from Figure 5.3 (a), the capacitance for $CaOx.H_2O$ suspensions were inversely proportional to the $CaOx.H_2O$ concentration; i.e., the sample with the highest amount of calcium oxalate powder generated the lowest curve, while the curves shifted to higher values with decreasing oxalate powder concentration. For the negative DC bias, all curves were almost

parallel; however, for the positive DC bias, the curves showed increasing trends. This phenomenon may be due to the change in the physical and dielectric properties of the calcium oxalate when the polarity of the applied voltage changes [256]. The average capacitance values over the negative applied voltage are 26.72μF, 18.8μF, 13.88μF and 11.40μF for the samples with oxalate powder concentrations of 10μg, 100μg, 1mg and 10mg per ml of urine, respectively.

The curves of the suspensions were expected to follow a direct relationship between the capacitance and CaOx.H$_2$O concentration in samples, i.e., for a higher calcium oxalate powder concentration, the capacitance value should be higher. Nevertheless, a contrasting trend was observed. This phenomenon can be attributed to the dynamic nature of urine, which varies over time. To verify the time dependence of urine, control samples from the suspended samples has been prepared, which acted as references for further measurements.
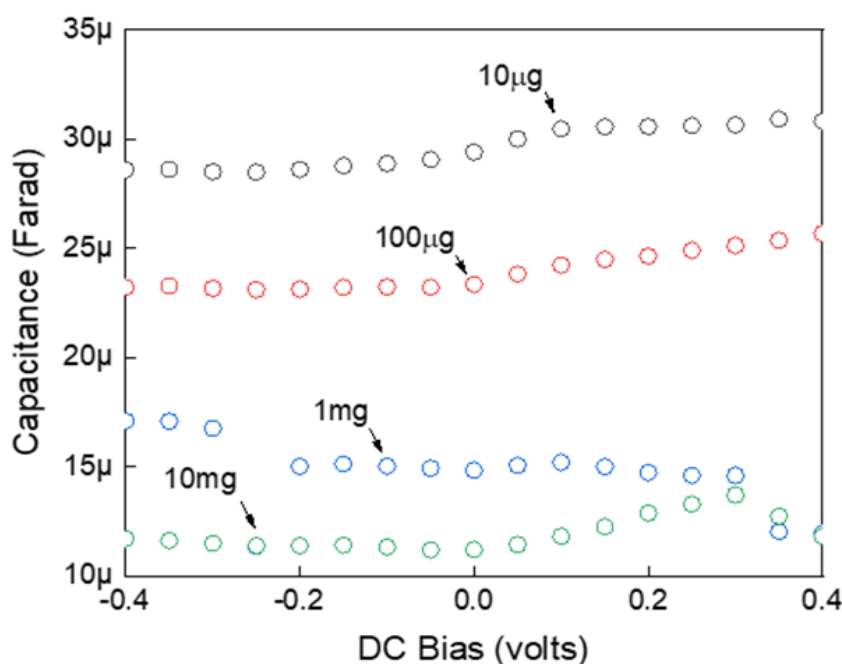


Figure 5.4:Capacitance-voltage (CV) profiles of control urine after centrifugation of suspensions with different masses.

After the measurements, to concoct control samples, the suspended samples were centrifuged and the supernatants were subjected to electrical measurements. The corresponding CV measurements of the control samples are depicted in Figure 5.4. Comparing both figures, Figure 5.3 and Figure 5.4, a homologous pattern of capacitive curves was observed. This comparison reveals that the control samples have higher values than the corresponding suspended samples. The extraction of the supernatant from its corresponding suspended samples excludes the effect of the sediment [257], leading to aberrations in the capacitive values for the control samples. Except for the 1 mg control sample, all the samples have an increasing slope for the positive applied voltage; however, for the negative DC bias, all curves are analogous. The average capacitance values over the negative DC bias are 28.76μF, 23.2μF, 15.8μF, and 11.48μF for the samples with oxalate powder concentrations of 10μg, 100μg, 1mg and 10mg per ml of urine, respectively.

The time-dependent dynamic nature of urine is shown in Figure 5.5. The chronological measurements were taken with an approximately 20-minute gap up to one hour to measure the control urine capacitance. As the overall urine properties and parameters critically depend on the time window, performing the study within the time period of 90 minutes is recommended [215, 258]. This curve shows a linear increase in the capacitance from 11.65μF to 28.7μF within an hour. This result indicated that the control sample undergoes some dynamic changes over time. The changes are mostly chemical, which can alter the electrical parameters, leading to a gradual increase in capacitance with time. A fitted curve was generated using a linear regression model with the extracted parameters, as depicted in the inset of Figure 5.5. The fitted and measured values exhibit approximately the same trend.
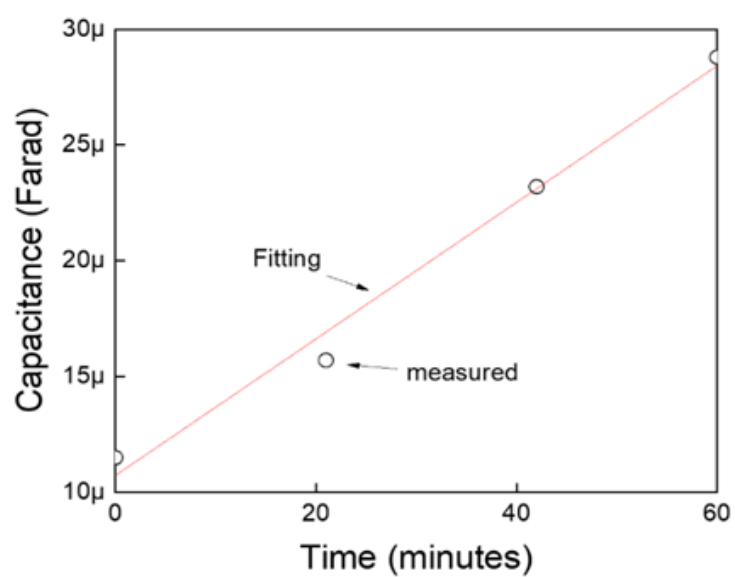
Figure 5.5: Time-dependent changes in urine sample capacitance, depicting measured data and the fitted curve. An inset table of the curve fitting parameters is also shown.
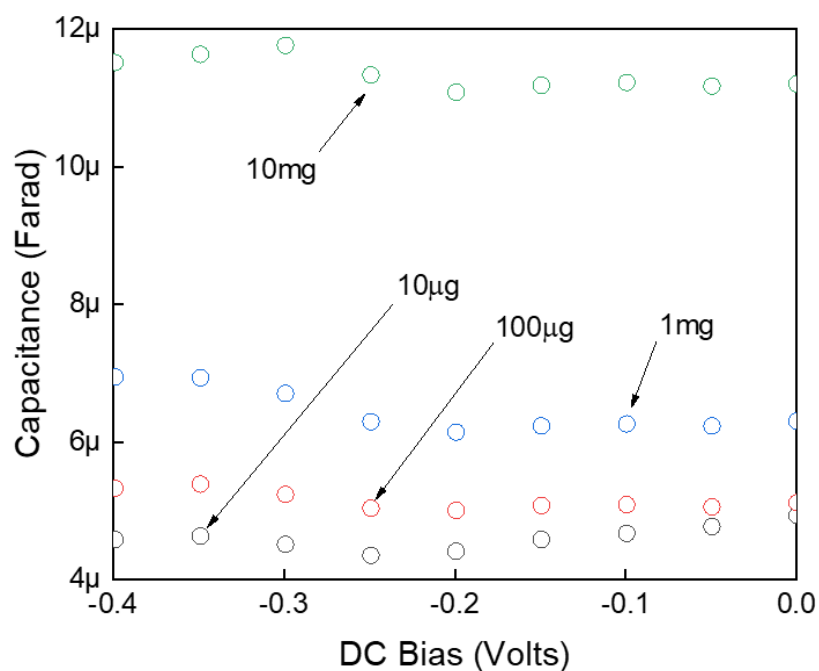


Figure 5.6: Capacitance-voltage (CV) profiles of oxalate powder suspensions after de-embedding the dynamic contributions of the urine for negative applied voltages.

The estimation model parameters show very little deviation from the actual empirical values of the data. The adjusted R-square value is 0.9812, approaching one, which indicates that the model well predicts the values in the target field. The rate of change of urine over time can be expressed as the slope of the fitted curve, which is 0.295µF/min.
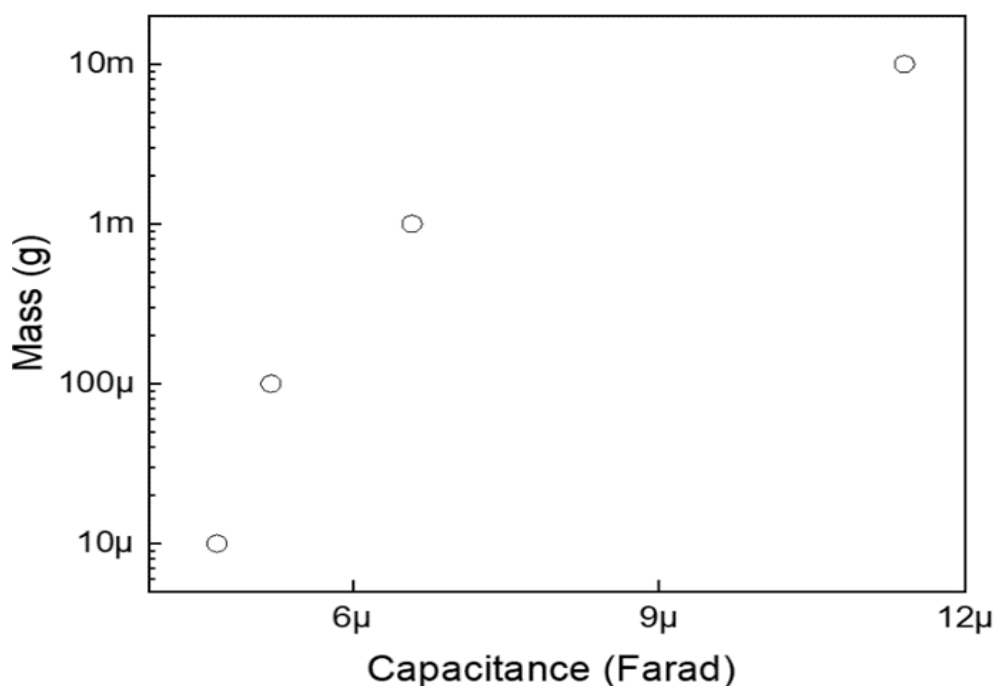


Figure 5.7: Capacitance-mass (CM) profile, with logarithmically increasing powder concentrations of 10 µg, 100 µg, 1 mg and 10 mg versus capacitance.

The rate of change of urine was used to de-embed the dynamic effect of urine from the suspended sample results. By performing this step, the capacitance values were corrected for any possible changes occurring over the experimental time window. After excluding the dynamic effect of the urine from the samples with various concentrations of suspended oxalate powder, the effective capacitance over the negative applied voltage was obtained, as shown in Figure 5.6. Specifically, the

capacitance values of each supernatant urine sample were deducted from those of the corresponding urine suspension of CaOx.$H_2$O powder. A reverse trend of normalized capacitance values can now be observed over the negative applied voltage compared to Figure 5.4, i.e., 10mg > 1mg > 100μg > 10 μg within the range of 4-12μF. Even the average magnitude is reduced, to 4.623μF, 5.164μF, 6.415μF and 11.3μF for the CaOx.$H_2$O concentrations of 10μg, 100μg, 1mg and 10mg per ml, respectively.

The capacitance-mass (CM) logarithmic profile for the saturation growth rate model of mass with respect to capacitance is depicted in Figure 5.7. With increasing CaOx.$H_2$O mass concentration from 10 μg to 100 μg, 1 mg and 10 mg, the capacitance ranges from 0-12 μF. The curve shows a gradual increase in the mass. The mass initially shows a steep increase and later tends to stabilize with increasing capacitance. Other studies also showed the change in the mass of stones. For instance, Ananth et al. investigated an in vitro method that manifests the change in the crystal size of calcium oxalate over time [244].

## Chapter 6: Conclusion and Future Scope

### 6.1 Conclusion

An innovative and easy technique for the detection of cells/stones in urine is proposed in this study. The method involves label-free identification and quantification of cells and calcium oxalate in urine based on electrical parameters without any preprocessing steps. This method is promising since biotic elements, such as DNA, viruses, cells appear in urine even before people are aware that they might have a trouble and accurate detection is important before the condition worsens. Urinalysis using dipsticks can be used to acquire preliminary information on the nature of the urine sample. However, a more sensitive method is required to confirm the nature of the risk posed and to determine the diagnosis.

The process is based on the use of Capacitance-Voltage measurements to detect the presence of blood cells and calculi suspended in urine. Any deviation from the normal constituents of urine can be detected because of the changes in the urine electrical parameters when exposed to an electric field. This technique can also sense dynamic variations in the sample that occur due to the diet and with the increasing lifetime of the sample. These dynamic variations can mask the actual values of the electrical parameters of the sample. By adding a de-embedding step in the process, this masking effect can be removed. Hence, the electrical variations become more appropriate and well correlated with the increasing amount of the quantities of the biological entities in the sample.

Electrical charging, capacitance-frequency and capacitance-voltage measurements were conducted to extract a set of dielectric constants and other electrical parameters that could determine the presence of cells and stones in urine. This recognition of

different diseases by analyzing the types of exfoliated particles inside the urine is promising. This technique can detect cell numbers as low as 100 cells per ml and CaOx.H$_2$O at a concentration as low as 10 µg/ml of urine. The comparison of proposed method with other available techniques has been depicted in Table 6.1.

Table 6.1: Comparison of Proposed Method with other available Techniques.

| | [259] | [260] | [261] | [200] | [262] |
|---|---|---|---|---|---|
| **Technique** | Phase-shifting Laser Microscopy (PLM) | Atomic Force Microscopy (AFM) | Gas Chromatography Mass Spectrometry (GC-MS) | Capacitive-Voltage and Capacitive-Frequency method | Electrical Impedance Spectroscopy (EIS) |
| **Parameters** | -Phase shifts and -Cancer-index | -Young's Modulus -Single Cell Elasticity | At 2 different pHs: pH-7 and pH-2: -Volatile profiling -Metabolomic Profiling -effect size -Percentage of variation | -Polarization -Dielectric properties | Resistance and capacitance at 4 phases of: -Growth -Confluence -Wounding -Healing |
| **Analysis** | Bird's eye view of Phase shifts analysis | Hertz–Sneddon model | Statistical Analysis: PCA and PLS-DA | Capacitive Modelling | -Feature Analysis and Selection with Linear Discriminant Analysis |
| **Pros** | -Less time taking -NN are flexible and used for both regression and classification problems. -Can model with nonlinear data with large number of inputs. -Once prepared, the predictions are fast. | -Resolution: --0.5–5 nm depth, --0.2–10.0 nm (lateral). -For conductive and non-conductive. -Can be used for nanocrystals and nanotubes as well | - Suitable for certain analytes. - Many well-established protocols. - Faster method development | -Fast -Sensitive -pre-processing steps are not required | -Consistent results -non-destructive techniques hence less material is required. -cell sorting -high resolution |

Table 6.1: Comparison of Proposed Method with other available Techniques.
[Contd.]

| | [259] | [260] | [261] | [200] | [262] |
|---|---|---|---|---|---|
| Cons | -Histograms of different cells are overlapping, hence sensitivity and specificity needs to improve. -The tableland and cone shapes are considered as the distinctive shape of normal and cancer cells, which is not a promising feature. | -Its clinical use needs more systematic studies. -Structural complexity and heterogeneity of tumors questions the relevance of elasticity measurements. | -The integration of Volatile Organic Compound (VOCs) in specific metabolic pathways is still very difficult, needs more studies. | -Capacitive values may vary from one investigational setup to another. - Single cell analysis is required to produce more precise results for the intrinsic properties of cells. | -To determine cancer cells in coculture inside a single well containing a set of spatially distributed microelectrodes. |
| Time | Few Hours | Few Hours- one day | Few days: as VCOs take at least 2 days. | Few minutes | Few days |
| Reliability | Less reliable | Less reliable due to: - small scan image size and restricted speed. - slow rate of scanning leads to thermal drift. - images affected by hysteresis property of the piezoelectric material. | Moderate reliable: as it doesn't produce accurate results for all cell lines. | Yes | Yes |
| Errors | Error in case of contamination only. | - | Separate errors for each sample | Error of 5% | Error of 4.5% |

This technique can also potentially be used for identifying the type of cells present by comparing the capacitance measurements, which could provide a valuable tool for discriminating different urine samples of different compositions. Knowing the individual electrical response of each cell component can help explain the effect observed when these responses are combined. This approach is a highly sensitive, safe,

low-cost and reliable method with minimal sample processing. This method can be considered a point-of-care test because the results can be instantaneously shared with the members of the medical team.

## 6.2 Future Scope

The development of innovative, cheap and rapid electrical detection methods for identifying cells and stones in patient samples could potentially provide significant public health benefits in terms of early disease detection. Based on these outcomes, the proposed method to be an initial point towards creating the foundation for label-free electrical-based identification and quantification of an unlimited number of nano-sized particles.
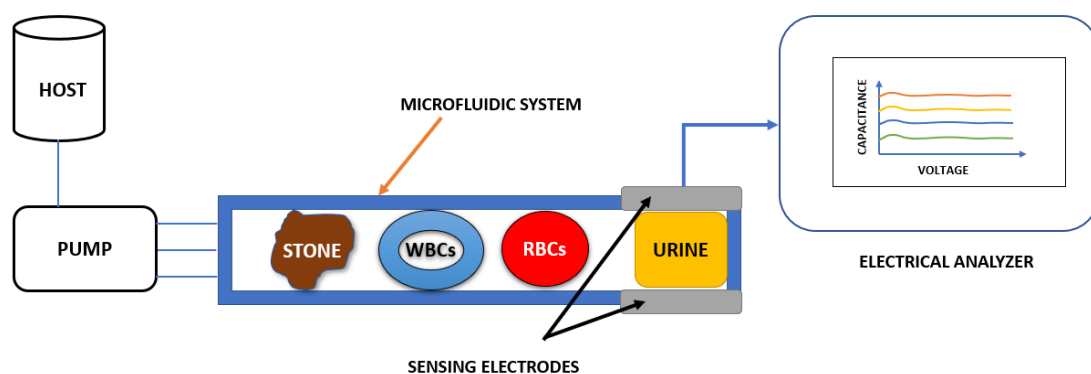


Figure 6.1: Overview of the microfluidic channel-based system.

The future scope of the study suggests that single entity characterization will be more precise towards development of this technique. The composition of biotic materials and suspensions on a unit level will help in better understanding of biochemical and physiological states. This will help in the exact identification of the type of particles present in the suspension. Currently, microfluidics is appropriate for this purpose

which has the potential to provide components identification with higher accuracy. Microfluidics can detect individual traits, molecular interactions, and behavior over long-time durations, etc. which are the basics of electrical biomarkers, especially in proposed methodology of capacitive-voltage detection.

The basic setup of any microfluidic channel has been depicted in Figure 6.1, which incorporates a host where the sample will be loaded. The sample is the urine suspension including the possible cells or stones. A pump which is a controlled system to regulate the pressure and flow of the sample in microfluidic chamber; a microfluidics system with sensing electrodes for analysis of the loaded material where the particles are confined. The electrical conditions for investigation can be applied with the help of the sensing electrodes. A dedicated embedded system/software for microfluidic channel which will provide the measurements and its analysis on computer.

Usually a microcontroller with a closed-loop control algorithm controls the output pressure at the requested level. The main part of the system is the electrical analyzer which takes sample (for instance, urine) with a regulated flow for its detailed research. This analyzer will examine the components (such as, WBCs. RBCs, salts) of the sample trapped within the sensing electrodes and provides the results, such as capacitance-voltage measurements, etc., when subjected to certain regulated conditions. With the slow motion of the flow inside and the size of the channel makes it easy to trap individual cells/molecules and explore it. The various pros of using microfluidics are to decrease in the sample volume and reagents; pressure, flow, temperature, and mixing can be controlled; wide range of fluidic geometries and small particles, etc.

# References

[1]     A. J. Lewington, J. Cerdá, and R. L. Mehta, "Raising Awareness of Acute Kidney Injury: A Global Perspective of a Silent Killer," *Kidney Int.*, vol. 84, no. 3, pp. 457–467, Sep. 2013, doi: 10.1038/ki.2013.153.

[2]     J. Delanghe and M. Speeckaert, "Preanalytical requirements of urinalysis," *Biochem. Medica*, vol. 24, no. 1, pp. 89–104, Feb. 2014, doi: 10.11613/BM.2014.011.

[3]     "Urine Boundless Anatomy and Physiology." Jan 2017 [Online]. Available: https://courses.lumenlearning.com/boundless-ap/chapter/urine/. [Accessed: 17-Dec-2018].

[4]     A. Al-Fraihat, A. W. Al-Mufti, U. Hashim, and T. Adam, "Potential of urine dielectric properties in classification of stages of breast carcinomas," in *2014 2nd International Conference on Electronic Design (ICED)*, 2014, pp. 305–308, doi: 10.1109/ICED.2014.7015819.

[5]     O. Herman-Saffar, Z. Boger, S. Libson, D. Lieberman, R. Gonen, and Y. Zeiri, "Early non-invasive detection of breast cancer using exhaled breath and urine analysis," *Comput. Biol. Med.*, vol. 96, pp. 227–232, May 2018, doi: 10.1016/j.compbiomed.2018.04.002.

[6]     R. N. Kore, C. S. Dow, and K. M. Desai, "A new automated system for urine analysis: a simple, cost-effective and reliable method for distinguishing between glomerular and nonglomerular sources of haematuria," *BJU Int.*, vol. 84, no. 4, pp. 454–460, Sep. 1999.

[7]     D. Roberts, "Electrical impedance of human urine," M.Sc. dissertation, University of Utah, 1980. Accessed on: Feb 24, 2020. [Online]. Available: https://collections.lib.utah.edu/dl_files/cd/cc/cdcc7741f473589a628f71dfaa23 ed4737b77592.pdf

[8]     Y. M. Fazil Marickar, "Electrical conductivity and total dissolved solids in urine," *Urol. Res.*, vol. 38, no. 4, pp. 233–235, Aug. 2010, doi: 10.1007/s00240-009-0228-y.

[9]     F. Hernández-Luis, S. Abdala, S. Dévora, D. Benjumea, and D. Martín-Herrera, "Electrical conductivity measurements of urine as a new simplified method to evaluate the diuretic activity of medicinal plants," *J. Ethnopharmacol.*, vol. 151, no. 2, pp. 1019–1022, Feb. 2014, doi: 10.1016/j.jep.2013.11.059.

[10]     C. Honrado and T. Dong, "A Capacitive Touch Screen Sensor for Detection of Urinary Tract Infections in Portable Biomedical Devices," *Sensors*, vol. 14, no. 8, pp. 13851–13862, Jul. 2014, doi: 10.3390/s140813851.

[11]     K. Settu, C.-J. Chen, J.-T. Liu, and J.-Z. Tsai, "Capacitance sensor for detecting Escherichia Coli in urinary tract infection diagnosis," *J. Microbiol. Immunol. Infect.*, vol. 48, no. 2, p. S81, Apr. 2015, doi: 10.1016/j.jmii.2015.02.287.

[12]     S. J. Han, H.-K. Park, and K. S. Kim, "Applications of Microfluidic Devices for Urology," *Int. Neurourol. J.*, vol. 21, no. Suppl 1, pp. S4-9, Apr. 2017, doi: 10.5213/inj.1734838.419.

[13]     V. Suresh, O. Qunya, B. L. Kanta, L. Y. Yuh, and K. S. L. Chong, "Non-invasive paper-based microfluidic device for ultra-low detection of urea through enzyme catalysis," *R. Soc. Open Sci.*, vol. 5, no. 3, p. 171980, Mar. 2018, doi: 10.1098/rsos.171980.

[14]     D. Sechi, B. Greer, J. Johnson, N. Hashemi, "Three-Dimensional Paper-Based Microfluidic Device for Assays of Protein and Glucose in Urine," *Analytical Chemistry (ACS Publications)*", vol. 85, no. 22, pp. 10733-10737, 2013, doi:10.1021/ac4014868.

[15]     Y. Yagyik, N. Lal, I. M. Talwar, and R. K. Jethi, "Electrical conductivity of kidney stones," *Biomaterials*, vol. 10, no. 4, pp. 281–285, May 1989.

[16]     D. Sinha, K. Anwar, K. Kumari, S. Jaishwal, S. Madeshwaran, S. Keshari, D. R. Babu, R. Vidya, N. A. N. Raj, "Studies on the Dielectric Properties of Natural Urinary Stones," *Advanced Materials Research*, vol. 584, pp. 484-488, Oct 2012.

[17]     G. P. Triberis and M. Dimakogianni, "DNA in the material world: electrical properties and nano-applications.," *Recent Pat. Nanotechnol.*, vol. 3, no. 2, pp. 135–153, 2009.

[18]     V. Hodzic, V. Hodzic, and R. W. Newcomb, "Modeling of the Electrical Conductivity of DNA," *IEEE Trans. Circuits Syst. Regul. Pap.*, vol. 54, no. 11, pp. 2360–2364, Nov. 2007, doi: 10.1109/TCSI.2007.907879.

[19]     M. Ouyang, W. J. Li, K. W. Wong, and W. K. Liu, "Investigation of electrical properties of DNA-attached carbon nano-particles for biological applications," *2012 7th IEEE Int. Conf. NanoMicro Eng. Mol. Syst. NEMS*, pp. 429–432, 2012, doi: 10.1109/NEMS.2012.6196810.

[20]  H. An, Q. Liu, Q. Ji, and B. Jin, "DNA binding and aggregation by carbon nanoparticles," *Biochem. Biophys. Res. Commun.*, vol. 393, no. 4, pp. 571–576, Mar. 2010, doi: 10.1016/j.bbrc.2010.02.006.

[21]  A. Yan *et al.*, "Biocompatible, Hydrophilic, Supramolecular Carbon Nanoparticles for Cell Delivery," *Adv. Mater.*, vol. 18, no. 18, pp. 2373–2378, 2006, doi: 10.1002/adma.200600838.

[22]  P. Chopade, S. H. Moh, V. Kanade, T. Kim, A. Kulkarni, and S. H. Park, "Distinct characteristics of DNA field effect transistors embedded with marine-derived porphyra-334 under UV illumination," *AIP Adv.*, vol. 9, no. 2, p. 0252121, Feb. 2019, doi: 10.1063/1.5079784.

[23]  S. Maeno *et al.*, "Electrical property of DNA field-effect transistor; Charge retention property," in *2012 IEEE International Meeting for Future of Electron Devices, Kansai*, 2012, pp. 1–2, doi: 10.1109/IMFEDK.2012.6218621.

[24]  N. Arshad and S. I. Farooqi, "Cyclic Voltammetric DNA Binding Investigations on Some Anticancer Potential Metal Complexes: a Review," *Appl. Biochem. Biotechnol.*, vol. 186, no. 4, pp. 1090–1110, Dec. 2018, doi: 10.1007/s12010-018-2818-z.

[25]  D. Jiang, G. Xiang, C. Liu, J. Yu, L. Liu, and X. Pu, "Development of a Cyclic Voltammetry Method for DNA Electrochemical Detection on Microfluidic Gene Chip," *Int J Electrochem Sci*, vol. 7, pp. 10607–10619, 2012.

[26]  C. H. Wohlgamuth, M. A. McWilliams, and J. D. Slinker, "DNA as a Molecular Wire: Distance and Sequence Dependence," Sep 2013. [Online]. Available: https://pubs.acs.org/doi/full/10.1021/ac401229q. [Accessed: 25-Mar-2019].

[27]  C. M. Bui, "Temperature effect on DNA molecular wires," *PhD Dissertation*, San Diego State University, USA, Jan 2016.

[28]  D. Mandal, S. Khatun, A. N. Gupta, and A. Chandra, "DNA supported graphene quantum dots for Ag ion sensing," *Nanotechnology*, vol. 30, no. 25, p. 255501, Feb. 2019, doi: 10.1088/1361-6528/ab084c.

[29]  S. Rafiei, M. Dadmehr, M. Hosseini, H. A. Kermani, and M. R. Ganjali, "A fluorometric study on the effect of DNA methylation on DNA interaction with graphene quantum dots," *Methods Appl. Fluoresc.*, vol. 7, no. 2, p. 025001, Jan. 2019, doi: 10.1088/2050-6120/aaff95.

[30]    A. Henning, Frank. F. Bier, and R. Hölzel, "Dielectrophoresis of DNA: Quantification by impedance measurements," *Biomicrofluidics*, vol. 4, no. 2, p. 022803 (1-9), Jun. 2010, doi: 10.1063/1.3430550.

[31]    M. Viefhues and R. Eichhorn, "DNA dielectrophoresis: Theory and applications a review," *Electrophoresis*, vol. 38, no. 11, pp. 1483–1506, Mar 2017, doi: 10.1002/elps.201600482.

[32]    N. G. A. Abrescia, D. H. Bamford, J. M. Grimes, and D. I. Stuart, "Structure unifies the viral universe," *Annu. Rev. Biochem.*, vol. 81, pp. 795–822, Jul 2012, doi: 10.1146/annurev-biochem-060910-095130.

[33]    X. Muñoz-Berbel, N. Godino, O. Laczka, E. Baldrich, F. X. Muñoz, and F. J. del Campo, "Impedance-Based Biosensors for Pathogen Detection," in *Principles of Bacterial Detection: Biosensors, Recognition Receptors and Microsystems*, Eds. New York, NY: Springer New York, pp. 341–376, 2008.

[34]    J.-H. Lee, B.-C. Kim, B.-K. Oh, and J.-W. Choi, "Highly Sensitive Electrical Detection of HIV-1 Virus Based on Scanning Tunneling Microscopy," *J. Nanosci. Nanotechnol.*, vol. 15, no. 2, pp. 1117–1122, Feb. 2015.

[35]    J.-H. Lee, B.-K. Oh, and J.-W. Choi, "Development of a HIV-1 Virus Detection System Based on Nanotechnology," *Sensors*, vol. 15, no. 5, pp. 9915–9927, Apr. 2015, doi: 10.3390/s150509915.

[36]    S. H. Kim, Y. J. Park, J. Woo, and B. Y. Majlis, "Highly selective dengue virus detection using carbon nanotubes: Effect of pulse biasing in serum," in *2015 IEEE 15th International Conference on Nanotechnology (IEEE-NANO)*, pp. 1066–1069, 2015, doi: 10.1109/NANO.2015.7388805.

[37]    D. Wasik, A. Mulchandani, and M. V. Yates, "A heparin-functionalized carbon nanotube-based affinity biosensor for dengue virus," *Biosens. Bioelectron.*, vol. 91, pp. 811–816, May 2017, doi: 10.1016/j.bios.2017.01.017.

[38]    D. M. Elsheikh, H. A. Elsadek, E. A. Abdallah, S. Atteya, and W. N. ELmazny, "Rapid detection of blood entero-viruses using microstrip antenna bio-sensor," in *2013 European Microwave Conference*, pp. 878–880, 2013, doi: 10.23919/EuMC.2013.6686797.

[39]    M. Nakano, Z. Ding, and J. Suehiro, "Dielectrophoresis and dielectrophoretic impedance detection of adenovirus and rotavirus," *Jpn. J. Appl. Phys.*, vol. 55, no. 1, p. 017001, Dec. 2015, doi: 10.7567/JJAP.55.017001.

[40]    M. Nakano, R. Obara, Z. Ding, and J. Suehiro, "Detection of norovirus and rotavirus by dielectrophoretic impedance measurement," in *2013 Seventh*

*International Conference on Sensing Technology (ICST)*, pp. 374–378, 2013, doi: 10.1109/ICSensT.2013.6727678.

[41] J. El-Ali, P. K. Sorger, and K. F. Jensen, "Cells on chips," *Nature*, vol. 442, pp. 403–411, Jul. 2006, doi: 10.1038/nature05063.

[42] S. Suresh, "Biomechanics and biophysics of cancer cells," *Acta Biomater.*, vol. 3, no. 4, pp. 413–438, Jul. 2007, doi: 10.1016/j.actbio.2007.04.002.

[43] H. M. Coley, F. H. Labeed, H. Thomas, and M. P. Hughes, "Biophysical characterization of MDR breast cancer cell lines reveals the cytoplasm is critical in determining drug sensitivity," *Biochim. Biophys. Acta*, vol. 1770, no. 4, pp. 601–608, Apr. 2007, doi: 10.1016/j.bbagen.2006.12.002.

[44] Y. Cho, H. S. Kim, A. B. Frazier, Z. G. Chen, D. M. Shin, and A. Han, "Whole-Cell Impedance Analysis for Highly and Poorly Metastatic Cancer Cells," *J. Microelectromechanical Syst.*, vol. 18, no. 4, pp. 808–817, Aug. 2009, doi: 10.1109/JMEMS.2009.2021821.

[45] Y. Zhao *et al.*, "A microfluidic system for cell type classification based on cellular size-independent electrical properties," *Lab. Chip*, vol. 13, no. 12, pp. 2272–2277, Jun. 2013, doi: 10.1039/c3lc41361f.

[46] S. Byun *et al.*, "Characterizing deformability and surface friction of cancer cells," *Proc. Natl. Acad. Sci.*, vol. 110, no. 19, pp. 7580–7585, May 2013, doi: 10.1073/pnas.1218806110.

[47] Y. Zhao *et al.*, "Tumor cell characterization and classification based on cellular specific membrane capacitance and cytoplasm conductivity," *Biosens. Bioelectron.*, vol. 57, pp. 245–253, Jul. 2014, doi: 10.1016/j.bios.2014.02.026.

[48] M. R. Nurliyana *et al.*, "The Detection Method of Escherichia coli in Water Resources: A Review," *J. Phys. Conf. Ser.*, vol. 995, p. 012065, Apr. 2018, doi: 10.1088/1742-6596/995/1/012065.

[49] K. Settu, C.-J. Chen, J.-T. Liu, C.-L. Chen, and J.-Z. Tsai, "Impedimetric method for measuring ultra-low E. coli concentrations in human urine," *Biosens. Bioelectron.*, vol. 66, pp. 244–250, Apr. 2015, doi: 10.1016/j.bios.2014.11.027.

[50] W. Roobsoong *et al.*, "A rapid sensitive, flow cytometry-based method for the detection of Plasmodium vivax-infected blood cells," *Malar. J.*, vol. 13, no. 1, p. 55 (1-11), Feb. 2014, doi: 10.1186/1475-2875-13-55.

[51] B. Malleret *et al.*, "A rapid and robust tri-color flow cytometry assay for monitoring malaria parasite development," *Sci. Rep.*, vol. 1, p. 118, Oct. 2011, doi: 10.1038/srep00118.

[52] F. Asphahani and M. Zhang, "Cellular Impedance Biosensors for Drug Screening and Toxin Detection," *The Analyst*, vol. 132, no. 9, pp. 835–841, Sep. 2007, doi: 10.1039/b704513a.

[53] K. E. Moeller, J. C. Kissack, R. S. Atayee, and K. C. Lee, "Clinical Interpretation of Urine Drug Tests," *Mayo Clin. Proc.*, vol. 92, no. 5, pp. 774–796, May 2017, doi: 10.1016/j.mayocp.2016.12.007.

[54] S.-I. Han, Y.-D. Joo, and K.-H. Han, "An electrorotation technique for measuring the dielectric properties of cells with simultaneous use of negative quadrupolar dielectrophoresis and electrorotation," *The Analyst*, vol. 138, no. 5, pp. 1529–1537, Mar. 2013, doi: 10.1039/c3an36261b.

[55] D. A. Dean, D. Machado-Aranda, T. Ramanathan, I. Molina, and R. Sundararajan, "Electrical Properties of Biological Tissues - An Impedance Spectroscopy Study," in *2006 IEEE Conference on Electrical Insulation and Dielectric Phenomena*, pp. 357–360, 2006, doi: 10.1109/CEIDP.2006.311943.

[56] S. Gabriel, R. W. Lau, and C. Gabriel, "The dielectric properties of biological tissues: III. Parametric models for the dielectric spectrum of tissues," *Phys. Med. Biol.*, vol. 41, no. 11, pp. 2271–2293, Nov. 1996, doi: 10.1088/0031-9155/41/11/003.

[57] G. M. Whitesides, "The origins and the future of microfluidics," *Nature*, vol. 442, pp. 368–373, Jul. 2006, doi: 10.1038/nature05058.

[58] J. Chen *et al.*, "A microfluidic device for simultaneous electrical and mechanical measurements on single cells," *Biomicrofluidics*, vol. 5, no. 1, pp. 14113(1-11), Mar. 2011, doi: 10.1063/1.3571530.

[59] E. Hodzic, "Single-cell analysis: Advances and future perspectives," *Bosn. J. Basic Med. Sci.*, vol. 16, no. 4, pp. 313–314, Nov. 2016, doi: 10.17305/bjbms.2016.1371.

[60] T. Stuart and R. Satija, "Integrative single-cell analysis," *Nat. Rev. Genet.*, vol. 20, pp. 257–272, Jan. 2019, doi: 10.1038/s41576-019-0093-7.

[61] B. F. Brehm-Stecher and E. A. Johnson, "Single-cell microbiology: tools, technologies, and applications," *Microbiol. Mol. Biol. Rev. MMBR*, vol. 68, no. 3, pp. 538–559, Sep. 2004, doi: 10.1128/MMBR.68.3.538-559.2004.

[62]    M. A. Mansor and M. R. Ahmad, "Single Cell Electrical Characterization Techniques," *Int. J. Mol. Sci.*, vol. 16, no. 6, pp. 12686–12712, Jun. 2015, doi: 10.3390/ijms160612686.

[63]    J. S. Marcus, W. F. Anderson, and S. R. Quake, "Microfluidic single-cell mRNA isolation and analysis," *Anal. Chem.*, vol. 78, no. 9, pp. 3084–3089, May 2006, doi: 10.1021/ac0519460.

[64]    A. Han, L. Yang, and A. B. Frazier, "Quantification of the heterogeneity in breast cancer cell lines using whole-cell impedance spectroscopy," *Clin. Cancer Res. Off. J. Am. Assoc. Cancer Res.*, vol. 13, no. 1, pp. 139–143, Jan. 2007, doi: 10.1158/1078-0432.CCR-06-1346.

[65]    F. Lang and C. Stournaras, "Ion channels in cancer: future perspectives and clinical potential," *Philos. Trans. R. Soc. B Biol. Sci.*, vol. 369, no. 1638, Mar. 2014, doi: 10.1098/rstb.2013.0108.

[66]    K. R. Foster, J. M. Bidinger, and D. O. Carpenter, "The electrical resistivity of cytoplasm," *Biophys. J.*, vol. 16, no. 9, pp. 991–1001, Sep. 1976, doi: 10.1016/S0006-3495(76)85750-5.

[67]    S.-B. Huang *et al.*, "A clogging-free microfluidic platform with an incorporated pneumatically driven membrane-based active valve enabling specific membrane capacitance and cytoplasm conductivity characterization of single cells," *Sens. Actuators B Chem.*, vol. 190, pp. 928–936, Jan. 2014, doi: 10.1016/j.snb.2013.09.070.

[68]    K. Wang *et al.*, "Specific membrane capacitance, cytoplasm conductivity and instantaneous Young's modulus of single tumour cells," *Sci. Data*, vol. 4, p. 170015, Feb. 2017, doi: 10.1038/sdata.2017.15.

[69]    L.-S. Jang and M.-H. Wang, "Microfluidic device for cell capture and impedance measurement," *Biomed. Microdevices*, vol. 9, no. 5, pp. 737–743, Oct. 2007, doi: 10.1007/s10544-007-9084-0.

[70]    M. Abdolahad, Z. Sanaee, M. Janmaleki, S. Mohajerzadeh, M. Abdollahi, and M. Mehran, "Vertically aligned multiwall-carbon nanotubes to preferentially entrap highly metastatic cancerous cells," *Carbon*, vol. 50, no. 5, pp. 2010–2017, Apr. 2012, doi: 10.1016/j.carbon.2012.01.001.

[71]    Y. Katsumoto, K. Tatsumi, T. Doi, and K. Nakabe, "Electrical classification of single red blood cell deformability in high-shear microchannel flows," *Int. J. Heat Fluid Flow*, vol. 31, no. 6, pp. 985–995, Dec. 2010, doi: 10.1016/j.ijheatfluidflow.2010.02.019.

[72]    A. M. Dondorp, P. A. Kager, J. Vreeken, and N. J. White, "Abnormal blood flow and red blood cell deformability in severe malaria," *Parasitol. Today Pers. Ed*, vol. 16, no. 6, pp. 228–232, Jun. 2000.

[73]    Y. Zhao, S. Inayat, D. A. Dikin, J. H. Singer, R. S. Ruoff, and J. B. Troy, "Patch clamp technique: Review of the current state of the art and potential contributions from nanoengineering," *Proc. Inst. Mech. Eng. Part N J. Nanoeng. Nanosyst.*, vol. 222, no. 1, pp. 1–11, Mar. 2008, doi: 10.1243/17403499JNN149.

[74]    B. G. Kornreich, "The patch clamp technique: principles and technical considerations," *J. Vet. Cardiol. Off. J. Eur. Soc. Vet. Cardiol.*, vol. 9, no. 1, pp. 25–37, May 2007, doi: 10.1016/j.jvc.2007.02.001.

[75]    E. Neher and B. Sakmann, "The Patch Clamp Technique," *Sci. Am.*, vol. 266, no. 3, pp. 44–51, 1992.

[76]    B. Sakmann and E. Neher, "Patch clamp techniques for studying ionic channels in excitable membranes," *Annu. Rev. Physiol.*, vol. 46, pp. 455–472, 1984, doi: 10.1146/annurev.ph.46.030184.002323.

[77]    O. P. Hamill, A. Marty, E. Neher, B. Sakmann, and F. J. Sigworth, "Improved patch-clamp techniques for high-resolution current recording from cells and cell-free membrane patches," *Pflugers Arch.*, vol. 391, no. 2, pp. 85–100, Aug. 1981.

[78]    S. Veitinger, "The Patch-Clamp Technique," Nov. 2011. [Online] Available: https://www.leica-microsystems.com/science-lab/the-patch-clamp-technique/ [Accessed: 02-Mar-2020]

[79]    L. J. DeFelice, *Electrical Properties of Cells: Patch Clamp for Biologists*. pp. 7-48, Springer US, 1997.

[80]    J. Zhang, R. M. Davidson, M. D. Wei, and L. M. Loew, "Membrane electric properties by combined patch clamp and fluorescence ratio imaging in single neurons," *Biophys. J.*, vol. 74, no. 1, pp. 48–53, Jan. 1998, doi: 10.1016/S0006-3495(98)77765-3.

[81]    A. Marty and E. Neher, "Tight-Seal Whole-Cell Recording," in *Single-Channel Recording*, B. Sakmann and E. Neher, Eds. Boston, MA: Springer US, 1995, pp. 31–52.

[82]    D. Ogden and P. Stanfield, "Chapter 4 Patch clamp techniques for single channel and whole-cell recording." (1999). [Online] Available: https://www.semanticscholar.org/paper/Chapter-4-Patch-clamp-techniques-for-single-channel-OgdenStanfield/b5ed4637b8a1cb4af6d84297efcc510ef329 555f. [Accessed: 02-Mar-2020]

[83]    M. Karmazínová and L. Lacinová, "Measurement of cellular excitability by whole cell patch clamp technique," *Physiol. Res.*, vol. 59 Suppl 1, pp. S1-7, 2010. Available: https://pubmed.ncbi.nlm.nih.gov/20626213/ [Accessed: 26-Mar-2020].

[84]    N. J. Willumsen, M. Bech, S.-P. Olesen, B. S. Jensen, M. P. G. Korsgaard, and P. Christophersen, "High throughput electrophysiology: new perspectives for ion channel drug discovery," *Receptors Channels*, vol. 9, no. 1, pp. 3–12, 2003.

[85]    M. Bébarová, "Advances in patch clamp technique: towards higher quality and quantity," *Gen. Physiol. Biophys.*, vol. 31, no. 2, pp. 131–140, Jun. 2012, doi: 10.4149/gpb_2012_016.

[86]    M. R. Ahmad, M. Nakajima, T. Fukuda, S. Kojima, and M. Homma, "Single cells electrical characterizations using nanoprobe via ESEM-nanomanipulator system," in *2009 9th IEEE Conference on Nanotechnology (IEEE-NANO)*, pp. 589–592, 2009.

[87]    A. H. M. Sulaiman and M. R. Ahmad, "Rigid and Conductive Dual Nanoprobe for Single Cell Analysis," *J. Teknol.*, vol. 69, no. 8, pp. 107-113, Jul. 2014, doi: 10.11113/jt.v69.3304.

[88]    D. Esteban-Ferrer, M. A. Edwards, L. Fumagalli, A. Juárez, and G. Gomila, "Electric Polarization Properties of Single Bacteria Measured with Electrostatic Force Microscopy," *ACS Nano*, vol. 8, no. 10, pp. 9843–9849, Oct. 2014, doi: 10.1021/nn5041476.

[89]    A. H. M. Sulaiman and M. R. Ahmad, "Integrated dual nanoprobe-microfluidic system for single cell penetration," in *2013 IEEE International Conference on Control System, Computing and Engineering*, pp. 568–572, 2013, doi: 10.1109/ICCSCE.2013.6720029.

[90]    M. A. Unger, H. P. Chou, T. Thorsen, A. Scherer, and S. R. Quake, "Monolithic microfabricated valves and pumps by multilayer soft lithography," *Science*, vol. 288, no. 5463, pp. 113–116, Apr. 2000.

[91]    C. Hansen and S. R. Quake, "Microfluidics in structural biology: smaller, faster em leader better," *Curr. Opin. Struct. Biol.*, vol. 13, no. 5, pp. 538–544, Oct. 2003.

[92] D. R. Reyes, D. Iossifidis, P.-A. Auroux, and A. Manz, "Micro Total Analysis Systems. 1. Introduction, Theory, and Technology," *Anal. Chem.*, vol. 74, no. 12, pp. 2623–2636, Jun. 2002, doi: 10.1021/ac0202435.

[93] M. Javanmard and R. W. Davis, "A microfluidic platform for electrical detection of DNA hybridization," *Sens. Actuators B Chem.*, vol. 154, no. 1, pp. 22–27, May 2011, doi: 10.1016/j.snb.2010.03.067.

[94] L. Yang, Y. Li, C. L. Griffis, and M. G. Johnson, "Interdigitated microelectrode (IME) impedance sensor for the detection of viable Salmonella typhimurium," *Biosens. Bioelectron.*, vol. 19, no. 10, pp. 1139–1147, May 2004, doi: 10.1016/j.bios.2003.10.009.

[95] P. M. Valencia, O. C. Farokhzad, R. Karnik, and R. Langer, "Microfluidic technologies for accelerating the clinical translation of nanoparticles," *Nat. Nanotechnol.*, vol. 7, no. 10, pp. 623–629, Oct. 2012, doi: 10.1038/nnano.2012.168.

[96] W.-C. Tian and E. Finehout, *Microfluidics for Biological Applications*, 1st ed. Springer Publishing Company, Incorporated, 2008.

[97] L. Huang, P. Zhao, and W. Wang, "3D cell electrorotation and imaging for measuring multiple cellular biophysical properties," *Lab. Chip*, vol. 18, no. 16, pp. 2359–2368, Aug. 2018, doi: 10.1039/C8LC00407B.

[98] J. Yang, Y. Huang, X. Wang, X. B. Wang, F. F. Becker, and P. R. Gascoyne, "Dielectric properties of human leukocyte subpopulations determined by electrorotation as a cell separation criterion," *Biophys. J.*, vol. 76, no. 6, pp. 3307–3314, Jun. 1999.

[99] E. G. Cen, C. Dalton, Y. Li, S. Adamia, L. M. Pilarski, and K. V. I. S. Kaler, "A combined dielectrophoresis, traveling wave dielectrophoresis and electrorotation microchip for the manipulation and characterization of human malignant cells," *J. Microbiol. Methods*, vol. 58, no. 3, pp. 387–401, Sep. 2004, doi: 10.1016/j.mimet.2004.05.002.

[100] W. M. Arnold and U. Zimmermann, "Rotating-Field-Induced Rotation and Measurement of the Membrane Capacitance of Single Mesophyll Cells of Avena sativa," *Z. Für Naturforschung C*, vol. 37, no. 10, pp. 908–915, 2014, doi: 10.1515/znc-1982-1010.

[101] C. Dalton, A. D. Goater, J. P. H. Burt, and H. V. Smith, "Analysis of parasites by electrorotation," *J. Appl. Microbiol.*, vol. 96, no. 1, pp. 24–32, 2004, doi: 10.1046/j.1365-2672.2003.02113.x.

[102] J. P. Huang and K. W. Yu, "First-principles approach to electrorotation assay," *J. Phys. Condens. Matter*, vol. 14, no. 6, pp. 1213–1221, Feb. 2002, doi: 10.1088/0953-8984/14/6/308.

[103] T. B. Jones, "Basic theory of dielectrophoresis and electrorotation," *IEEE Eng. Med. Biol. Mag.*, vol. 22, no. 6, pp. 33–42, Nov. 2003, doi: 10.1109/MEMB.2003.1304999.

[104] J. P. Huang, K. W. Yu, and G. Q. Gu, "Electrorotation of a pair of spherical particles," *Phys. Rev. E Stat. Nonlin. Soft Matter Phys.*, vol. 65, no. 2, p. 021401, Feb. 2002, doi: 10.1103/PhysRevE.65.021401.

[105] H. Morgan and N. G. Green, "AC electrokinetics: colloids and nanoparticles," 2003. [Online]. Available: http://eprints.gla.ac.uk/33024/. [Accessed: 25-Mar-2019].

[106] Y. Zheng, J. Nguyen, Y. Wei, and Y. Sun, "Recent advances in microfluidic techniques for single-cell biophysical characterization," *Lab. Chip*, vol. 13, no. 13, pp. 2464–2483, Jun. 2013, doi: 10.1039/C3LC50355K.

[107] X. F. Zhou, G. H. Markx, and R. Pethig, "Effect of biocide concentration on electrorotation spectra of yeast cells," *Biochim. Biophys. Acta*, vol. 1281, no. 1, pp. 60–64, May 1996.

[108] R. Hölzel, "Non-invasive determination of bacterial single cell properties by electrorotation," *Biochim. Biophys. Acta*, vol. 1450, no. 1, pp. 53–60, May 1999.

[109] C. Dalton, A. D. Goater, J. Drysdale, and R. Pethig, "Parasite viability by electrorotation," *Colloids Surf. Physicochem. Eng. Asp.*, vol. 195, no. 1, pp. 263–268, Dec. 2001, doi: 10.1016/S0927-7757(01)00850-0.

[110] A. D. Goater, J. P. H. Burt, and R. Pethig, "A combined travelling wave dielectrophoresis and electrorotation device: applied to the concentration and viability determination of Cryptosporidium," *J. Phys. Appl. Phys.*, vol. 30, no. 18, pp. L65–L69, Sep. 1997, doi: 10.1088/0022-3727/30/18/001.

[111] C. Dalton, A. D. Goater, J. P. H. Burt, and H. V. Smith, "Analysis of parasites by electrorotation," *J. Appl. Microbiol.*, vol. 96, no. 1, pp. 24–32, 2004.

[112] D. H. Smetherman, "Screening, Imaging, and Image-Guided Biopsy Techniques for Breast Cancer," *Surg. Clin.*, vol. 93, no. 2, pp. 309–327, Apr. 2013, doi: 10.1016/j.suc.2013.01.004.

[113]  M. S. Linet *et al.*, "Cancer risks associated with external radiation from diagnostic imaging procedures," *CA. Cancer J. Clin.*, vol. 62, no. 2, pp. 75–100, Apr. 2012, doi: 10.3322/caac.21132.

[114]  "Radiography (Plain X-rays)," *Understanding Medical Radiation,* 2017. [Online]. Available: https://www.medicalradiation.com/types-of-medical-imaging/ imaging-using-x-rays/radiography-plain-x-rays/. [Accessed: 26-Mar-2019].

[115]  Y. Abbosh, "Breast Cancer Diagnosis using Microwave and Hybrid Imaging Methods," vol.5, no.3 pp. 41-48, 2014, doi:10.5121/ijcses.2014.5304.

[116]  H. Zhao, L. Zou, X. Geng, and S. Zheng, "Limitations of mammography in the diagnosis of breast diseases compared with ultrasonography: a single-center retrospective analysis of 274 cases," *Eur. J. Med. Res.*, vol. 20, no. 1, p. 49, Apr. 2015, doi: 10.1186/s40001-015-0140-6.

[117]  M. Morrow, J. Waters, and E. Morris, "MRI for breast cancer screening, diagnosis, and treatment," *Lancet Lond. Engl.*, vol. 378, no. 9805, pp. 1804–1811, Nov. 2011, doi: 10.1016/S0140-6736(11)61350-0.

[118]  B. Schweber "Magnetic resonance imaging (MRI), Part 1: How it works," *Analog IC Tips*, 11-Mar-2019. [Online]. Available: https://www.analogictips.com/magnetic-resonance-imaging-part-1-how-it-works-faq/. [Accessed: 26-Mar-2019].

[119]  H. D. Cheng, J. Shan, W. Ju, Y. Guo, and L. Zhang, "Automated Breast Cancer Detection and Classification Using Ultrasound Images: A Survey," *Pattern Recogn*, vol. 43, no. 1, pp. 299–317, Jan. 2010, doi: 10.1016/j.patcog.2009.05.012.

[120]  P. B. Gordon, "Ultrasound for breast cancer screening and staging," *Radiol. Clin. North Am.*, vol. 40, no. 3, pp. 431–441, May 2002.

[121]  F. M. Bengel, T. Higuchi, M. S. Javadi, and R. Lautamäki, "Cardiac Positron Emission Tomography," *J. Am. Coll. Cardiol.*, vol. 54, no. 1, pp. 1–15, Jun. 2009, doi: 10.1016/j.jacc.2009.02.065.

[122]  Md. Z. Mahmud, M. T. Islam, N. Misran, A. F. Almutairi, and M. Cho, "Ultra-Wideband (UWB) Antenna Sensor Based Microwave Breast Imaging: A Review," *Sensors*, vol. 18, no. 9, p. 2951, Sep. 2018, doi: 10.3390/s18092951.

[123]  G. M. Fiedler *et al.*, "Standardized peptidome profiling of human urine by magnetic bead separation and matrix-assisted laser desorption/ionization time-

of-flight mass spectrometry," *Clin. Chem.*, vol. 53, no. 3, pp. 421–428, Mar. 2007, doi: 10.1373/clinchem.2006.077834.

[124] H. L. Köhling *et al.*, "Direct identification of bacteria in urine samples by matrix-assisted laser desorption/ionization time-of-flight mass spectrometry and relevance of defensins as interfering factors," *J. Med. Microbiol.*, vol. 61, no. Pt 3, pp. 339–344, Mar. 2012, doi: 10.1099/jmm.0.032284-0.

[125] L. Ferreira, F. Sánchez-Juanes, J. L. Muñoz-Bellido, and J. M. González-Buitrago, "Rapid method for direct identification of bacteria in urine and blood culture samples by matrix-assisted laser desorption ionization time-of-flight mass spectrometry: intact cell vs. extraction method," *Clin. Microbiol. Infect. Off. Publ. Eur. Soc. Clin. Microbiol. Infect. Dis.*, vol. 17, no. 7, pp. 1007–1012, Jul. 2011, doi: 10.1111/j.1469-0691.2010.03339.x.

[126] L. Ferreira *et al.*, "Direct identification of urinary tract pathogens from urine samples by matrix-assisted laser desorption ionization-time of flight mass spectrometry," *J. Clin. Microbiol.*, vol. 48, no. 6, pp. 2110–2115, Jun. 2010, doi: 10.1128/JCM.02215-09.

[127] X.-H. Wang, G. Zhang, Y.-Y. Fan, X. Yang, W.-J. Sui, and X.-X. Lu, "Direct identification of bacteria causing urinary tract infections by combining matrix-assisted laser desorption ionization-time of flight mass spectrometry with UF-1000i urine flow cytometry," *J. Microbiol. Methods*, vol. 92, no. 3, pp. 231–235, Mar. 2013, doi: 10.1016/j.mimet.2012.12.016.

[128] D. G. Grier, "A revolution in optical manipulation," *Nature*, vol. 424, pp. 810–816, Aug. 2003, doi: 10.1038/nature01935.

[129] A. L. Birkbeck, R. A. Flynn, M. Ozkan, D. Song, M. Gross, and S. C. Esener, "VCSEL Arrays as Micromanipulators in Chip-Based Biosystems," *Biomed. Microdevices*, vol. 5, no. 1, pp. 47–54, Mar. 2003, doi: 10.1023/A:1024463316562.

[130] D. J. Odde and M. J. Renn, "Laser-guided direct writing of living cells," *Biotechnol. Bioeng.*, vol. 67, no. 3, pp. 312–318, 2000, doi: 10.1002/(SICI)1097-0290(20000205)67:3<312::AID-BIT7>3.0.CO;2-F.

[131] D. J. Odde and M. J. Renn, "Laser-guided direct writing for applications in biotechnology," *Trends Biotechnol.*, vol. 17, no. 10, pp. 385–389, Oct. 1999, doi: 10.1016/S0167-7799(99)01355-4.

[132] D. Bazou, G. P. Dowthwaite, I. M. Khan, C. W. Archer, J. R. Ralphs, and W. T. Coakley, "Gap junctional intercellular communication and cytoskeletal organization in chondrocytes in suspension in an ultrasound trap," *Mol.*

*Membr. Biol.*, vol. 23, no. 2, pp. 195–205, Apr. 2006, doi: 10.1080/09687860600555906.

[133] D. Bazou, L. A. Kuznetsova, and W. T. Coakley, "Physical enviroment of 2-D animal cell aggregates formed in a short pathlength ultrasound standing wave trap," *Ultrasound Med. Biol.*, vol. 31, no. 3, pp. 423–430, Mar. 2005, doi: 10.1016/j.ultrasmedbio.2004.12.007.

[134] M. Tanase, E. J. Felton, D. S. Gray, A. Hultgren, C. S. Chen, and D. H. Reich, "Assembly of multicellular constructs and microarrays of cells using magnetic nanowires," *Lab. Chip*, vol. 5, no. 6, pp. 598–605, Jun. 2005, doi: 10.1039/b500243e.

[135] K. Ino, A. Ito, and H. Honda, "Cell patterning using magnetite nanoparticles and magnetic force," *Biotechnol. Bioeng.*, vol. 97, no. 5, pp. 1309–1317, Aug. 2007, doi: 10.1002/bit.21322.

[136] G. H. Markx, "The use of electric fields in tissue engineering," *Organogenesis*, vol. 4, no. 1, pp. 11–17, 2008, doi: 10.4161/org.5799

[137] P. Linkov, M. Artemyev, A. E. Efimov, and I. Nabiev, "Comparative advantages and limitations of the basic metrology methods applied to the characterization of nanomaterials," *Nanoscale*, vol. 5, no. 19, pp. 8781–8798, Oct. 2013, doi: 10.1039/c3nr02372a.

[138] C. Henry, "XII. An account of some attempts to imitate the effects of the torpedo by electricity.," *Philos. Trans. R. Soc. Lond.*, vol. 66, pp. 196–225, Jan. 1776, doi: 10.1098/rstl.1776.0013.

[139] "G. S. Ohm (Five Papers, 1825-1853)," *JF Ptak Science Books Blog Bookstore* 2017. [Online]. Available: https://longstreet.typepad.com/books/2017 /08/georg-simon-ohm-five-papers-1825-1853.html. [Accessed: 07-May-2019].

[140] J. Bernstein and A. Tschermak, "Untersuchungen zur Thermodynamik der bioelektrischen Ströme," *Arch. Für Gesamte Physiol. Menschen Tiere*, vol. 112, no. 9, pp. 439–521, Jun. 1906, doi: 10.1007/BF01676972.

[141] R. Höber, "Eine Methode, die elektrische Leitfähigkeit im Innern von Zellen zu messen," *Pflüg. Arch. Für Gesamte Physiol. Menschen Tiere*, vol. 133, no. 4, pp. 237–253, Jul. 1910, doi: 10.1007/BF01680330.

[142] R. Höber, "Messungen der inneren Leitfähigkeit von Zellen," *Pflüg. Arch. Für Gesamte Physiol. Menschen Tiere*, vol. 150, no. 1, pp. 15–45, Feb. 1913, doi: 10.1007/BF01681047.

[143] V. Raicu and Y. Feldman, *Dielectric Relaxation in Biological Systems: Physical Principles, Methods, and Applications*. OUP Oxford, 2015.

[144] H. Fricke and S. Morse, "The Electric Resistance and Capacity of Blood for Frequencies Between 800 and 4½ Million Cycles," *J. Gen. Physiol.*, vol. 9, no. 2, pp. 153–167, Nov. 1925.

[145] K. S. Cole and R. F. Baker, "Longitudinal Impedance of the Squid Giant Axon," *J. Gen. Physiol.*, vol. 24, no. 6, pp. 771–788, Jul. 1941.

[146] R. Pethig and D. B. Kell, "The passive electrical properties of biological systems: their significance in physiology, biophysics and biotechnology," *Phys. Med. Biol.*, vol. 32, no. 8, pp. 933–970, Aug. 1987.

[147] H. P. Schwan, "Electrical properties of tissue and cell suspensions," *Adv. Biol. Med. Phys.*, vol. 5, pp. 147–209, 1957.

[148] "Kramers–Kronig relations," *Wikipedia,* 2005. [Online] Available: https://en.wikipedia.org/wiki/Kramers%E2%80%93Kronig_relations [Accessed: 02-Mar-2020]

[149] K. R. Waters, M. S. Hughes, J. Mobley, and J. G. Miller, "Differential forms of the Kramers-Kronig dispersion relations," *IEEE Trans. Ultrason. Ferroelectr. Fr Equation Control*, vol. 50, no. 1, pp. 68–76, Jan. 2003, doi: 10.1109/TUFFC.2003.1176526.

[150] J. S. Toll, "Causality and the Dispersion Relation: Logical Foundations," *Phys. Rev.*, vol. 104, no. 6, pp. 1760–1770, Dec. 1956, doi: 10.1103/PhysRev.104.1760.

[151] J. P. Grant, "Measurements, medical significance and applications of the dielectric properties of biological materials.," Doctoral, University of Surrey, Guildford, 1984.

[152] R. R. Pethig, *Dielectrophoresis: Theory, Methodology and Biological Applications*, vol.2, John Wiley & Sons, 2017.

[153] K. Asami, "Characterization of biological cells by dielectric spectroscopy," *J. Non Cryst. Solids*, vol. 305, pp. 268–277, Jul. 2002, doi: 10.1016/S0022-3093(02)01110-9.

[154] M. Gotz, L. Karsch, and J. Pawelke, "A new model for volume recombination in plane-parallel chambers in pulsed fields of high dose-per-pulse," *Phys. Med. Biol.*, vol. 62, no. 22, pp. 8634–8654, Nov. 2017, doi: 10.1088/1361-6560/aa8985.

[155] K. R. Foster and H. P. Schwan, "Dielectric properties of tissues and biological materials: a critical review," *Crit. Rev. Biomed. Eng.*, vol. 17, no. 1, pp. 25–104, 1989.

[156] M.-R. Tofighi, "Chapter 2 - Interaction between electromagnetic waves and biological materials," in *Principles and Applications of RF/Microwave in Healthcare and Biosensing*, C. Li, M.-R. Tofighi, D. Schreurs, and T.-S. J. Horng, Eds. Academic Press, pp. 53–101, 2017.

[157] S. Riniker, A.-P. E. Kunz, and W. F. van Gunsteren, "On the Calculation of the Dielectric Permittivity and Relaxation of Molecular Models in the Liquid Phase," *J. Chem. Theory Comput.*, vol. 7, no. 5, pp. 1469–1475, May 2011, doi: 10.1021/ct100610v.

[158] L. Gun, D. Ning, and Z. Liang, "Effective Permittivity of Biological Tissue: Comparison of Theoretical Model and Experiment," *Mathematical Problems in Engineering*, 2017. [Online]. Available: https://www.hindawi.com/journals/mpe/2017/7249672/. [Accessed: 06-May-2019].

[159] E. Talebian and M. Talebian, "A general review on the derivation of Clausius–Mossotti relation," *Optik*, vol. 124, no. 16, pp. 2324–2326, Aug. 2013, doi: 10.1016/j.ijleo.2012.06.090.

[160] N. E. Hill, *Dielectric properties and molecular behaviour*. London; New York: Van Nostrand Reinhold, 1969.

[161] Shodhganga, "Theories of Dielectric and Thermodynamic Parameters," INFLIBNET Centre, Gujarat, India, 2020, {online] Available: https://shodhganga.inflibnet.ac.in/bitstream/10603/8332/13/13_chapter%202.pdf. [Accessed: 02-Mar-2020].

[162] K. S. Cole and R. H. Cole, "Dispersion and Absorption in Dielectrics I. Alternating Current Characteristics," *J. Chem. Phys.*, vol. 9, pp. 341–351, Apr. 1941, doi: 10.1063/1.1750906.

[163] P. Debye, *"Polar Molecules"*, Chemical Catalog, New York, NY, USA, 1929.

[164] T. Sun and H. Morgan, "Single-cell microfluidic impedance cytometry: a review," *Microfluid. Nanofluidics*, vol. 8, no. 4, pp. 423–443, Apr. 2010, doi: 10.1007/s10404-010-0580-9.

[165] T. Hanai, N. Koizumi, and A. Irimajiri, "A method for determining the dielectric constant and the conductivity of membrane-bounded particles of biological relevance," *Biophys. Struct. Mech.*, vol. 1, no. 4, pp. 285–294, Dec. 1975, doi: 10.1007/BF00537642.

[166] T. Hanai, K. Asami, and N. Koizumi, "Dielectric Theory of Concentrated Suspensions of Shell-Spheres in Particular Reference to the Analysis of Biological Cell Suspensions," pp. 297–305, 1979. {online} Available: https://core.ac.uk/download/pdf/39209395.pdf. [Accessed: 18-Mar-2020].

[167] D. Das, F. A. Kamil, K. Biswas, and S. Das, "Evaluation of single cell electrical parameters from bioimpedance of a cell suspension," *RSC Adv.*, vol. 4, no. 35, pp. 18178–18185, Apr. 2014, doi: 10.1039/C4RA00400K.

[168] J. C. Maxwell, "A Treatise on Electricity and Magnetism." vol.1, Macmillan and Co. Publishing, London, 1873.

[169] M. Apostol, *Magnetic and Electric Resonance*. vol. 2, Cambridge Scholars Publishing, 2018.

[170] "The Clausius–Mossotti Factor," in *Dielectrophoresis*, John Wiley & Sons, Ltd, 2017, pp. 119–144.

[171] K. W. Wagner, "Erklärung der dielektrischen Nachwirkungsvorgänge auf Grund Maxwellscher Vorstellungen," *Arch. Für Elektrotechnik*, vol. 2, no. 9, pp. 371–387, Sep. 1914, doi: 10.1007/BF01657322.

[172] T. Hanai, "Theory of the dielectric dispersion due to the interfacial polarization and its application to emulsions," *Kolloid-Z.*, vol. 171, no. 1, pp. 23–31, Jul. 1960, doi: 10.1007/BF01520320.

[173] A. Irimajiri, Y. Doida, T. Hanai, and A. Inouye, "Passive electrical properties of cultured murine lymphoblast (L5178Y) with reference to its cytoplasmic membrane, nuclear envelope, and intracellular phases," *J. Membr. Biol.*, vol. 38, no. 3, pp. 209–232, Jan. 1978.

[174] T. Hanai, H. Z. Zhang, K. Sekine, K. Asaka, and K. Asami, "The number of interfaces and the associated dielectric relaxations in heterogeneous systems," *Ferroelectrics*, vol. 86, no. 1, pp. 191–204, Oct. 1988, doi: 10.1080/00150198808227014.

[175] M. Sahay, S. Kalra, and T. Bandgar, "Renal endocrinology: The new frontier," *Indian J. Endocrinol. Metab.*, vol. 16, no. 2, pp. 154–155, 2012, doi: 10.4103/2230-8210.93729.

[176] R. Thomas, A. Kanso, and J. R. Sedor, "Chronic kidney disease and its complications," *Prim. Care*, vol. 35, no. 2, pp. 329–344, vii, Jun. 2008, doi: 10.1016/j.pop.2008.01.008.

[177] National Kidney Foundation-Executive Summary, "KDOQI Clinical Practice Guidelines and Clinical Practice Recommendations for Anemia in Chronic

Kidney Disease," *Am. J. Kidney Dis. Off. J. Natl. Kidney Found.*, vol. 47, no. 5 Suppl 3, pp. S11-145, May 2006, doi: 10.1053/j.ajkd.2006.03.010.

[178] J. Coresh, B. C. Astor, T. Greene, G. Eknoyan, and A. S. Levey, "Prevalence of chronic kidney disease and decreased kidney function in the adult US population: Third National Health and Nutrition Examination Survey," *Am. J. Kidney Dis. Off. J. Natl. Kidney Found.*, vol. 41, no. 1, pp. 1–12, Jan. 2003, doi: 10.1053/ajkd.2003.50007.

[179] L. G. Feld, W. R. Waz, L. M. Pérez, and D. B. Joseph, "Hematuria. An integrated medical and surgical approach," *Pediatr. Clin. North Am.*, vol. 44, no. 5, pp. 1191–1210, Oct. 1997.

[180] G. D. Grossfeld *et al.*, "Asymptomatic microscopic hematuria in adults: summary of the AUA best practice policy recommendations," *Am. Fam. Physician*, vol. 63, no. 6, pp. 1145–1154, Mar. 2001.

[181] K. H. Pade and D. R. Liu, "An evidence-based approach to the management of hematuria in children in the emergency department," *Pediatr. Emerg. Med. Pract.*, vol. 11, no. 9, pp. 1–13, Sep. 2014. Available: https://pubmed.ncbi.nlm.nih.gov/25296518/ [Accessed: 02-Jun-2020].

[182] S. M. Jalalah, I. H. Alzahrani, and P. N. Furness, "Glomerular changes in microscopic haematuria, studied by quantitative immunoelectron microscopy and in situ zymography," *Nephrol. Dial. Transplant. Off. Publ. Eur. Dial. Transpl. Assoc. - Eur. Ren. Assoc.*, vol. 17, no. 9, pp. 1586–1593, Sep. 2002.

[183] R. J. Johnson *et al.*, "Morphologic correlates of glomerular oxidant injury induced by the myeloperoxidase-hydrogen peroxide-halide system of the neutrophil," *Lab. Investig. J. Tech. Methods Pathol.*, vol. 58, no. 3, pp. 294–301, Mar. 1988.

[184] M. C. M. Vissers and C. C. Winterbourn, "Gelatinase Contributes to the Degradation of Glomerular Basement Membrane Collagen by Human Neutrophils," *Coll. Relat. Res.*, vol. 8, no. 2, pp. 113–122, Mar. 1988, doi: 10.1016/S0174-173X(88)80023-2.

[185] M. J. Tracz, J. Alam, and K. A. Nath, "Physiology and pathophysiology of heme: implications for kidney disease," *J. Am. Soc. Nephrol. JASN*, vol. 18, no. 2, pp. 414–420, Feb. 2007, doi: 10.1681/ASN.2006080894.

[186] J. M. Rifkind and E. Nagababu, "Hemoglobin Redox Reactions and Red Blood Cell Aging," *Antioxid. Redox Signal.*, vol. 18, no. 17, pp. 2274–2283, Jun. 2013, doi: 10.1089/ars.2012.4867.

[187] Y. I. Miller, S. M. Altamentova, and N. Shaklai, "Oxidation of low-density lipoprotein by hemoglobin stems from a heme-initiated globin radical: antioxidant role of haptoglobin," *Biochemistry*, vol. 36, no. 40, pp. 12189–12198, Oct. 1997, doi: 10.1021/bi970258a.

[188] E. Homsi, P. Janino, and J. B. L. de Faria, "Role of caspases on cell death, inflammation, and cell cycle in glycerol-induced acute renal failure," *Kidney Int.*, vol. 69, no. 8, pp. 1385–1392, Apr. 2006, doi: 10.1038/sj.ki.5000315.

[189] T. Shima, "Hematuria is a risk factor towards end-stage renal disease - A propensity score analysis," *Nephrol. Ren. Dis.*, vol. 2, no. 2, pp. 1-6, 2017, doi: 10.15761/NRD.1000120.

[190] J. A. Moreno *et al.*, "Haematuria: the forgotten CKD factor?," *Nephrol. Dial. Transplant. Off. Publ. Eur. Dial. Transpl. Assoc. - Eur. Ren. Assoc.*, vol. 27, no. 1, pp. 28–34, Jan. 2012, doi: 10.1093/ndt/gfr749.

[191] K. D. Phadke, M. Vijayakumar, J. Sharma, A. Iyengar, and Indian Pediatric Nephrology Group, "Consensus statement on evaluation of hematuria," *Indian Pediatr.*, vol. 43, no. 11, pp. 965–973, Nov. 2006.

[192] P. Veerreddy, "Hemoglobinuria Misidentified as Hematuria: Review of Discolored Urine and Paroxysmal Nocturnal Hemoglobinuria," *Clin. Med. Insights*, vol. 6, pp. 7–17, Jun. 2013, doi: 10.4137/CMBD.S11517.

[193] P. Kincaid-Smith and K. Fairley, "The investigation of hematuria," *Semin. Nephrol.*, vol. 25, no. 3, pp. 127–135, May 2005.

[194] S. C. Freni, G. J. Heederik, and C. Hol, "Centrifugation techniques and reagent strips in the assessment of microhaematuria," *J. Clin. Pathol.*, vol. 30, no. 4, pp. 336–340, Apr. 1977.

[195] W. W. Jou and R. D. Powers, "Utility of dipstick urinalysis as a guide to management of adults with suspected infection or hematuria," *South. Med. J.*, vol. 91, no. 3, pp. 266–269, Mar. 1998.

[196] A. Bataille, M. Wetzstein, A. Hertig, S. Vimont, E. Rondeau, and P. Galichon, "Evidence of dipstick superiority over urine microscopy analysis for detection of hematuria," *BMC Res. Notes*, vol. 9, no. 1, p. 435 Sep. 2016, doi: 10.1186/s13104-016-2240-y.

[197] V. Khejonnit, B. Pratumvinit, K. Reesukumal, S. Meepanya, C. Pattanavin, and P. Wongkrajang, "Optimal criteria for microscopic review of urinalysis following use of automated urine analyzer," *Clin. Chim. Acta Int. J. Clin. Chem.*, vol. 439, pp. 1–4, Jan. 2015, doi: 10.1016/j.cca.2014.09.027.

[198] Z. Zaman, G. B. Fogazzi, G. Garigali, M. D. Croci, G. Bayer, and T. Kránicz, "Urine sediment analysis: Analytical and diagnostic performance of sediMAX - a new automated microscopy image-based urine sediment analyser," *Clin. Chim. Acta Int. J. Clin. Chem.*, vol. 411, no. 3–4, pp. 147–154, Feb. 2010, doi: 10.1016/j.cca.2009.10.018.

[199] F. D. İnce, H. Y. Ellidağ, M. Koseoğlu, N. Şimşek, H. Yalçın, and M. O. Zengin, "The comparison of automated urine analyzers with manual microscopic examination for urinalysis automated urine analyzers and manual urinalysis," *Pract. Lab. Med.*, vol. 5, pp. 14–20, Aug. 2016, doi: 10.1016/j.plabm.2016.03.002.

[200] M. A. Ahmad, F. Mustafa, L. M. Ali, and T. A. Rizvi, "Virus detection and quantification using electrical parameters," *Sci. Rep.*, vol. 4, p. 6831, Oct. 2014, doi: 10.1038/srep06831.

[201] M. Wolf, R. Gulich, P. Lunkenheimer, and A. Loidl, "Broadband dielectric spectroscopy on human blood," *Biochim. Biophys. Acta BBA - Gen. Subj.*, vol. 1810, no. 8, pp. 727–740, Aug. 2011, doi: 10.1016/j.bbagen.2011.05.012.

[202] P. S. Mun, H. N. Ting, T. A. Ong, C. M. Wong, K. H. Ng, and Y. B. Chong, "A Study of Dielectric Properties of Proteinuria between 0.2 GHz and 50 GHz," *PLOS ONE*, vol. 10, no. 6, p. e0130011, Jun. 2015, doi: 10.1371/journal.pone.0130011.

[203] H. N. Ting, P. S. Mun, T. A. Ong, Y. B. Chong, and K. H. Ng, "Dielectric Properties of Urine for Diabetes Mellitus and Chronic Kidney Disease between 0.2 GHz and 50 GHz," in *World Congress on Medical Physics and Biomedical Engineering, June 7-12, 2015, Toronto, Canada*, 2015, pp. 1257–1260.

[204] A. Lonappan, V. Hamsakkutty, G. Bindu, J. Jacob, V. Thomas, and K. T. Mathew, "Dielectric properties of human urine at microwave frequencies," *Microw. Opt. Technol. Lett.*, vol. 42, no. 6, pp. 500–503, 2004, doi: 10.1002/mop.20349.

[205] A. Lonappan, G. Bindu, V. Thomas, J. Jacob, C. Rajasekaran, and K. T. Mathew, "Diagnosis of Diabetes Mellitus using Microwaves," *J. Electromagn. Waves Appl.*, vol. 21, no. 10, pp. 1393–1401, Jan. 2007, doi: 10.1163/156939307783239429.

[206] P. S. Mun, H. N. Ting, Y. B. Chong, and T. A. Ong, "Dielectric properties of glycosuria at 0.2-50 GHz using microwave spectroscopy," *J. Electromagn. Waves Appl.*, vol. 29, no. 17, pp. 2278–2292, Nov. 2015, doi: 10.1080/09205071.2015.1072480.

[207] P. S. Mun, H. N. Ting, S. M. Mirhassani, T. A. Ong, C. M. Wong, and Y. B. Chong, "Prediction of chronic kidney disease using urinary dielectric properties and support vector machine," *J. Microw. Power Electromagn. Energy*, vol. 50, no. 3, pp. 201–213, Jul. 2016, doi: 10.1080/08327823.2016.1230927.

[208] T. A. Larsen and W. Gujer, "Separate management of anthropogenic nutrient solutions (human urine)," *Water Sci. Technol.*, vol. 34, no. 3, pp. 87–94, Jan. 1996, doi: 10.1016/0273-1223(96)00560-4.

[209] I. Fittschen and H. H. Hahn, "Characterization of the municipal wastewaterpart human urine and a preliminary comparison with liquid cattle excretion," *Water Sci. Technol.*, vol. 38, no. 6, pp. 9–16, Jan. 1998, doi: 10.1016/S0273-1223(98)00562-9.

[210] H. L. Mobley and R. P. Hausinger, "Microbial ureases: significance, regulation, and molecular characterization," *Microbiol. Rev.*, vol. 53, no. 1, pp. 85–108, Mar. 1989.

[211] Z. Liu, Q. Zhao, K. Wang, D. Lee, W. Qiu, and J. Wang, "Urea hydrolysis and recovery of nitrogen and phosphorous as MAP from stale human urine," *J. Environ. Sci.*, vol. 20, no. 8, pp. 1018–1024, Jan. 2008, doi: 10.1016/S1001-0742(08)62202-0.

[212] P. Froom, B. Bieganiec, Z. Ehrenrich, and M. Barak, "Stability of common analytes in urine refrigerated for 24 h before automated analysis by test strips," *Clin. Chem.*, vol. 46, no. 9, pp. 1384–1386, Sep. 2000.

[213] X. You, M. Misra, S. Gregori, and A. K. Mohanty, "Preparation of an Electric Double Layer Capacitor (EDLC) Using Miscanthus-Derived Biocarbon," *ACS Sustain. Chem. Eng.*, vol. 6, no. 1, pp. 318–324, Jan. 2018, doi: 10.1021/acssuschemeng.7b02563.

[214] S. Abdalla, S. S. Al-ameer, and S. H. Al-Magaishi, "Electrical properties with relaxation through human blood," *Biomicrofluidics*, vol. 4, no. 3, pp 034101(1-16), Jul. 2010, doi: 10.1063/1.3458908.

[215] H. A. Fink *et al.*, "Medical management to prevent recurrent nephrolithiasis in adults: a systematic review for an American College of Physicians Clinical Guideline," *Ann. Intern. Med.*, vol. 158, no. 7, pp. 535–543, Apr. 2013, doi: 10.7326/0003-4819-158-7-201304020-00005.

[216] S. H. Obligado and D. S. Goldfarb, "The association of nephrolithiasis with hypertension and obesity: a review," *Am. J. Hypertens.*, vol. 21, no. 3, pp. 257–264, Mar. 2008, doi: 10.1038/ajh.2007.62.

[217] C. D. Scales, A. C. Smith, J. M. Hanley, C. S. Saigal, and Urologic Diseases in America Project, "Prevalence of kidney stones in the United States," *Eur. Urol.*, vol. 62, no. 1, pp. 160–165, Jul. 2012, doi: 10.1016/j.eururo.2012.03.052.

[218] E. N. Taylor, M. J. Stampfer, and G. C. Curhan, "Diabetes mellitus and the risk of nephrolithiasis," *Kidney Int.*, vol. 68, no. 3, pp. 1230–1235, Sep. 2005, doi: 10.1111/j.1523-1755.2005.00516.x.

[219] M. Daudon and P. Jungers, "Diabetes and nephrolithiasis," *Curr. Diab. Rep.*, vol. 7, no. 6, pp. 443–448, Dec. 2007.

[220] J. C. Lieske *et al.*, "Diabetes mellitus and the risk of urinary tract stones: a population-based case-control study," *Am. J. Kidney Dis. Off. J. Natl. Kidney Found.*, vol. 48, no. 6, pp. 897–904, Dec. 2006, doi: 10.1053/j.ajkd.2006.09.002.

[221] E. N. Taylor, M. J. Stampfer, and G. C. Curhan, "Obesity, weight gain, and the risk of kidney stones," *JAMA*, vol. 293, no. 4, pp. 455–462, Jan. 2005, doi: 10.1001/jama.293.4.455.

[222] F. P. Cappuccio, P. Strazzullo, and M. Mancini, "Kidney stones and hypertension: population based study of an independent clinical association.," *BMJ*, vol. 300, no. 6734, pp. 1234–1236, May 1990.

[223] N. Johri, B. Cooper, W. Robertson, S. Choong, D. Rickards, and R. Unwin, "An update and practical guide to renal stone management," *Nephron Clin. Pract.*, vol. 116, no. 3, pp. c159-171, 2010, doi: 10.1159/000317196.

[224] J. Shoag, J. Halpern, D. S. Goldfarb, and B. H. Eisner, "Risk of chronic and end stage kidney disease in patients with nephrolithiasis," *J. Urol.*, vol. 192, no. 5, pp. 1440–1445, Nov. 2014, doi: 10.1016/j.juro.2014.05.117.

[225] M. T. Keddis and A. D. Rule, "Nephrolithiasis and loss of kidney function," *Curr. Opin. Nephrol. Hypertens.*, vol. 22, no. 4, pp. 390–396, Jul. 2013, doi: 10.1097/MNH.0b013e32836214b9.

[226] Z. M. El-Zoghby *et al.*, "Urolithiasis and the risk of ESRD," *Clin. J. Am. Soc. Nephrol. CJASN*, vol. 7, no. 9, pp. 1409–1415, Sep. 2012, doi: 10.2215/CJN.03210312.

[227] A. D. Rule, A. E. Krambeck, and J. C. Lieske, "Chronic kidney disease in kidney stone formers," *Clin. J. Am. Soc. Nephrol. CJASN*, vol. 6, no. 8, pp. 2069–2075, Aug. 2011, doi: 10.2215/CJN.10651110.

[228] B. Finlayson, "Physicochemical aspects of urolithiasis," *Kidney Int.*, vol. 13, no. 5, pp. 344–360, May 1978, doi: 10.1038/ki.1978.53.

[229] V. K. Singh and P. K. Rai, "Kidney stone analysis techniques and the role of major and trace elements on their pathogenesis: a review," *Biophys. Rev.*, vol. 6, no. 3–4, pp. 291–310, Dec. 2014, doi: 10.1007/s12551-014-0144-4.

[230] D. Bazin, P. Chevallier, G. Matzen, P. Jungers, and M. Daudon, "Heavy elements in urinary stones," *Urol. Res.*, vol. 35, no. 4, pp. 179–184, Aug. 2007, doi: 10.1007/s00240-007-0099-z.

[231] I. H. Atakan, M. Kaplan, G. Seren, T. Aktoz, H. Gül, and O. Inci, "Serum, urinary and stone zinc, iron, magnesium and copper levels in idiopathic calcium oxalate stone patients," *Int. Urol. Nephrol.*, vol. 39, no. 2, pp. 351–356, Jun. 2007, doi: 10.1007/s11255-006-9050-4.

[232] D. Bazin, E. Letavernier, J.-P. Haymann, F. Tielens, A. Kellum, and M. Daudon, "Shedding light on the morphology of calcium oxalate monohydrate crystallites present in kidney biopsies in the case of hyperoxaluria," *Comptes Rendus Chim.*, vol. 19, no. 11, pp. 1548–1557, Nov. 2016, doi: 10.1016/j.crci.2016.02.004.

[233] M. Daudon, J.-C. Doré, P. Jungers, and B. Lacour, "Changes in stone composition according to age and gender of patients: a multivariate epidemiological approach," *Urol. Res.*, vol. 32, no. 3, pp. 241–247, Jun. 2004, doi: 10.1007/s00240-004-0421-y.

[234] G. Schubert, "Stone analysis," *Urol. Res.*, vol. 34, no. 2, pp. 146–150, Apr. 2006, doi: 10.1007/s00240-005-0028-y.

[235] G. P. Kasidas, C. T. Samuell, and T. B. Weir, "Renal stone analysis: why and how?," *Ann. Clin. Biochem.*, vol. 41, no. Pt 2, pp. 91–97, Mar. 2004, doi: 10.1258/000456304322879962.

[236] D. Bazin, M. Daudon, C. Combes, and C. Rey, "Characterization and some physicochemical aspects of pathological microcalcifications," *Chem. Rev.*, vol. 112, no. 10, pp. 5092–5120, Oct. 2012, doi: 10.1021/cr200068d.

[237] V. K. Singh and A. K. Rai, "Prospects for laser-induced breakdown spectroscopy for biomedical applications: a review," *Lasers Med. Sci.*, vol. 26, no. 5, pp. 673–687, Sep. 2011, doi: 10.1007/s10103-011-0921-2.

[238] E. Moreno-Gordaliza *et al.*, "Elemental bioimaging in kidney by LA-ICP-MS as a tool to study nephrotoxicity and renal protective strategies in cisplatin

therapies," *Anal. Chem.*, vol. 83, no. 20, pp. 7933–7940, Oct. 2011, doi: 10.1021/ac201933x.

[239] M. Daudon and D. Bazin, "When the Synchrotron radiations highlight the Randall's plaques and kidney concretions," *J. Phys. Conf. Ser.*, vol. 425, no. 2, p. 022006, 2013, doi: 10.1088/1742-6596/425/2/022006.

[240] A. Basiri, M. Taheri, and F. Taheri, "What is the state of the stone analysis techniques in urolithiasis?," *Urol. J.*, vol. 9, no. 2, pp. 445–454, 2012.

[241] C. A. Wagner and N. Mohebbi, "Urinary pH and stone formation," *J. Nephrol.*, vol. 23 Suppl 16, pp. S165-169, Dec. 2010.

[242] P. G. Rainsbury, M. Fabricius, and E. McLarty, "Management of Urinary Incontinence in Primary Care," *InnovAiT*, vol. 4, no. 1, pp. 23–30, Jan. 2011, doi: 10.1093/innovait/inq041.

[243] "Urine pH: Normal ranges and what they mean," *Medical News Today,* 2018. [Online]. Available: https://www.medicalnewstoday.com/articles/323957.php. [Accessed: 12-Mar-2019].

[244] K. Ananth, J. P. Kavanagh, R. C. Walton, and P. N. Rao, "Enlargement of calcium oxalate stones to clinically significant size in an in-vitro stone generator," *BJU Int.*, vol. 90, no. 9, pp. 939–944, Dec. 2002.

[245] "Oxalate (Urine) - Health Encyclopedia - University of Rochester Medical Center, 2020." [Online]. Available: https://www.urmc.rochester.edu/ encyclopedia/content.aspx?contenttypeid=167&contentid=oxalate_urine. [Accessed: 25-Jul-2018].

[246] G. Bihl and A. Meyers, "Recurrent renal stone disease-advances in pathogenesis and clinical management," *Lancet Lond. Engl.*, vol. 358, no. 9282, pp. 651–656, Aug. 2001, doi: 10.1016/S0140-6736(01)05782-8.

[247] M. Daudon, E. Letavernier, V. Frochot, J.-P. Haymann, D. Bazin, and P. Jungers, "Respective influence of calcium and oxalate urine concentration on the formation of calcium oxalate monohydrate or dihydrate crystals," *Comptes Rendus Chim.*, vol. 19, no. 11, pp. 1504–1513, Nov. 2016, doi: 10.1016/j.crci.2016.08.009.

[248] A. Conte, C. Genestar, and F. Grases, "Relation between calcium oxalate hydrate form found in renal calculi and some urinary parameters," *Urol. Int.*, vol. 45, no. 1, pp. 25–27, 1990, doi: 10.1159/000281653.

[249] D. M. Roxe, "Urinalysis," in *Clinical Methods: The History, Physical, and Laboratory Examinations*, 3rd ed., H. K. Walker, W. D. Hall, and J. W. Hurst, Eds. Boston: Butterworths, 1990.

[250] H. T. F. Barniville and R. Misk, "Urinary Glucuronic Acid Excretion in Liver Disease and the Effect of a Salicylamide Load," *Br Med J*, vol. 1, no. 5118, pp. 337–340, Feb. 1959, doi: 10.1136/bmj.1.5118.337.

[251] J. D. Williams and G. A. Coles, "Proteinuria--a direct cause of renal morbidity?," *Kidney Int.*, vol. 45, no. 2, pp. 443–450, Feb. 1994.

[252] "Specific Gravity: Reference Range, Interpretation, Collection and Panels," Aug. 2018. [Online]. Available: https://emedicine.medscape.com/article/2090711-overviewhttps://www.analogictips.com/magnetic-resonance-imaging-part-1-how-it-works-faq/. [Accessed: 18-Mar-2020].

[253] J. Golowasch *et al.*, "Membrane capacitance measurements revisited: dependence of capacitance value on measurement method in nonisopotential neurons," *J. Neurophysiol.*, vol. 102, no. 4, pp. 2161–2175, Oct. 2009, doi: 10.1152/jn.00160.2009.

[254] M. C. R. Medeiros *et al.*, "An electrical method to measure low-frequency collective and synchronized cell activity using extracellular electrodes," *Sens. Bio-Sens. Res.*, vol. 10, pp. 1–8, Sep. 2016, doi: 10.1016/j.sbsr.2016.06.002.

[255] J. Z. Bao, C. C. Davis, and R. E. Schmukler, "Frequency domain impedance measurements of erythrocytes. Constant phase angle impedance characteristics and a phase transition," *Biophys. J.*, vol. 61, no. 5, pp. 1427–1434, May 1992, doi: 10.1016/S0006-3495(92)81948-3.

[256] C. F. Habeger, C. E. Condon, S. R. Khan, and J. H. Adair, "Evaluation of the calcium oxalate monohydrate Hamaker constant based on static dielectric constant determination and electronic polarization," *Colloids Surf. B Biointerfaces*, vol. 10, no. 1, pp. 13–21, Oct. 1997, doi: 10.1016/S0927-7765(97)00044-1.

[257] T. Szarvas *et al.*, "Deletion analysis of tumor and urinary DNA to detect bladder cancer: urine supernatant versus urine sediment," *Oncol. Rep.*, vol. 18, no. 2, pp. 405–409, Aug. 2007.

[258] R. C. Dolscheid-Pommerich, U. Klarmann-Schulz, R. Conrad, B. Stoffel-Wagner, and B. Zur, "Evaluation of the appropriate time period between sampling and analyzing for automated urinalysis," *Biochem. Medica*, vol. 26, no. 1, pp. 82–89, Feb. 2016, doi: 10.11613/BM.2016.008.

[259] M. Takagi and N. Tokunaga, "Noninvasive discrimination between human normal and cancer cells by analysis of intracellular distribution of phase-shift data," *Cytotechnology*, vol. 67, no. 4, pp. 733–739, Aug. 2015, doi: 10.1007/s10616-015-9865-x.

[260] M. Lekka, "Discrimination Between Normal and Cancerous Cells Using AFM," *BioNanoScience*, vol. 6, pp. 65–80, 2016, doi: 10.1007/s12668-016-0191-3.

[261] A. R. Lima *et al.*, "Discrimination between the human prostate normal and cancer cell exometabolome by GC-MS," *Sci. Rep.*, vol. 8, no. 1, pp. 1–12, Apr. 2018, doi: 10.1038/s41598-018-23847-9.

[262] F. E. Giana, F. J. Bonetto, and M. I. Bellotti, "Assay based on electrical impedance spectroscopy to discriminate between normal and cancerous mammalian cells," *Phys. Rev. E*, vol. 97, no. 3–1, p. 032410, Mar. 2018, doi: 10.1103/PhysRevE.97.032410.

[263] I. E. Khuda, "Feasibility of the Detection of Breast Cancer Using Ultra-Wide Band (UWB) Technology in Comparison with Other Screening Techniques," *UWB Technol. Its Appl.*, Nov. 2018, doi: 10.5772/intechopen.79679.

# List of Publications

- N. Nasir, S. Raji, F. Mustafa, T. A. Rizvi, Z. A. Natour, A. H. A. Naqbi and M. A. Ahmad, "Electrical Detection of Blood Cells in Urine" - vol. 6, no. 1, pp. e03102 (1-10), Jan 2020.

- N. Nasir and M. A. Ahmad, "Cells Electrical Characterization: Dielectric Properties, Mixture and Modelling theories" *Journal of Engineering*, vol. 2020, no. 1, pp. 9475490 (1-17), Jan 2020.

- M. A. Ahmad, A. Najar, A. Moutaouakil, N. Nasir, M. Hussein, S. Raji and A. H. Naqbi, "Label-Free Cancer Cells Detection using Optical Sensors" *IEEE Access*, vol 6, pp. 55807-55814, 2018.

- N. Nasir, M. A. Ahmad and A. A. Murad, "Capacitive Detection and Quantification of Water Suspended Solids" *The International Conference on Electrical and Computing Technologies and Applications (ICECTA),* UAE, Nov 2019.

- N. Nasir and M. A. Ahmad, "Optical Characterization of Calcium Oxalate Hydrate in Urine" *5th IEEE International Conference on Engineering Technologies and Applied Sciences (ICETAS),* Thailand, Nov 2018.

- N. Nasir, M. A. Ahmad, A. Najar, "Optical Detection of Dissolved Solids in Water Samples" *5th IEEE International Conference on Engineering Technologies and Applied Sciences (ICETAS),* Thailand, Nov 2018.

- N. Nasir, M. Al Ahmad, "Measuring transmittance of human female breast cells through spectrophotometry and generating its equivalent circuit by prony modelling," *4th IEEE International Conference on Engineering Technologies and Applied Sciences (ICETAS),* Bahrain, Dec (2017).

# Appendix

Table A.1: Differentiation of Diverse Electric Field Procedures for Cell Manipulation [136]

| Force Field | Equipment needed | Spatial resolution achievable | Field effect on the cell viability | Manipulation directly in the growth medium? | Number of cells that can be manipulated simultaneously | Typical volume handled |
|---|---|---|---|---|---|---|
| Optical | -Microscope -NIR laser -Motorized stage | very high, nanometers | -Low heating | Possible | Few hundreds of cells | pL |
| Electrical | Microelectrodes -Frequency generator | typically micrometers | -Heating -Breaking down of the membrane at high fields | Challenging | Single cell to millions of cells | µL-mL |
| Magnetic | -Magnet | typically micrometers | -Needs magnetizable cells; otherwise negligible | Possible | Single cell to millions of cells | µL-mL |
| Ultrasound | -Resonance chamber -Resonance-based piezoelectric transducer -1–10 MHz frequency range | low, tens of micrometers | Slight | Possible | Multimillions of cells | mL |

Table A.2: Comparison of Basic Nanometrology Techniques, Electron Microscopy Methods [137]

| ELECTRON MICROSCOPY METHODS | | |
|---|---|---|
| Approaches | Scanning Electron Microscopy | Transmission Electron Microscopy |
| Nano-system Analyzed | -Atomically flat surfaces<br>-nanoparticles<br>-nanocrystals<br>-multilayered materials<br>-nanowires<br>-carbon nanotubes<br>-nanofibers<br>-biomolecules | -Clusters<br>-biomolecules<br>-nanocrystals<br>-nanotubes<br>-nanoparticles<br>-quantum dots<br>-nanowires<br>-dendrimers |
| Parameter Measured | -Topography<br>-morphology<br>-composition<br>-crystallography | -Morphology<br>-crystallography<br>-compositional data<br>-phase data<br>-topography<br>-elemental mapping |
| Resolution | -0.5–5 nm depth,<br>-1–20 nm (lateral) | -0.1 nm (lateral) |
| Problems | -SEM requires conductive samples<br>-needs high vacuum<br>- wet materials and biological samples | -Thickness bound is 200 nm<br>-time consuming<br>-small field of view<br>-electron beam can damage biological portions<br>-for atomic-scale resolution ultrahigh vacuum is required<br>-light atoms exhibit contrast |

Table A.3: Comparison of Basic Nanometrology Techniques, Scanning Probe
Microscopy Methods [137]

| SCANNING PROBE MICROSCOPY METHODS | | |
|---|---|---|
| Methods | Scanning Tunneling Microscopy (STM) | Atomic Force Microscopy (AFM) or Scanning Force Microscopy |
| Nanosystem Analyzed | -Conductive materials<br>-nanocrystals<br>-thin films<br>-nanotubes<br>-molecules | -Conductive and nonconductive materials<br>-nanocrystals<br>-nanotubes<br>-biological samples |
| Parameter Measured | Surface-oriented:<br>-topology<br>-properties<br>-structures<br>-reactions<br>-faults | -Topography<br>-total density<br>-morphology<br>-frictional characteristics<br>-elasticity of the surface<br>-magnetic characteristics of the surface<br>-specific molecular interactions |
| Resolution | -0.5–5 nm depth<br>-2–10 nm (lateral) | -0.5–5 nm depth<br>-0.2–10.0 nm (lateral) |
| Problems | - conductive samples<br>- noise reduction required | - small scan image size<br>- scanning speed is restricted<br>- slow rate of scanning leads to thermal drift<br>- images affected by hysteresis property of the piezoelectric material |

Table A.4: Comparison of Basic Nanometrology Techniques, Optical Methods [137]

| OPTIC METHODS | | |
|---|---|---|
| Methods | Dynamic Light Scattering And Fluorescence Correlation Spectroscopy | Absorption Spectroscopy |
| Nanosystem Analyzed | -Colloidal suspensions<br>-polymer solutions/melts<br>-gels/ liquid crystals<br>-amino acids and proteins | -Colloidal solutions<br>-suspensions<br>-thin films<br>-powders |
| Parameter Measured | -Size<br>-particle diffusion rate<br>- radius<br>-structural variations of macromolecules | -Volume<br>-particle size |
| Resolution | 0.5 nm – micrometer range | |
| Problems | -Average particle size, error when larger atoms or impurity elements are present in a sample<br>-In the nanoparticle sample, the analysis is biased toward highly refractile particles | -Error due to scattering via solid particles in heterogeneous samples<br>-Restricted to turbid samples |

Table A.5: Comparison of Basic Nanometrology Techniques, X-ray Methods [137]

| X-RAY METHODS | | |
|---|---|---|
| Procedures | X-ray Diffraction | X-ray Photoelectron Spectroscopy |
| Nanosystem Analyzed | -Nanoparticles<br>-virus particles<br>-polymers<br>-thin films<br>-biomolecules | -Nanoparticles<br>-nanowires<br>-thin films<br>-semiconductors<br>-polymers<br>-biomaterials |
| Parameter Measured | -Surface topology<br>-crystallographic information<br>-structure<br>-composition<br>-physical traits | -Quantitative and qualitative elemental composition in external layers<br>-identification of chemical state of the sample elements<br>-binding energy and density of states |
| Resolution | - | -0.5–10 nm depth<br>-0.005–50 µm lateral resolution |
| Problems | Broad peaks from small crystals, making it problematic to verify the crystalline orientation. | -Errors in the chemical analysis for heterogeneous exteriors<br>-Degradation during study<br>-High vacuum is required |

Table A.6: Comparison of Cancer and Tumor Detection Techniques [263].

| Diagnostic Procedure | Sensitivity (%) | Specificity (%) | Positive Predicted Value (%) | Accuracy (%) |
|---|---|---|---|---|
| Mammography | 68 | 75 | 86 | 70.2 |
| MRI | 94.4 | 26 | 73.6 | 73 |
| Clinical Checkup | 50.4 | 92.1 | 94.3 | 64 |
| Ultrasound | 83.1 | 34 | 73.4 | 68 |
| Mammogram and Medical Checkup | 77.4 | 72 | 59 | 76 |
| Mammogram and Ultrasound | 91 | 24 | 71 | 70 |
| Mammogram, Medical Checkup, and Ultrasound | 93 | 23 | 71 | 70 |
| Mammogram, Clinical Checkup, and MRI | 99.5 | 7.0 | 70 | 70.4 |